LAWRENCE
LIVERMORE
NATIONAL
LABORATORY

LLNL-JRNL-472171

Extracting Scattering Phase-Shifts in Higher Partial-Waves from Lattice QCD Calculations

T. Luu, M. J. Savage

March 7, 2011

Physical Review D

Disclaimer

This document was prepared as an account of work sponsored by an agency of the United States government. Neither the United States government nor Lawrence Livermore National Security, LLC, nor any of their employees makes any warranty, expressed or implied, or assumes any legal liability or responsibility for the accuracy, completeness, or usefulness of any information, apparatus, product, or process disclosed, or represents that its use would not infringe privately owned rights. Reference herein to any specific commercial product, process, or service by trade name, trademark, manufacturer, or otherwise does not necessarily constitute or imply its endorsement, recommendation, or favoring by the United States government or Lawrence Livermore National Security, LLC. The views and opinions of authors expressed herein do not necessarily state or reflect those of the United States government or Lawrence Livermore National Security, LLC, and shall not be used for advertising or product endorsement purposes.

NT@UW-11-01

Extracting Scattering Phase-Shifts in Higher Partial-Waves from Lattice QCD Calculations

Thomas Luu[1,*] and Martin J. Savage[2,†]

[1] *N Section, Lawrence Livermore National Laboratory, Livermore, CA 94551, USA*
[2] *Department of Physics, University of Washington, Seattle, WA 98195-1560, USA*

(Dated: January 18, 2011)

Abstract

Lüscher's method is routinely used to determine meson-meson, meson-baryon and baryon-baryon s-wave scattering amplitudes below inelastic thresholds from Lattice QCD calculations - presently at unphysical light-quark masses. In this work we review the formalism and develop the requisite expressions to extract phase-shifts describing meson-meson scattering in partial-waves with angular-momentum $l \leq 6$ and $l = 9$. The implications of the underlying cubic symmetry, and strategies for extracting the phase-shifts from Lattice QCD calculations, are presented, along with a discussion of the signal-to-noise problem that afflicts the higher partial-waves.

*tluu@llnl.gov
†mjs5@u.washington.edu

Contents

I. Introduction 3

II. Formalism 4

III. Energy-Eigenvalues, Sources and Sinks 7
- A. Positive Parity Systems 8
  - 1. A_1^+ Representation 8
  - 2. A_2^+ Representation 15
  - 3. E^+ Representation 17
  - 4. T_1^+ Representation 22
  - 5. T_2^+ Representation 26
- B. Negative Parity Systems 32
  - 1. A_2^- Representation 32
  - 2. E^- Representation 34
  - 3. T_1^- Representation 36
  - 4. T_2^- Representation 42
  - 5. A_1^- Representation 44

IV. Discussion 50
- A. Strategy for Extracting Phase-Shifts from Lattice QCD 50
- B. Expectations for the $\pi\pi$ Energy-Eigenvalues 51
- C. Signal-to-Noise Issues 54

V. Conclusion 55

A. Block-Diagonalization of $F^{(FV)}$ 56
- 1. Odd-Parity Sector with $\delta_{1,3} \neq 0$ 56
- 2. Even-Parity Sector with $\delta_{0,2,4} \neq 0$ 61

B. $\mathcal{Z}_{l,m}(1;\tilde{q}^2)$ Functions 64

C. Perturbative Expressions 66

Acknowledgments 75

References 77

I. INTRODUCTION

The s-wave interactions between hadrons are being calculated with Lattice QCD (LQCD) with increasing precision. Presently, such calculations are being performed at unphysical light-quark masses, and in the case of mesonic interactions, extrapolations to the physical light-quark masses are made possible by chiral perturbation theory (χPT). Unfortunately, such extrapolations are presently not reliable for baryon-baryon interactions, and it is likely that LQCD calculations at, or very near, the physical light-quark masses will be required to make precise predictions for these interactions due to the fine-tunings that are known to exist in nuclear physics. In most LQCD calculations, periodic boundary-conditions (BC's) are imposed on the quark and gluons fields in the spatial-directions of the lattice volume and Lüscher's method [1, 2] can be used to extract scattering phase-shifts from the energy-eigenvalues of two-hadron states that lie below inelastic thresholds. As it is the irreducible representations (irreps) of the cubic group that determine the degeneracies of the eigenstates in the (cubic) lattice volume, it is difficult to determine the phase-shifts, δ_l, beyond the lowest few partial-waves. Each of the irreps of the cubic group have a non-zero overlap with infinitely many irreps of SO(3), and as a result, the energy-eigenvalues of two-hadron states transforming as a certain irrep of the cubic group receive contributions from the phase-shifts in an infinite number of partial-waves. In contrast, two-particle systems confined in a harmonic oscillator potential have a one-to-one relation between phase shifts and the energy-eigenvalues since the potential respects SO(3) symmetry [3, 4] [1]. The mixing of angular momentum in cubic irreps consequently limits the precision with which the phase-shift in any given partial-wave can be extracted in a LQCD calculation. This was made obvious in the work of Mandula, Zweig and Govaerts,[6], and explicitly detailed in Lüscher's papers [1, 2]. Lüscher calculated the energies of states in the A_1^+ irrep of the cubic group as a function of δ_0 and δ_4, and gave general expressions for the energies of states transforming in each of the cubic irreps in terms of the δ_l. The extension of this formalism to systems with non-zero center-of-mass (CM) momentum was performed by Rummukainen and Gottlieb [7], and later by Kim, Sharpe and Sachrajda [8]. Recently finite-volume expressions for three-nucleon systems within cubic volumes have been investigated [9–11].

Fully-dynamical $n_f = 2+1$ LQCD calculations of meson-meson interactions in the isospin-stretch-states (*i.e.* no disconnected diagrams) are presently enabling predictions of the s-wave interactions with percent-level precision [12–17] (for a recent review, see Ref. [18]), and very recently a preliminary calculation of the $\pi^+\pi^+$ d-wave phase-shift has been performed [20]. Further, preliminary calculations of $I = 0$ $\pi\pi$ scattering, which contain disconnected diagrams, have been performed [21]. These calculations were preceded by quenched LQCD calculations [22–40], and by early $n_f = 2$ LQCD calculations [41]. Meson-baryon systems are starting to be explored in the channels for which disconnected diagrams are not required in the LQCD calculations [42]. Further, LQCD calculations of baryon-baryon interactions are beginning to become reliable at unphysical pion masses [43–46], and recently the binding energy of the H-dibaryon has been calculated [47]. Now that the methodology for extracting s-wave interactions has been shown to be effective, it is appropriate to explore the higher partial-waves. In the meson sector, a determination of the p-wave phase-shifts has direct implications for post-dicting the mass and width of the ρ-meson [48, 49], but this

[1] The same is true when a "spherical-wall" is imposed on the separation between hadrons, as has been demonstrated in recent lattice effective field theory (LEFT) calculations [5].

requires evaluating disconnected diagrams in LQCD - calculations that are computationally expensive. In nucleon-nuclei scattering, the experimentally determined p-wave phase-shifts are thought to be at the heart of the "A_y-puzzle" in nucleon-deuteron scattering. Further, it is found phenomenologically that only the phase-shifts in partial waves with $l \lesssim 4$ are required to perform relatively precise calculations of nuclear structure and reactions (at the physical pion mass).

The formalism required to analyze the $J = 1$ coupled-channels, in which the deuteron is the ground-state, has been put in place by Liu, Feng and He [50], and exploratory quenched calculations of the s-d mixing parameter, ε, at pion masses of $m_\pi \sim 730, 530$ and 380 MeV have been performed in a small number of lattice volumes [51]. Further, there has been recent work in developing the phenomenology that goes beyond Lüschers formalism in an attempt to explore resonances (and couplings to multi-hadron final-states) in the single baryon and meson sectors[52].

It is appropriate to point out that there is a substantial amount of information and technology that is directly relevant to this subject, in particular space-groups, that has been developed for study of condensed matter systems. Much of the work in this paper draws directly from various applications found in these fields. Discussions of space-groups can be found in texts, such as Ref. [53] or Ref. [54], as are discussions of point-groups, and other formalisms that impact the present calculations.

While the papers by Lüscher [1, 2] contain the required formalism, we take this opportunity to present the explicit relations between the energy-eigenvalues of two-meson states in a cubic volume and the phase-shifts in the partial-waves with $l \leq 6$ and $l = 9$. The experimentally measured phase-shifts describing $\pi\pi$ scattering in the lowest-lying partial-waves, appropriately parameterized, are used to perform estimates of the energy-eigenvalues that are expected in LQCD calculations of such systems over a range of lattice volumes. We also discuss the issue of signal-to-noise degradation while performing lattice calculations in higher partial waves.

II. FORMALISM

In the absence of interactions, the states in the cubic volume can be defined by their behavior under transformations of the cubic group and by their energy. As the momentum in the volume is quantized in integer multiples of $2\pi/L$, where L is the spatial-extent of the volume, the energy quantum number can be replaced by the magnitude of the integer triplet defining the momentum, $|\mathbf{n}|^2$, where $\mathbf{n} = (n_x, n_y, n_z)$. Instead of the energy, it is convenient to refer to the particular $|\mathbf{n}|^2$-shell. For each partial-wave with $l \leq 6$ and $l = 9$, an irrep of the cubic group is identified for which δ_l provides the dominant contribution to the interaction energy. Sources and sinks used in LQCD calculations that are constructed to transform under such irreps will allow for a determination of the δ_l at some level of precision. The energy of states with $|\mathbf{n}|^2 \leq 6$ are required to lie below the inelastic threshold in order to obtain all of the phase-shifts with $l \leq 6$, thereby requiring relatively large lattice volumes. Further, the energy of a state in the $|\mathbf{n}|^2 = 14$-shell is required to obtain the $l = 9$ phase-shift.

A non-zero phase-shift in a given partial-wave will, in general, contribute to the energy-eigenvalues of two-hadron states in the volume that transform as one or more irreducible

TABLE I: Decomposition of the orbital angular momentum eigenstates, $|l,m\rangle$, into irreps of the cubic group, $\Gamma^{(i)}$, for $l \leq 9$ (see, for instance, Ref. [53]).

Angular Momentum, l	Irreps of the Cubic Group, $\Gamma^{(i)}$
0	A_1^+
1	T_1^-
2	$E^+ \oplus T_2^+$
3	$A_2^- \oplus T_1^- \oplus T_2^-$
4	$A_1^+ \oplus E^+ \oplus T_1^+ \oplus T_2^+$
5	$E^- \oplus T_1^{-(1)} \oplus T_1^{-(2)} \oplus T_2^-$
6	$A_1^+ \oplus A_2^+ \oplus E^+ \oplus T_1^+ \oplus T_2^{+(1)} \oplus T_2^{+(2)}$
7	$A_2^- \oplus E^- \oplus T_1^{-(1)} \oplus T_1^{-(2)} \oplus T_2^{-(1)} \oplus T_2^{-(2)}$
8	$A_1^+ \oplus E^{+(1)} \oplus E^{+(2)} \oplus T_1^{+(1)} \oplus T_1^{+(2)} \oplus T_2^{+(1)} \oplus T_2^{+(2)}$
9	$A_1^- \oplus A_2^- \oplus E^- \oplus T_1^{-(1)} \oplus T_1^{-(2)} \oplus T_1^{-(3)} \oplus T_2^{-(1)} \oplus T_2^{-(2)}$

representations of the full cubic group, $\Gamma^{(i)}$. [2] Table I shows the decomposition of the orbital angular momentum eigenstates, $|l,m\rangle$, into the $\Gamma^{(i)}$ for $l \leq 9$, from which it is straightforward to determine the $\Gamma^{(i)}$ that have energy-eigenvalues that depend upon a given phase-shift δ_l [3]. A cursory study of table I shows that A_1^+-states will, in general, receive contributions to their energy from interactions with $l = 0, 4, 6, 8, ...$, as is well known [6], and similarly for the other $\Gamma^{(i)}$. As the dimensionality of an SO(3) irrep (which is $2l+1$ for $|l,m\rangle$) must be equal to the sum of the dimensionalities of the cubic irreps in its decomposition, cubic irreps will, in general, appear multiple times (with multiplicities denoted by $N(\Gamma^{(i)}, l)$) in the decomposition of an SO(3) irrep. Multiplicities greater than one occur for $l \geq 5$. The space associated with the jth occurrence of $\Gamma^{(i)}$ in the decomposition of $|l,m\rangle$ is spanned by the orthonormal basis $\{\ |\Gamma^{(i)}, L_z; l; j\rangle\ \}$, where the number of values of L_z equals the dimensionality of $\Gamma^{(i)}$, e.g. for $l = 5$, the 3-dimensional irrep T_1^- occurs twice, and the space associated with the second occurrence is spanned by $\{\ |T_1^-, 0; 5; 2\rangle\ ,\ |T_1^-, 1; 5; 2\rangle\ ,\ |T_1^-, 3; 5; 2\rangle\}$ [4]. When calculating observables in a cubic volume, operators transforming as a component of a spherical tensor of rank-S, $\hat{O}_S^{(\mu)}$, are most conveniently written as

$$\hat{O}_S^{(\mu)} = \sum_{i,j,L_z} \theta^{(\Gamma^{(i)},j,L_z;S,\mu)}\ |\Gamma^{(i)}, L_z; S; j\rangle\langle\Gamma^{(i)}, L_z; S; j| \quad , \tag{1}$$

where the values of the $\theta^{(\Gamma^{(i)},j,L_z;S,\mu)}$ are simply determined by matrix elements of $\hat{O}_S^{(\mu)}$

[2] The irreps of the full cubic group are $\Gamma^{(i)} = A_1^\pm, A_2^\pm, E^\pm, T_1^\pm$, and $T_2^\pm$, and have dimensionality $1, 1, 2, 3$ and 3 respectively. The superscript denotes the parity of $\Gamma^{(i)}$.

[3] Each $\Gamma^{(i)}$ appears at least once in the decomposition of the $|l,m\rangle$ with $l \leq 6$ except A_1^- which first appears in the decomposition of the $l = 9$ irrep [53]. It is important to note that the decompositions of the $l = 7$ and $l = 8$ irreps contain only $\Gamma^{(i)}$ that also appear in the decomposition of the $l \leq 6$ irreps, and consequently there is no $\Gamma^{(i)}$ for which the dominant contribution to the interaction energy (in the large volume limit) is from the $l = 7$ and $l = 8$ partial-waves.

[4] The L_z quantum number indicates that a phase of $e^{iL_z\phi}$ results from a (cubic) rotation of $\phi = n\pi/2$ about the z-axis, with n an integer. $L_z = 3$ is equivalent to a $L_z = -1$ and $L_z = 2$ is equivalent to $L_z = -2$.

between $|l,m\rangle$, or $|\Gamma^{(i)},L_z;S;j\rangle$, or any states forming a basis in which the projections onto $|\Gamma^{(i)},L_z;S;j\rangle$ are known. In determining the energy-eigenvalues of the states in the volume, it is the scattering amplitude in a given partial-wave that is written in the form of eq. (1), with $S=l$.

The relations between the energy-eigenvalues of two-hadrons in a cubic volume and their scattering phase-shifts below the inelastic threshold, originally derived in the context of non-relativistic quantum mechanics, were shown to be valid in quantum field theory (QFT) without modification by Lüscher [1, 2]. The energy-shifts of scattering states due to the interactions exhibit power-law dependence upon the volume when the range of the interaction is negligible compared to the spatial-extent of the volume. Corrections arising from the range of the interaction (for the case of $\pi^+\pi^+$ the range is set by $R\sim 1/(2m_\pi)$, while for nucleon-nucleon interactions it is set by $R\sim 1/m_\pi$) are exponentially suppressed for $L\gg R$, and of the form $\sim e^{-L/R}$ [55]. In this work, it is assumed that these finite-range corrections are negligible compared to the power-law energy-shifts due to the interactions. It is straightforward to calculate a two-hadron Green function resulting from an arbitrary source and sink. The Green-function is generated by the bubble-diagrams with non-interacting two-hadron states propagating from the source through multiple insertions of the T-matrix, and then to the sink. In free-space, the Green function exhibits poles at the location of bound-states and cuts along the positive real axis. In the finite-volume, modifications to the propagation of the two non-interacting hadrons eliminates the cuts on the positive real axis, replacing them with poles at the location of the energy-eigenstates. Further, these modifications shift the location of the poles on the negative real axis (if present in infinite volume). The energy-eigenvalues, corresponding to both bound-states and continuum states in the infinite-volume limit are determined by solutions to [8],

$$\det\left[\ \cos\delta-\sin\delta\ F^{(FV)}\ \right]\ =\ 0\quad , \tag{2}$$

where $\cot\delta$, $\sin\delta$ and $F^{(FV)}$ are $(l^{\max}+1)^2\times(l^{\max}+1)^2$ dimensional matrices when the phase-shifts δ_l are non-zero for $l\leq l^{\max}$ and vanish for $l>l^{\max}$. Initially, it is convenient to work in the $|l,m\rangle$ basis in which, for uncoupled channels, $\cot\delta$ and $\sin\delta$ are diagonal matrices of the form

$$\cos\delta\ =\ \cos\delta_{l_1}\ \delta_{l_1,l_2}\ \delta_{m_1,m_2}\quad ,\quad \sin\delta\ =\ \sin\delta_{l_1}\ \delta_{l_1,l_2}\ \delta_{m_1,m_2}\quad , \tag{3}$$

for $l_{1,2}\leq l^{\max}$, but in which $F^{(FV)}$ has off-diagonal elements, in general. $F^{(FV)}$ is a matrix that is a function of the dimensionless quantity $\tilde{q}=\frac{qL}{2\pi}$, where q is related to the energy of the interacting two-hadron state, $E_{H_1H_2}=\sqrt{q^2+m_{H_1}^2}+\sqrt{q^2+m_{H_2}^2}$. Its matrix elements are of the form

$$\overline{F}^{(FV)}_{l_1m_1;l_2m_2}\ =\ \frac{(-)^{m_2}}{\tilde{q}\ \pi^{3/2}}\ \sqrt{(2l_1+1)(2l_2+1)}\ \sum_{\bar{l}=|l_1-l_2|}^{|l_1+l_2|}$$
$$\sum_{\overline{m}=-\bar{l}}^{\bar{l}}\ \frac{\sqrt{2\bar{l}+1}}{\tilde{q}^{\bar{l}}}\begin{pmatrix} l_1 & \bar{l} & l_2\\ 0 & 0 & 0\end{pmatrix}\begin{pmatrix} l_1 & \bar{l} & l_2\\ -m_1 & -\overline{m} & m_2\end{pmatrix}\ \mathcal{Z}_{\bar{l},\overline{m}}(1;\tilde{q}^2)\quad , \tag{4}$$

where the functions $\mathcal{Z}_{l,m}(1;\tilde{q}^2)$ are those defined by Lüscher [1, 2],

$$\mathcal{Z}_{l,m}(s;\tilde{q}^2)\ =\ \sum_{\mathbf{n}}\ \frac{|\mathbf{n}|^l\ Y_{lm}(\Omega_{\mathbf{n}})}{[\ |\mathbf{n}|^2-\tilde{q}^2\ ]^s}\quad , \tag{5}$$

where $Y_{lm}(\Omega)$ are the spherical harmonics. The function $\mathcal{Z}_{0,0}(1;\tilde{q}^2)$ is UV-divergent and is defined with the same renormalization scheme used to define the infinite-volume scattering amplitude. It is useful to first diagonalize the blocks of $F^{(FV)}$ with $l_1 = l_2 = l$, $\overline{F}^{(FV)}_{lm_1,lm_2}$, which diagonalizes $F^{(FV)}$ into blocks with dimensions dictated by the number of occurrences of each $\Gamma^{(i)}$ for $l \leq l^{\max}$, while leaving the $\sin\delta$ and $\cos\delta$ matrices diagonal. Further diagonalizations that may be required are confined within each $\Gamma^{(i)}$. The determinant in eq. (2) becomes the product of determinants resulting from each $\Gamma^{(i)}$, and therefore, for $l^{\max} = 6$, this procedure requires dealing with matrices of size 4×4 or smaller.

Despite the fact that eq. (2) requires forming the determinant of a finite dimensional matrix, it has infinitely many solutions. It is derived from a Green-function between arbitrary sources and sinks which, in principle, can couple to all of the eigenstates in the volume, manifested in the infinite-sums over integer-triplets that define the $\mathcal{Z}_{l,m}$-functions. Therefore, the zero's of the determinant in eq. (2) define all of the energy-eigenvalues and hence eigenstates. As discussed previously, the energy-spectrum of two non-interacting hadrons in the cubic volume with periodic BC's, and with vanishing total momentum can be defined by triplets of integers, $\mathbf{n}$,

$$\begin{aligned} E &= \sqrt{|\mathbf{q}_1|^2 + m_1^2} \; + \; \sqrt{|\mathbf{q}_2|^2 + m_2^2} \; \rightarrow \; \sqrt{\left(\frac{2\pi}{L}\right)^2 |\mathbf{n}|^2 + m_1^2} \; + \; \sqrt{\left(\frac{2\pi}{L}\right)^2 |\mathbf{n}|^2 + m_2^2} \\ &= \frac{|\mathbf{q}_1|^2}{2m_1} \; + \; \frac{|\mathbf{q}_2|^2}{2m_2} \; + \; ... \; \rightarrow \; \frac{2\pi^2}{\mu L^2} \, |\mathbf{n}|^2 \; + \; ... \quad . \end{aligned} \tag{6}$$

where one hadron carries momentum $\mathbf{q}_1 = \frac{2\pi}{L}\mathbf{n}$ and the other carries momentum $\mathbf{q}_2 = -\frac{2\pi}{L}\mathbf{n}$, and the reduced mass of the system is $\mu^{-1} = m_1^{-1} + m_2^{-1}$. This (non-interacting) spectrum is recovered in the above formalism, in particular eq. (2), in the limit that $\delta_l \rightarrow 0$ in each partial-wave from the poles in the $\mathcal{Z}_{l,m}$-functions that exist along the positive real axis. The degeneracy of any given $|\mathbf{n}|^2$-shell is straightforward to determine and is recovered from the number of states in the $\Gamma^{(i)}$ that span the $|\mathbf{n}|^2$-shell, as shown in table II. As the (single hadron) momentum eigenstates in a given $|\mathbf{n}|^2$-shell are degenerate, the corresponding $\Gamma^{(i)}$ are also degenerate. These degeneracies are lifted by two-particle interactions that induce non-zero δ_l's. Table II shows that all but one of the $\Gamma^{(i)}$ are required to describe the eigenstates for $|\mathbf{n}|^2 \leq 6$, and from table I it can be concluded that for $\delta_l \neq 0$ for $l \leq 6$ all of the eigenstates with $|\mathbf{n}|^2 \leq 6$ are shifted from the non-interacting two-hadron energy due to interactions. However, the A_1^- irrep first occurs in the $|\mathbf{n}|^2 = 14$ shell and its energy is dependent upon interactions with $l \geq 9$.

III. ENERGY-EIGENVALUES, SOURCES AND SINKS

Lüschers formalism, as detailed in the previous section, is used to construct explicit relations between the energy-eigenvalues of the $\Gamma^{(i)}$ and the interaction phase-shifts for $l \leq l^{max} = 6$, the results of which are presented in this section. Sources and sinks for LQCD calculations that transform as a given $\Gamma^{(i)}$ are constructed from the single-hadron momentum-eigenstates, and Fourier transformed into position-space. One pair of these sources and sinks would couple only to a single energy-eigenstate in the absence of interactions between the hadrons. As the interactions do not induce mixing between distinct $\Gamma^{(i)}$, these sources and sinks couple, in principle, to all states that transform in the same $\Gamma^{(i)}$. To keep the presentation

TABLE II: The degeneracies of, and the number of occurrences of each $\Gamma^{(i)}$ in, the lowest-lying $|\mathbf{n}|^2$-shells. Note: the A_1^- irrep first appears in the $|\mathbf{n}|^2 = 14$ shell.

$\|\mathbf{n}\|^2$	degeneracy	A_1^+	A_2^+	T_1^+	T_2^+	E^+	A_1^-	A_2^-	T_1^-	T_2^-	E^-
0	1	1	-	-	-	-	-	-	-	-	-
1	6	1	-	-	-	1	-	-	1	-	-
2	12	1	-	-	1	1	-	-	1	1	-
3	8	1	-	-	1	-	-	1	1	-	-
4	6	1	-	-	-	1	-	-	1	-	-
5	24	1	1	1	1	2	-	-	2	2	-
6	24	1	-	1	2	1	-	1	2	1	1
$\vdots$											
14	48	1	1	3	3	2	1	1	3	3	2

of results simple, explicit derivations are deferred to Appendix A, where calculations of the even- and odd-parity systems with $l^{max} = 4$ are detailed, and which straightforwardly generalize to any l^{max}.

As the hadronic interactions considered in this work result from QCD with the strong CP-violating parameter θ set equal to zero, and without the electroweak interactions, parity is a good quantum number. Consequently, the contributions to the finite-volume function $F^{(FV)}$ do not mix states of opposite parity, and therefore the required calculations decompose into the parity-even and parity-odd sectors. If weak-interactions are included in the analysis, as will necessarily be the case when hadronic parity-violating interactions are calculated with LQCD, mixing between the parity-sectors will occur.

A. Positive Parity Systems

There are five positive parity irreps of the cubic group, A_1^+, A_2^+, E^+, T_1^+, and T_2^+ with dimensions $1, 1, 2, 3,$and 3 respectively. Table I shows how the interactions in a given partial-wave contribute to each $\Gamma^{(i)}$. The energy-eigenvalues, sources and sinks for the even-parity states are presented in the following sections: III A 1, III A 2, III A 3, III A 4 and III A 5.

1. A_1^+ Representation

The energy-eigenvalues of A_1^+ states depend upon the phase-shifts in the $l = 0, 4, 6, 8, ...$ partial-waves, as can be seen in table I. Diagonalization of the blocks in the finite-volume function of the form $F_{l;l}^{(FV)}$ for $l = 0, 4, 6$ gives the states $|A_1^+, L_z; l; j\rangle$, as defined immediately

before eq. (1), with

$$
\begin{aligned}
|A_1^+,0;0;1\rangle &= |0,0\rangle \\
|A_1^+,0;4;1\rangle &= \frac{1}{2}\sqrt{\frac{5}{6}}\,|4,4\rangle \;+\; \frac{1}{2}\sqrt{\frac{7}{3}}\,|4,0\rangle \;+\; \frac{1}{2}\sqrt{\frac{5}{6}}\,|4,-4\rangle \\
|A_1^+,0;6;1\rangle &= \frac{\sqrt{7}}{4}\,|6,4\rangle \;-\; \frac{1}{2\sqrt{2}}\,|6,0\rangle \;+\; \frac{\sqrt{7}}{4}\,|6,-4\rangle
\end{aligned}
\tag{7}
$$

for the A_1^+ eigenstate of each $\overline{F}^{(FV)}_{l;l}$ in the orbital angular momentum (spherical-wave) basis $|l,m\rangle$. With these states and the corresponding eigenvalues from $\overline{F}^{(FV)}_{l;l}$, the procedures described in Appendix A allow for the contribution to eq. (2) from A_1^+ states to be written as

$$
\det\left[\begin{pmatrix} \cot\delta_0 & 0 & 0 \\ 0 & \cot\delta_4 & 0 \\ 0 & 0 & \cot\delta_6 \end{pmatrix} - \begin{pmatrix} \overline{F}^{(FV,A_1^+)}_{0;0} & \overline{F}^{(FV,A_1^+)}_{0;4} & \overline{F}^{(FV,A_1^+)}_{0;6} \\ \overline{F}^{(FV,A_1^+)}_{4;0} & \overline{F}^{(FV,A_1^+)}_{4;4} & \overline{F}^{(FV,A_1^+)}_{4;6} \\ \overline{F}^{(FV,A_1^+)}_{6;0} & \overline{F}^{(FV,A_1^+)}_{6;4} & \overline{F}^{(FV,A_1^+)}_{6;6} \end{pmatrix}\right] \;=\; 0 \quad , \tag{8}
$$

where the finite-volume contributions are

$$
\begin{aligned}
\overline{F}^{(FV,A_1^+)}_{0;0} &= \frac{\mathcal{Z}_{0,0}\left(1;\tilde{q}^2\right)}{\pi^{3/2}\tilde{q}} \\
\overline{F}^{(FV,A_1^+)}_{0;4} &= \frac{2\sqrt{\frac{3}{7}}\mathcal{Z}_{4,0}\left(1;\tilde{q}^2\right)}{\pi^{3/2}\tilde{q}^5} \\
\overline{F}^{(FV,A_1^+)}_{0;6} &= -\frac{2\sqrt{2}\mathcal{Z}_{6,0}\left(1;\tilde{q}^2\right)}{\pi^{3/2}\tilde{q}^7} \\
\overline{F}^{(FV,A_1^+)}_{4;4} &= \frac{\mathcal{Z}_{0,0}\left(1;\tilde{q}^2\right)}{\pi^{3/2}\tilde{q}} + \frac{108\mathcal{Z}_{4,0}\left(1;\tilde{q}^2\right)}{143\pi^{3/2}\tilde{q}^5} + \frac{80\mathcal{Z}_{6,0}\left(1;\tilde{q}^2\right)}{11\sqrt{13}\pi^{3/2}\tilde{q}^7} + \frac{560\mathcal{Z}_{8,0}\left(1;\tilde{q}^2\right)}{143\sqrt{17}\pi^{3/2}\tilde{q}^9} \\
\overline{F}^{(FV,A_1^+)}_{4;6} &= -\frac{40\sqrt{\frac{6}{91}}\mathcal{Z}_{4,0}\left(1;\tilde{q}^2\right)}{11\pi^{3/2}\tilde{q}^5} + \frac{42\sqrt{42}\mathcal{Z}_{6,0}\left(1;\tilde{q}^2\right)}{187\pi^{3/2}\tilde{q}^7} - \frac{224\sqrt{\frac{42}{221}}\mathcal{Z}_{8,0}\left(1;\tilde{q}^2\right)}{209\pi^{3/2}\tilde{q}^9} \\
&\quad - \frac{1008\sqrt{\frac{2}{13}}\mathcal{Z}_{10,0}\left(1;\tilde{q}^2\right)}{323\pi^{3/2}\tilde{q}^{11}} \\
\overline{F}^{(FV,A_1^+)}_{6;6} &= \frac{\mathcal{Z}_{0,0}\left(1;\tilde{q}^2\right)}{\pi^{3/2}\tilde{q}} - \frac{126\mathcal{Z}_{4,0}\left(1;\tilde{q}^2\right)}{187\pi^{3/2}\tilde{q}^5} - \frac{160\sqrt{13}\mathcal{Z}_{6,0}\left(1;\tilde{q}^2\right)}{3553\pi^{3/2}\tilde{q}^7} + \frac{840\mathcal{Z}_{8,0}\left(1;\tilde{q}^2\right)}{209\sqrt{17}\pi^{3/2}\tilde{q}^9} \\
&\quad - \frac{2016\sqrt{21}\mathcal{Z}_{10,0}\left(1;\tilde{q}^2\right)}{7429\pi^{3/2}\tilde{q}^{11}} + \frac{30492\mathcal{Z}_{12,0}\left(1;\tilde{q}^2\right)}{37145\pi^{3/2}\tilde{q}^{13}} - \frac{1848\sqrt{1001}\mathcal{Z}_{12,4}\left(1;\tilde{q}^2\right)}{37145\pi^{3/2}\tilde{q}^{13}} \quad ,
\end{aligned}
$$

and $\overline{F}^{(FV,\Gamma^{(i)})}_{i;j} = \overline{F}^{(FV,\Gamma^{(i)})}_{j;i}$. Equation (8) yields an infinite number of energy-eigenvalues and eigenstates, each of which depend upon the phase-shift in the l =0, 4, and 6 partial waves.

In the $|\mathbf{n}|^2$-shells for which there is just one A_1^+ state, as shown in table II, its energy-shift due to interactions receives contributions from the $l = 0, 4, 6, ...$ partial-waves. However, in the $|\mathbf{n}|^2$-shells in which there are multiple A_1^+ states (first occurring at $|\mathbf{n}|^2 = 9$), the energy-eigenstates are linear combinations of these states. In the large-volume limit, the shift in the energy-eigenvalue of one combination is dominated by the interactions in the $l = 0$

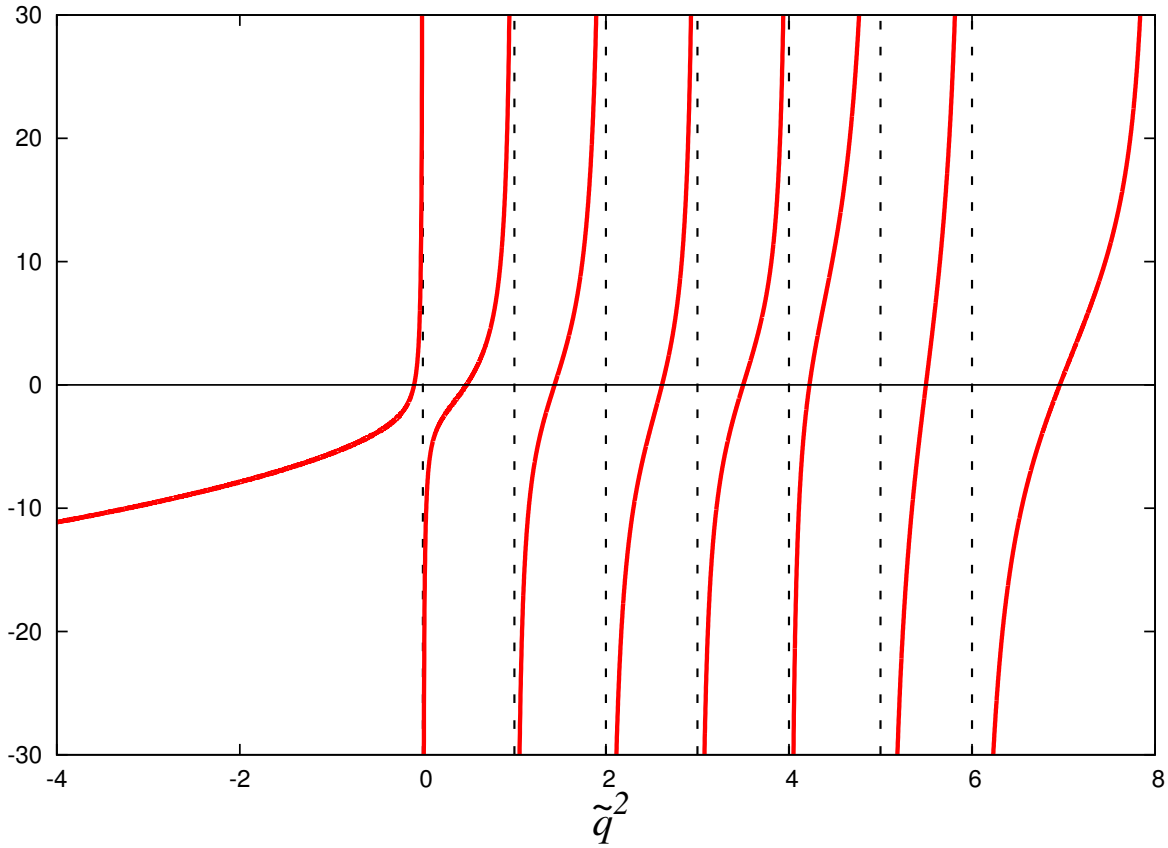

FIG. 1: The function $\mathcal{Z}_{0,0}\left(1;\tilde{q}^2\right)$. The vertical dashed lines denote the position of the poles of the function corresponding to the non-interacting energy-eigenvalues.

partial-wave, the shift in a second combination is dominated by the interactions in the $l=4$ partial-wave, the shift in a third combination is dominated by the interactions in the $l=6$ partial-wave, and so on. So while the naive argument that A_1^+ states receive contributions from interactions in the $l=0,4,6,...$ partial-waves is generally true, linear combinations of A_1^+ states are formed such that it is not true in the infinite-volume limit. The energy-shift of each occurrence of an A_1^+ energy-eigenstate in a given $|\mathbf{n}|^2$-shell is dominated by the interaction in a different partial-wave in the infinite-volume limit. To demonstrate this point, consider the situation where the phase-shift in the $l=6$ partial-wave vanishes, in which case eq. (8) becomes a 2×2 matrix with the following two solutions:

$$\frac{\cot\delta_0}{2}+\frac{\cot\delta_4}{2}-\frac{\mathcal{Z}_{0,0}\left(1;\tilde{q}^2\right)}{\pi^{3/2}\tilde{q}}-\frac{280\mathcal{Z}_{8,0}\left(1;\tilde{q}^2\right)}{143\sqrt{17}\pi^{3/2}\tilde{q}^9}-\frac{40\mathcal{Z}_{6,0}\left(1;\tilde{q}^2\right)}{11\sqrt{13}\pi^{3/2}\tilde{q}^7}-\frac{54\mathcal{Z}_{4,0}\left(1;\tilde{q}^2\right)}{143\pi^{3/2}\tilde{q}^5}$$
$$\pm\frac{1}{2}\sqrt{\left(\frac{560\mathcal{Z}_{8,0}\left(1;\tilde{q}^2\right)}{143\sqrt{17}\pi^{3/2}\tilde{q}^9}+\frac{80\mathcal{Z}_{6,0}\left(1;\tilde{q}^2\right)}{11\sqrt{13}\pi^{3/2}\tilde{q}^7}+\frac{108\mathcal{Z}_{4,0}\left(1;\tilde{q}^2\right)}{143\pi^{3/2}\tilde{q}^5}+\cot\delta_0-\cot\delta_4\right)^2+\frac{48\mathcal{Z}_{4,0}\left(1;\tilde{q}^2\right)^2}{7\pi^3\tilde{q}^{10}}}$$
$$=0\ . \quad (9)$$

In the case of $\tan\delta_4 \ll \tan\delta_0$, the $l=0$ dominated solution is

$$q\cot\delta_0 \;=\; \frac{2}{\sqrt{\pi}L}\mathcal{Z}_{0,0}\left(1;\tilde{q}^2\right) \;+\; \frac{12288\pi^7}{7L^{10}}\frac{\mathcal{Z}_{4,0}\left(1;\tilde{q}^2\right)^2}{[q^9\cot\delta_4]} \;+\; O\left(\tan^2\delta_4\right) \quad , \qquad (10)$$

and is valid for all $|\mathbf{n}|^2$-shells. If phase shifts in both the $l = 4$ and $l = 6$ partial-waves vanish, eq. (8) and eq. (10) reduce to the familiar result found by Lüscher [5],

$$q\cot\delta_0 \;=\; \frac{2}{\sqrt{\pi}L}\;\mathcal{Z}_{0,0}\left(1;\tilde{q}^2\right) \quad , \tag{11}$$

where the function $\mathcal{Z}_{0,0}\left(1;\tilde{q}^2\right)$ is shown in fig. 1. Performing a large-volume expansion of the solution (as discussed in Appendix C) to eq. (11) in the $|\mathbf{n}|^2 = 9$-shell gives the energy-eigenvalue

$$E_{A_1^{+(1)}} \;=\; \frac{1}{2\mu}\left[\frac{36\pi^2}{L^2} \;-\; \frac{20\tan\delta_0(|\mathbf{n}|^2=9)}{L^2} \;+\; \mathcal{O}(\tan^2\delta_0) \;+\; ...\right] \quad , \tag{12}$$

while the second solution to eq. (9) has a perturbative expansion of the form

$$E_{A_1^{+(2)}} \;=\; \frac{1}{2\mu}\left[\frac{36\pi^2}{L^2} \;-\; \frac{8960\tan\delta_4(|\mathbf{n}|^2=9)}{243\;L^2} \;+\; \mathcal{O}(\tan\delta_6) \;+\; ...\right] \quad , \tag{13}$$

where the contribution from the $l = 0$ partial-wave is strongly suppressed in the large-volume limit. While the two basis states, $||\mathbf{n}|^2 = 9; A_1^+(1)\rangle$ and $||\mathbf{n}|^2 = 9; A_1^+(2)\rangle$, both have a non-vanishing overlap with $|l, m\rangle = |0, 0\rangle$, it is obvious that a linear combination can be formed that has vanishing overlap. Inserting the interactions once, as is appropriate for determining the energy-eigenvalues in large volumes (*i.e.* first order perturbation theory in $1/L$), dictates the form of the expansions in eq. (12) and eq. (13).

Sources and sinks that have an overlap, and in general a range of overlaps, with the finite-volume energy-eigenstates of hadronic systems are required for LQCD calculations. While the interactions between hadrons gives rise to energy-eigenstates that are not products of single-hadron eigenstates of the linear-momentum operator, sources and sinks can be constructed from the single-hadron momentum eigenstates that transform as a given $\Gamma^{(i)}$, that will have non-zero overlap with the energy-eigenstates in the same irrep. Constructing sources and sinks from single hadrons that have equal and opposite momenta ensures that the total momentum of the combined system vanishes. The relative-momentum-eigenstates of definite parity, $\mathcal{P}$, are denoted by

$$|\vec{n}\;,\;\mathcal{P}\rangle \;=\; \begin{cases} \frac{|\vec{n}\rangle \;+\; \mathcal{P}\;|-\vec{n}\rangle}{\sqrt{2}} & (\vec{n}\neq\vec{0}) \\ |\vec{n}\rangle & (\vec{n}=\vec{0} \text{ and } \mathcal{P}=+1)\;, \end{cases} \tag{14}$$

where $\mathcal{P}$ is the parity of the state ($\mathcal{P} = \pm 1$) and $\vec{n} = (n_x, n_y, n_z)$ is the triplet of integers that define the relative momentum of the two-body system. The states in eq. (14) are eigenstates of the relative kinetic energy operator $T_{\rm rel}$, with the eigenvalues displayed in eq. (6). By taking appropriate linear combinations of these momentum-eigenstates, states in the A_1^+ representation (or any other irrep) can be constructed in each $|\mathbf{n}|^2$-shell if the shell supports it (see table II and Ref. [53]). For example, in the $|\mathbf{n}|^2 = 0$ shell the basis-state is

$$||\mathbf{n}|^2 = 0;\;A_1^+\rangle \;=\; |(0,0,0)\;,\;\mathcal{P}=+1\rangle\;,$$

[5] The "S-function", $S(\tilde{q}^2)$, used in, for example, Ref. [56], is related to $\mathcal{Z}_{0,0}(1;\tilde{q}^2)$ by $S(\tilde{q}^2) = \sqrt{4\pi}\mathcal{Z}_{0,0}(1;\tilde{q}^2)$.

TABLE III: The momentum-space structure of A_1^+ sources and sinks for $|\mathbf{n}|^2$=0-3. These are shown graphically in figs. 2 and 3.

$\|\mathbf{n}\|^2$=0	$\|\mathbf{n}\|^2$=1	$\|\mathbf{n}\|^2$=2	$\|\mathbf{n}\|^2$=3
$\|(0,0,0)\ ,\ +1\rangle$ 1	$\|(1,0,0)\ ,\ +1\rangle$ $\frac{1}{\sqrt{3}}$ $\|(0,1,0)\ ,\ +1\rangle$ $\frac{1}{\sqrt{3}}$ $\|(0,0,1)\ ,\ +1\rangle$ $\frac{1}{\sqrt{3}}$	$\|(1,1,0)\ ,\ +1\rangle$ $\frac{1}{\sqrt{6}}$ $\|(1,0,1)\ ,\ +1\rangle$ $\frac{1}{\sqrt{6}}$ $\|(1,0,-1)\ ,\ +1\rangle$ $\frac{1}{\sqrt{6}}$ $\|(1,-1,0)\ ,\ +1\rangle$ $\frac{1}{\sqrt{6}}$ $\|(0,1,1)\ ,\ +1\rangle$ $\frac{1}{\sqrt{6}}$ $\|(0,1,-1)\ ,\ +1\rangle$ $\frac{1}{\sqrt{6}}$	$\|(1,1,1)\ ,\ +1\rangle$ $\frac{1}{2}$ $\|(1,1,-1)\ ,\ +1\rangle$ $\frac{1}{2}$ $\|(1,-1,1)\ ,\ +1\rangle$ $\frac{1}{2}$ $\|(1,-1,-1)\ ,\ +1\rangle$ $\frac{1}{2}$

TABLE IV: The momentum-space structure of A_1^+ sources and sinks for $|\mathbf{n}|^2$=4-6. These are shown graphically in figs. 3 and 4.

$\|\mathbf{n}\|^2$=4	$\|\mathbf{n}\|^2$=5		$\|\mathbf{n}\|^2$=6	
$\|(2,0,0)\ ,\ +1\rangle$ $\frac{1}{\sqrt{3}}$ $\|(0,2,0)\ ,\ +1\rangle$ $\frac{1}{\sqrt{3}}$ $\|(0,0,2)\ ,\ +1\rangle$ $\frac{1}{\sqrt{3}}$	$\|(2,1,0)\ ,\ +1\rangle$ $\frac{1}{2\sqrt{3}}$ $\|(2,0,-1)\ ,\ +1\rangle$ $\frac{1}{2\sqrt{3}}$ $\|(1,2,0)\ ,\ +1\rangle$ $\frac{1}{2\sqrt{3}}$ $\|(1,0,-2)\ ,\ +1\rangle$ $\frac{1}{2\sqrt{3}}$ $\|(0,2,1)\ ,\ +1\rangle$ $\frac{1}{2\sqrt{3}}$ $\|(0,1,2)\ ,\ +1\rangle$ $\frac{1}{2\sqrt{3}}$	$\|(2,0,1)\ ,\ +1\rangle$ $\frac{1}{2\sqrt{3}}$ $\|(2,-1,0)\ ,\ +1\rangle$ $\frac{1}{2\sqrt{3}}$ $\|(1,0,2)\ ,\ +1\rangle$ $\frac{1}{2\sqrt{3}}$ $\|(1,-2,0)\ ,\ +1\rangle$ $\frac{1}{2\sqrt{3}}$ $\|(0,2,-1)\ ,\ +1\rangle$ $\frac{1}{2\sqrt{3}}$ $\|(0,1,-2)\ ,\ +1\rangle$ $\frac{1}{2\sqrt{3}}$	$\|(2,1,1)\ ,\ +1\rangle$ $\frac{1}{2\sqrt{3}}$ $\|(2,-1,1)\ ,\ +1\rangle$ $\frac{1}{2\sqrt{3}}$ $\|(1,2,1)\ ,\ +1\rangle$ $\frac{1}{2\sqrt{3}}$ $\|(1,1,2)\ ,\ +1\rangle$ $\frac{1}{2\sqrt{3}}$ $\|(1,-1,2)\ ,\ +1\rangle$ $\frac{1}{2\sqrt{3}}$ $\|(1,-2,1)\ ,\ +1\rangle$ $\frac{1}{2\sqrt{3}}$	$\|(2,1,-1)\ ,\ +1\rangle$ $\frac{1}{2\sqrt{3}}$ $\|(2,-1,-1)\ ,\ +1\rangle$ $\frac{1}{2\sqrt{3}}$ $\|(1,2,-1)\ ,\ +1\rangle$ $\frac{1}{2\sqrt{3}}$ $\|(1,1,-2)\ ,\ +1\rangle$ $\frac{1}{2\sqrt{3}}$ $\|(1,-1,-2)\ ,\ +1\rangle$ $\frac{1}{2\sqrt{3}}$ $\|(1,-2,-1)\ ,\ +1\rangle$ $\frac{1}{2\sqrt{3}}$

while for $|\mathbf{n}|^2 = 1$, the basis-state is

$$||\mathbf{n}|^2 = 1;\ A_1^+\rangle \ = \ \frac{|(1,0,0)\ ,\ \mathcal{P}=+1\rangle \ + \ |(0,1,0)\ ,\ \mathcal{P}=+1\rangle \ + \ |(0,0,1)\ ,\ \mathcal{P}=+1\rangle}{\sqrt{3}} \quad .$$

In general the coefficients of these basis vectors are valid up to an arbitrary phase. The complete momentum-space basis for the A_1^+ sources and sinks in each $|\mathbf{n}|^2$-shell are presented in table III for $|\mathbf{n}|^2 \leq 6$.

The momentum-space representations of the sources and sinks (the left panels in figs. 2-4) show the $\mathbf{n}$-vectors that transform as an A_1^+ in the given $|\mathbf{n}|^2$-shells. The widths of the vectors are proportional to the magnitude of their amplitudes and their color denotes the sign (red=positive, blue=negative). The position-space representations of the sources and sinks (the right panels in figs. 2-4) show the surfaces of constant $\rho_{\mathbf{n},\mathcal{P}}(\mathbf{r})$, defined by

$$\rho_{\mathbf{n},\mathcal{P}}(\mathbf{r}) \ = \ |\langle\ \mathbf{r}\ |\ (n_x, n_y, n_z)\ ,\ \mathcal{P}\ \rangle|^2 \quad , \tag{15}$$

which are obtained by Fourier transform. In the position-space representations, $\mathbf{r}$ refers to the relative distance between the two particles and in the figures $\tilde{\mathbf{r}}$ is defined to be $\tilde{\mathbf{r}} = \mathbf{r}/L$.

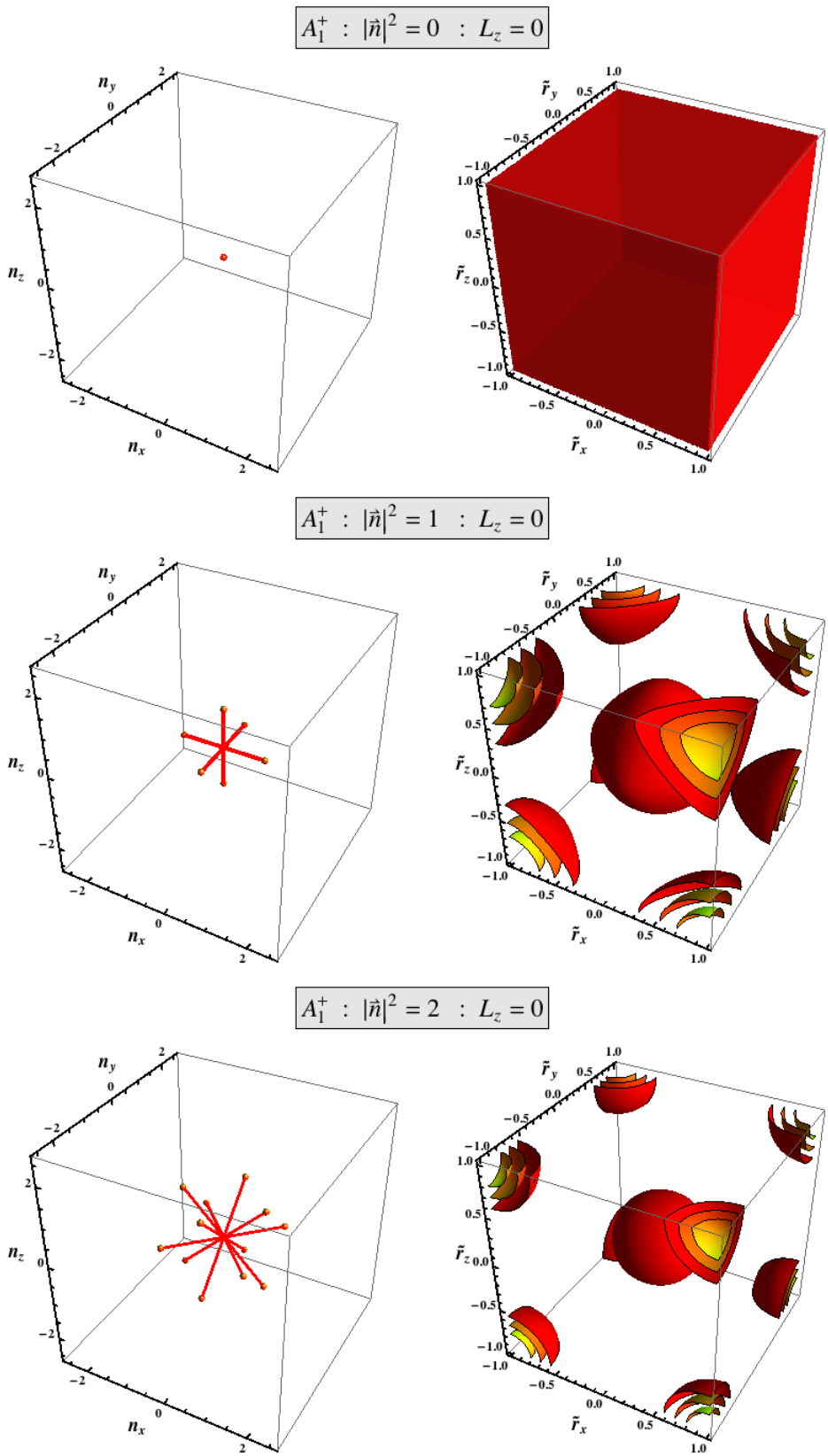

FIG. 2: The momentum-space representations (left) and position-space representations (right) of two-body relative states in the A_1^+ representation for select $|\mathbf{n}|^2$ shells. Here $\tilde{r} = r/L$.

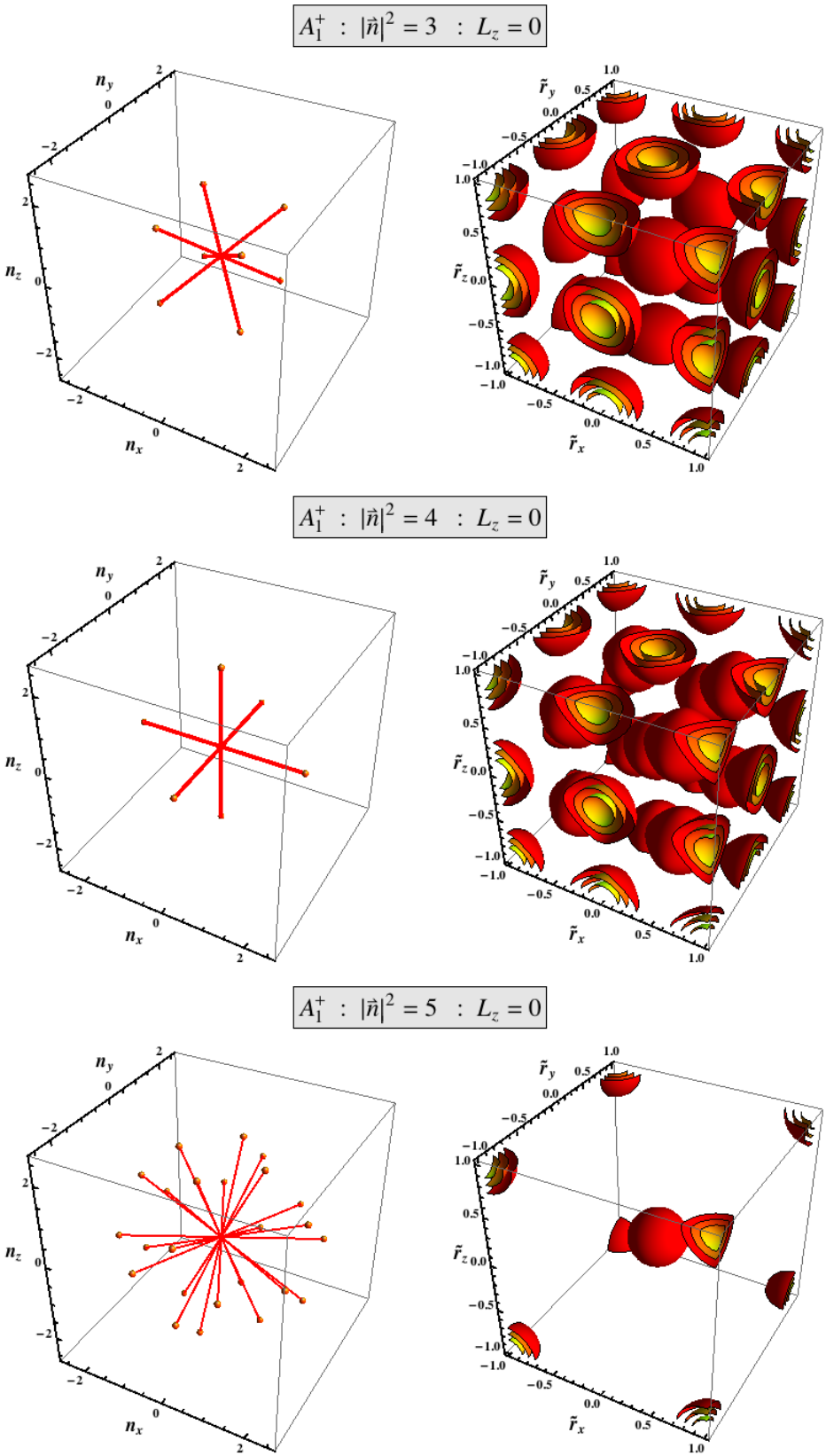

FIG. 3: The momentum-space representations (left) and position-space representations (right) of two-body relative states in the A_1^+ representation for select $|\mathbf{n}|^2$-shells.

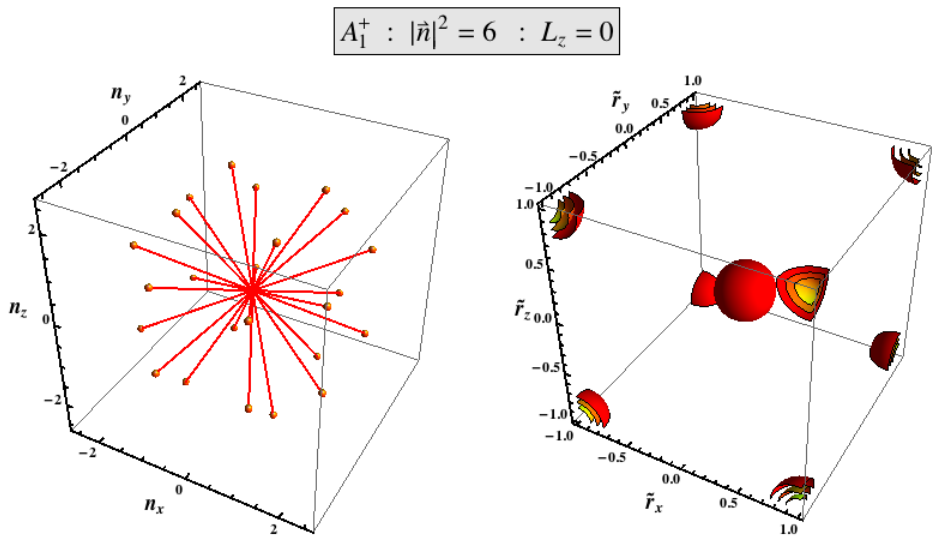

FIG. 4: The momentum-space representations (left) and position-space representations (right) of two-body relative states in the A_1^+ representation for $|\mathbf{n}|^2$=6 shell.

2. A_2^+ Representation

The other one-dimensional positive-parity irrep of the cubic group is the A_2^+. Due to its complexity, the lowest-lying state transforming as a A_2^+ is in the $|\mathbf{n}|^2 = 5$ shell, as indicated in table II. Further, the lowest partial-wave contributing to its energy is $l = 6$, and as this analysis is truncated to partial-waves with $l \leq 6$, the contribution to the determinant in eq. (2) has the solution

$$\begin{aligned} q^{13}\cot\delta_6 &= \left(\frac{2\pi}{L}\right)^{13} \frac{1}{\pi^{3/2}} \times \\ &\left(\tilde{q}^{12}\mathcal{Z}_{0,0}\left(1;\tilde{q}^2\right) + \frac{6\tilde{q}^8\mathcal{Z}_{4,0}\left(1;\tilde{q}^2\right)}{17} - \frac{160\sqrt{13}\tilde{q}^6\mathcal{Z}_{6,0}\left(1;\tilde{q}^2\right)}{323} - \frac{40\tilde{q}^4\mathcal{Z}_{8,0}\left(1;\tilde{q}^2\right)}{19\sqrt{17}}\right. \\ &\left. - \frac{2592\sqrt{21}\tilde{q}^2\mathcal{Z}_{10,0}\left(1;\tilde{q}^2\right)}{7429} + \frac{1980\mathcal{Z}_{12,0}\left(1;\tilde{q}^2\right)}{7429} + \frac{264\sqrt{1001}\mathcal{Z}_{12,4}\left(1;\tilde{q}^2\right)}{7429}\right) \\ &\equiv \left(\frac{2\pi}{L}\right)^{13} \frac{1}{\pi^{3/2}}\mathcal{X}_{A_2}^+\left(\tilde{q}^2\right) \ . \end{aligned} \tag{16}$$

and the associated eigenstate of the $\overline{F}_{6;6}^{(FV)}$ block is

$$|A_2^+, 2:6;1\rangle \ = \ \frac{1}{4}\sqrt{\frac{11}{2}}|6,2\rangle \ + \ \frac{1}{4}\sqrt{\frac{11}{2}}|6,-2\rangle \ - \ \frac{1}{4}\sqrt{\frac{5}{2}}|6,6\rangle \ - \ \frac{1}{4}\sqrt{\frac{5}{2}}|6,-6\rangle \quad . \tag{17}$$

The function $\mathcal{X}_{A_2}^+$ is shown in fig. 5 as a function of $\tilde{q}^2$. Its pole at $\tilde{q}^2$=5, denoted by the vertical dashed line, corresponds to the non-interacting ($\delta_6 = 0$) energy-eigenvalue. This is the only $|\mathbf{n}|^2$-shell with $|\mathbf{n}|^2 < 6$ which supports the A_2^+ irrep, as shown in table II. In fig. 6 we give the graphical representations of the source and sink that generates this irrep

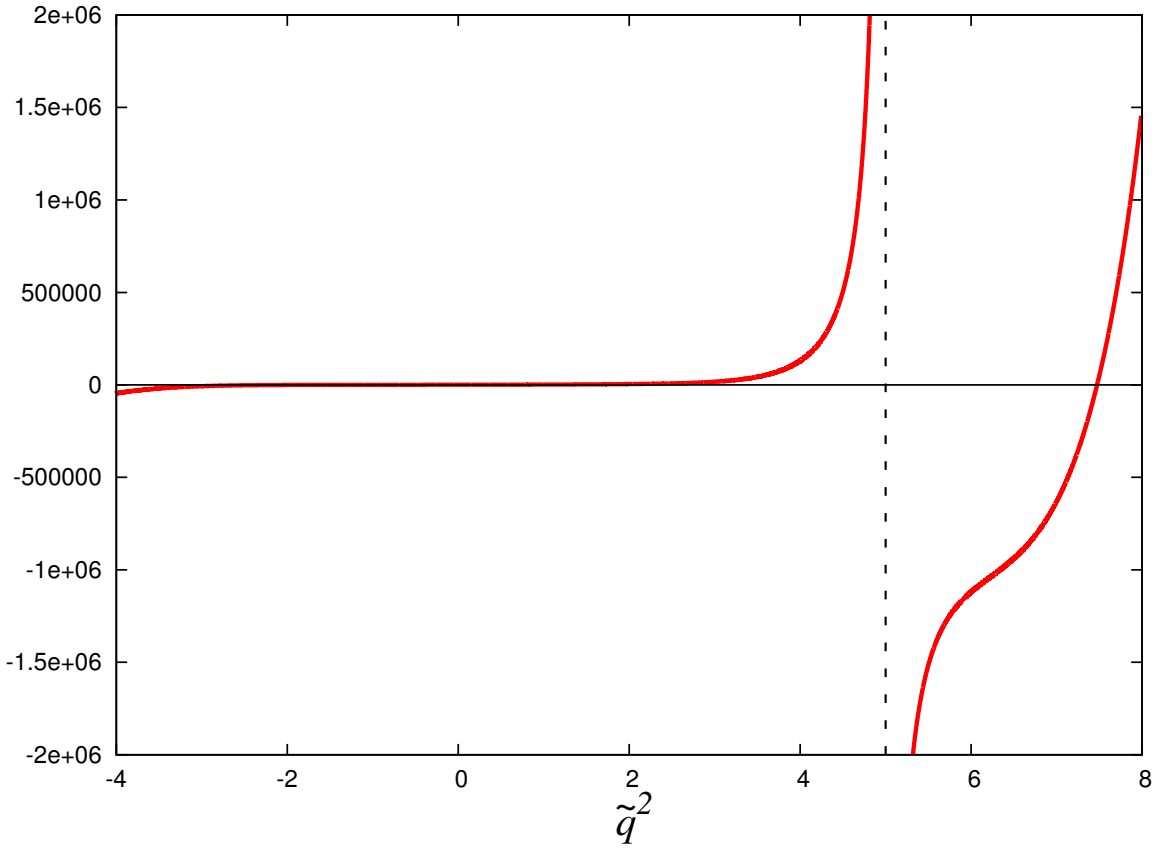

FIG. 5: The function $\mathcal{X}^{+}_{A_2}$, as defined in eq. (16), as a function of $\tilde{q}^2$. The vertical dashed line denotes the position of the pole of the function corresponding to the non-interacting energy-eigenvalues.

TABLE V: The momentum-space structure of the A_2^+ source and sink in the $|\mathbf{n}|^2 = 5$-shell. They are shown graphically in fig. 6.

$\lvert\mathbf{n}\rvert^2$=5			
$\lvert(2,1,0)\ ,\ +1\rangle$	$-\frac{1}{2\sqrt{3}}$	$\lvert(2,0,1)\ ,\ +1\rangle$	$\frac{1}{2\sqrt{3}}$
$\lvert(2,0,-1)\ ,\ +1\rangle$	$\frac{1}{2\sqrt{3}}$	$\lvert(2,-1,0)\ ,\ +1\rangle$	$-\frac{1}{2\sqrt{3}}$
$\lvert(1,2,0)\ ,\ +1\rangle$	$\frac{1}{2\sqrt{3}}$	$\lvert(1,0,2)\ ,\ +1\rangle$	$-\frac{1}{2\sqrt{3}}$
$\lvert(1,0,-2)\ ,\ +1\rangle$	$-\frac{1}{2\sqrt{3}}$	$\lvert(1,-2,0)\ ,\ +1\rangle$	$\frac{1}{2\sqrt{3}}$
$\lvert(0,2,1)\ ,\ +1\rangle$	$-\frac{1}{2\sqrt{3}}$	$\lvert(0,2,-1)\ ,\ +1\rangle$	$-\frac{1}{2\sqrt{3}}$
$\lvert(0,1,2)\ ,\ +1\rangle$	$\frac{1}{2\sqrt{3}}$	$\lvert(0,1,-2)\ ,\ +1\rangle$	$\frac{1}{2\sqrt{3}}$

in the $|\mathbf{n}|^2 = 5$-shell. As this is the lowest-lying state whose energy-eigenvalue is insensitive to $l < 6$ interactions, it is LQCD correlation functions constructed to transform in the A_2^+ irrep that will enable a calculation of δ_6. However, as the lowest energy contributing to an A_2^+ correlation function occurs in the $|\mathbf{n}^2| = 5$-shell, relatively large lattice volumes will be required in order to have this state lie below the inelastic threshold. The momentum-space structure of the source and sink that couple to the A_2^+ state in the $|\mathbf{n}|^2 = 5$-shell is given in

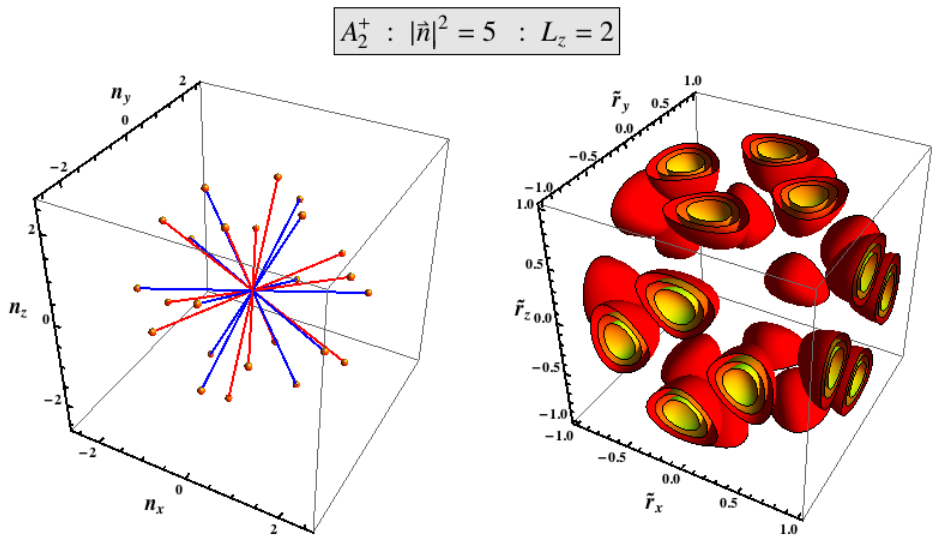

FIG. 6: The momentum-space representation (left) and position-space representation (right) of two-body relative states in the A_2^+ representation for the $|\mathbf{n}|^2 = 5$ shell.

table V.

3. E^+ Representation

The energy-eigenvalues of states transforming in the E^+ irrep receive contributions from interactions in the $l = 2, 4, 6, ...$ partial-waves. As the E^+ irrep is two-dimensional, the contribution to the determinant in eq. (2) results from a 6×6 matrix when $l \leq 6$. However, as the two states in the E^+ irrep (with $L_z = 0$ and $L_z = 2$) are degenerate, and orbital-angular momentum is conserved by the interactions (unlike the situation in the baryon-sector), the analysis can be reduced to that of a 3×3 matrix. The E^+ $L_z = 0$ states associated with the $\overline{F}^{(FV)}_{2;2}$, $\overline{F}^{(FV)}_{4;4}$, and $\overline{F}^{(FV)}_{6;6}$ blocks are

$$\begin{aligned}
|E^+, 0; 2; 1\rangle &= |2, 0\rangle \\
|E^+, 0; 4; 1\rangle &= \frac{1}{2}\sqrt{\frac{7}{6}}|4, 4\rangle \; - \; \frac{1}{2}\sqrt{\frac{5}{3}}|4, 0\rangle \; + \; \frac{1}{2}\sqrt{\frac{7}{6}}|4, -4\rangle \\
|E^+, 0; 6; 1\rangle &= \frac{1}{4}|6, 4\rangle \; + \; \frac{1}{2}\sqrt{\frac{7}{2}}|6, 0\rangle \; + \; \frac{1}{4}|6, -4\rangle \quad ,
\end{aligned} \tag{18}$$

and the contribution to eq. (2) becomes

$$\det\left[\begin{pmatrix} \cot\delta_2 & 0 & 0 \\ 0 & \cot\delta_4 & 0 \\ 0 & 0 & \cot\delta_6 \end{pmatrix} - \begin{pmatrix} \overline{F}^{(FV,E^+)}_{2;2} & \overline{F}^{(FV,E^+)}_{2;4} & \overline{F}^{(FV,E^+)}_{2;6} \\ \overline{F}^{(FV,E^+)}_{4;2} & \overline{F}^{(FV,E^+)}_{4;4} & \overline{F}^{(FV,E^+)}_{4;6} \\ \overline{F}^{(FV,E^+)}_{6;2} & \overline{F}^{(FV,E^+)}_{6;4} & \overline{F}^{(FV,E^+)}_{6;6} \end{pmatrix}\right] = 0 \; , \tag{19}$$

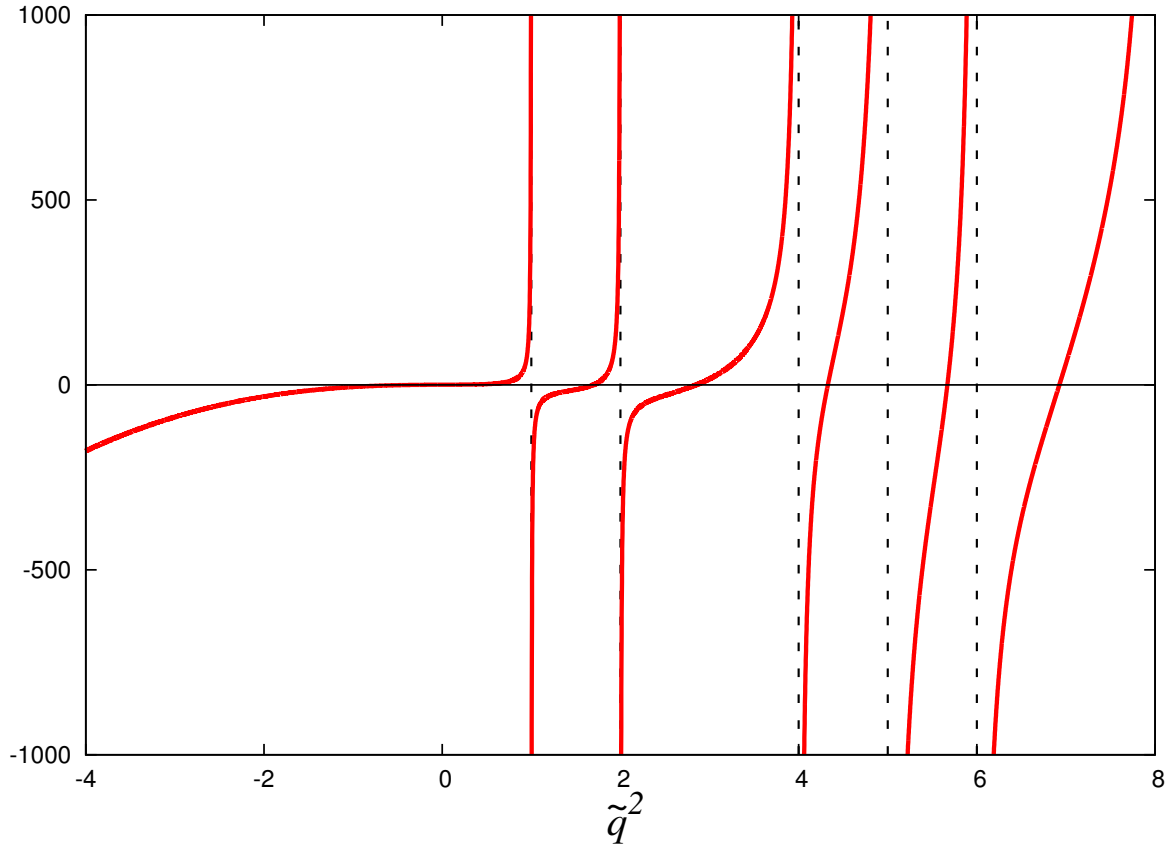

FIG. 7: The function $\mathcal{X}_E^+$, as defined in eq. (21), as a function of $\tilde{q}^2$. The vertical dashed lines denote the position of the poles in the function corresponding to the non-interacting energy-eigenvalues.

where

$$\overline{F}_{2;2}^{(FV,E^+)} = \frac{\mathcal{Z}_{0,0}\left(1;\tilde{q}^2\right)}{\pi^{3/2}\tilde{q}} + \frac{6\mathcal{Z}_{4,0}\left(1;\tilde{q}^2\right)}{7\pi^{3/2}\tilde{q}^5}$$

$$\overline{F}_{2;4}^{(FV,E^+)} = -\frac{30\sqrt{\frac{3}{13}}\mathcal{Z}_{6,0}\left(1;\tilde{q}^2\right)}{11\pi^{3/2}\tilde{q}^7} - \frac{40\sqrt{3}\mathcal{Z}_{4,0}\left(1;\tilde{q}^2\right)}{77\pi^{3/2}\tilde{q}^5}$$

$$\overline{F}_{2;6}^{(FV,E^+)} = \frac{8\sqrt{\frac{14}{1105}}\mathcal{Z}_{8,0}\left(1;\tilde{q}^2\right)}{\pi^{3/2}\tilde{q}^9} + \frac{4\sqrt{\frac{14}{5}}\mathcal{Z}_{6,0}\left(1;\tilde{q}^2\right)}{11\pi^{3/2}\tilde{q}^7} + \frac{30\sqrt{\frac{10}{91}}\mathcal{Z}_{4,0}\left(1;\tilde{q}^2\right)}{11\pi^{3/2}\tilde{q}^5}$$

$$\overline{F}_{4;4}^{(FV,E^+)} = \frac{\mathcal{Z}_{0,0}\left(1;\tilde{q}^2\right)}{\pi^{3/2}\tilde{q}} + \frac{392\mathcal{Z}_{8,0}\left(1;\tilde{q}^2\right)}{143\sqrt{17}\pi^{3/2}\tilde{q}^9} - \frac{64\mathcal{Z}_{6,0}\left(1;\tilde{q}^2\right)}{11\sqrt{13}\pi^{3/2}\tilde{q}^7} + \frac{108\mathcal{Z}_{4,0}\left(1;\tilde{q}^2\right)}{1001\pi^{3/2}\tilde{q}^5}$$

$$\overline{F}_{4;6}^{(FV,E^+)} = -\frac{1512\sqrt{\frac{2}{65}}\mathcal{Z}_{10,0}\left(1;\tilde{q}^2\right)}{323\pi^{3/2}\tilde{q}^{11}} - \frac{128\sqrt{\frac{210}{221}}\mathcal{Z}_{8,0}\left(1;\tilde{q}^2\right)}{209\pi^{3/2}\tilde{q}^9} - \frac{18\sqrt{210}\mathcal{Z}_{6,0}\left(1;\tilde{q}^2\right)}{187\pi^{3/2}\tilde{q}^7} - \frac{8\sqrt{\frac{30}{91}}\mathcal{Z}_{4,0}\left(1;\tilde{q}^2\right)}{11\pi^{3/2}\tilde{q}^5}$$

$$\overline{F}_{6;6}^{(FV,E^+)} = \frac{\mathcal{Z}_{0,0}\left(1;\tilde{q}^2\right)}{\pi^{3/2}\tilde{q}} + \frac{30492\mathcal{Z}_{12,0}\left(1;\tilde{q}^2\right)}{37145\pi^{3/2}\tilde{q}^{13}} + \frac{264\sqrt{1001}\mathcal{Z}_{12,4}\left(1;\tilde{q}^2\right)}{37145\pi^{3/2}\tilde{q}^{13}} + \frac{1152\sqrt{21}\mathcal{Z}_{10,0}\left(1;\tilde{q}^2\right)}{7429\pi^{3/2}\tilde{q}^{11}}$$
$$+ \frac{280\mathcal{Z}_{8,0}\left(1;\tilde{q}^2\right)}{209\sqrt{17}\pi^{3/2}\tilde{q}^9} + \frac{480\sqrt{13}\mathcal{Z}_{6,0}\left(1;\tilde{q}^2\right)}{3553\pi^{3/2}\tilde{q}^7} + \frac{114\mathcal{Z}_{4,0}\left(1;\tilde{q}^2\right)}{187\pi^{3/2}\tilde{q}^5} \quad .$$

TABLE VI: The momentum-space structure of E^+, $L_z = 0$ sources and sinks for $|\mathbf{n}|^2$=1,2, and 4.

$\|\mathbf{n}\|^2$=1		$\|\mathbf{n}\|^2$=2		$\|\mathbf{n}\|^2$=4	
$\|(1,1,0)\ ,+1\rangle$	$\frac{1}{\sqrt{3}}$				
$\|(1,0,1)\ ,+1\rangle$	$-\frac{1}{2\sqrt{3}}$				
$\|(1,0,-1)\ ,+1\rangle$	$-\frac{1}{2\sqrt{3}}$				
$\|(1,-1,0)\ ,+1\rangle$	$\frac{1}{\sqrt{3}}$				
$\|(0,1,1)\ ,+1\rangle$	$-\frac{1}{2\sqrt{3}}$				
$\|(0,1,-1)\ ,+1\rangle$	$-\frac{1}{2\sqrt{3}}$				
$\|(1,0,0)\ ,+1\rangle$	$\frac{1}{\sqrt{6}}$			$\|(2,0,0)\ ,+1\rangle$	$\frac{1}{\sqrt{6}}$
$\|(0,1,0)\ ,+1\rangle$	$\frac{1}{\sqrt{6}}$			$\|(0,2,0)\ ,+1\rangle$	$\frac{1}{\sqrt{6}}$
$\|(0,0,1)\ ,+1\rangle$	$-\sqrt{\frac{2}{3}}$			$\|(0,0,2)\ ,+1\rangle$	$-\sqrt{\frac{2}{3}}$

It is obvious that the solutions of eq. (19) depend upon the $l = 2$, 4, and 6 partial-waves in a non-trivial manner.

In the limit of vanishing interactions in partial-waves with $l > 4$, the contribution from the E^+ irrep to eq. (19) results from a 2×2 matrix, and has solutions

$$\frac{\cot\delta_2}{2} + \frac{\cot\delta_4}{2} - \frac{\mathcal{Z}_{0,0}\left(1;\tilde{q}^2\right)}{\pi^{3/2}q} - \frac{196\mathcal{Z}_{8,0}\left(1;\tilde{q}^2\right)}{143\sqrt{17}\pi^{3/2}\tilde{q}^9} + \frac{32\mathcal{Z}_{6,0}\left(1;\tilde{q}^2\right)}{11\sqrt{13}\pi^{3/2}\tilde{q}^7} - \frac{69\mathcal{Z}_{4,0}\left(1;\tilde{q}^2\right)}{143\pi^{3/2}\tilde{q}^5} =$$
$$\pm\frac{1}{2}\left[\left(\frac{392\mathcal{Z}_{8,0}\left(1;\tilde{q}^2\right)}{143\sqrt{17}\pi^{3/2}\tilde{q}^9} - \frac{64\mathcal{Z}_{6,0}\left(1;\tilde{q}^2\right)}{11\sqrt{13}\pi^{3/2}\tilde{q}^7} - \frac{750\mathcal{Z}_{4,0}\left(1;\tilde{q}^2\right)}{1001\pi^{3/2}\tilde{q}^5} + \cot\delta_2 - \cot\delta_4\right)^2\right.$$
$$\left. +4\left(\frac{30\sqrt{\frac{3}{13}}\mathcal{Z}_{6,0}\left(1;\tilde{q}^2\right)}{11\pi^{3/2}\tilde{q}^7} + \frac{40\sqrt{3}\mathcal{Z}_{4,0}\left(1;\tilde{q}^2\right)}{77\pi^{3/2}\tilde{q}^5}\right)^2\right]^{1/2} . \quad (20)$$

In the limit that $\tan\delta_4 << \tan\delta_2$, the $l = 2$ dominated solutions to eq. (20) result from

$$q^5\cot\delta_2 = \left(\frac{2\pi}{L}\right)^5 \frac{1}{\pi^{3/2}}\left(\tilde{q}^4\mathcal{Z}_{0,0}\left(1;\tilde{q}^2\right) + \frac{6}{7}\mathcal{Z}_{4,0}\left(1;\tilde{q}^2\right)\right) = \left(\frac{2\pi}{L}\right)^5 \frac{1}{\pi^{3/2}}\mathcal{X}_E^+\left(\tilde{q}^2\right) , \quad (21)$$

where function $\mathcal{X}_E^+$ is shown in fig. 7 as a function $\tilde{q}^2$ [6]. The graphical representations of the sources and sinks that generate this irrep for $|\mathbf{n}|^2 \leq 6$-shell are shown in figs. 8 and 9 in the case of $L_z = 0$, and the momentum-space structures are given explicitly in table VI and table VIII.

There are two occurrences of the E^+ irrep in the $|\mathbf{n}|^2 = 5$-shell. Linear combinations of the basis states can be formed: one that is dominated by δ_2, and one that is dominated by δ_4 in the infinite-volume limit, as shown in table VI and table VIII. The states are defined by $\langle l, m||\mathbf{n}|^2_l;\Gamma^{(i)}, L_z\rangle = \langle 2, 0|5_4; E^+, 0\rangle = 0$, and the orthogonal combination $|5_2; E^+, 0\rangle$. As is the case in the A_1^+ sector, these states are not energy-eigenstates since they have a non-zero projection, in principle, onto all E^+ states. The perturbative expansions of the energy-eigenvalues in the large-volume limit can be found in Appendix C.

[6] This expression has been derived previously by R. Briceno [19].

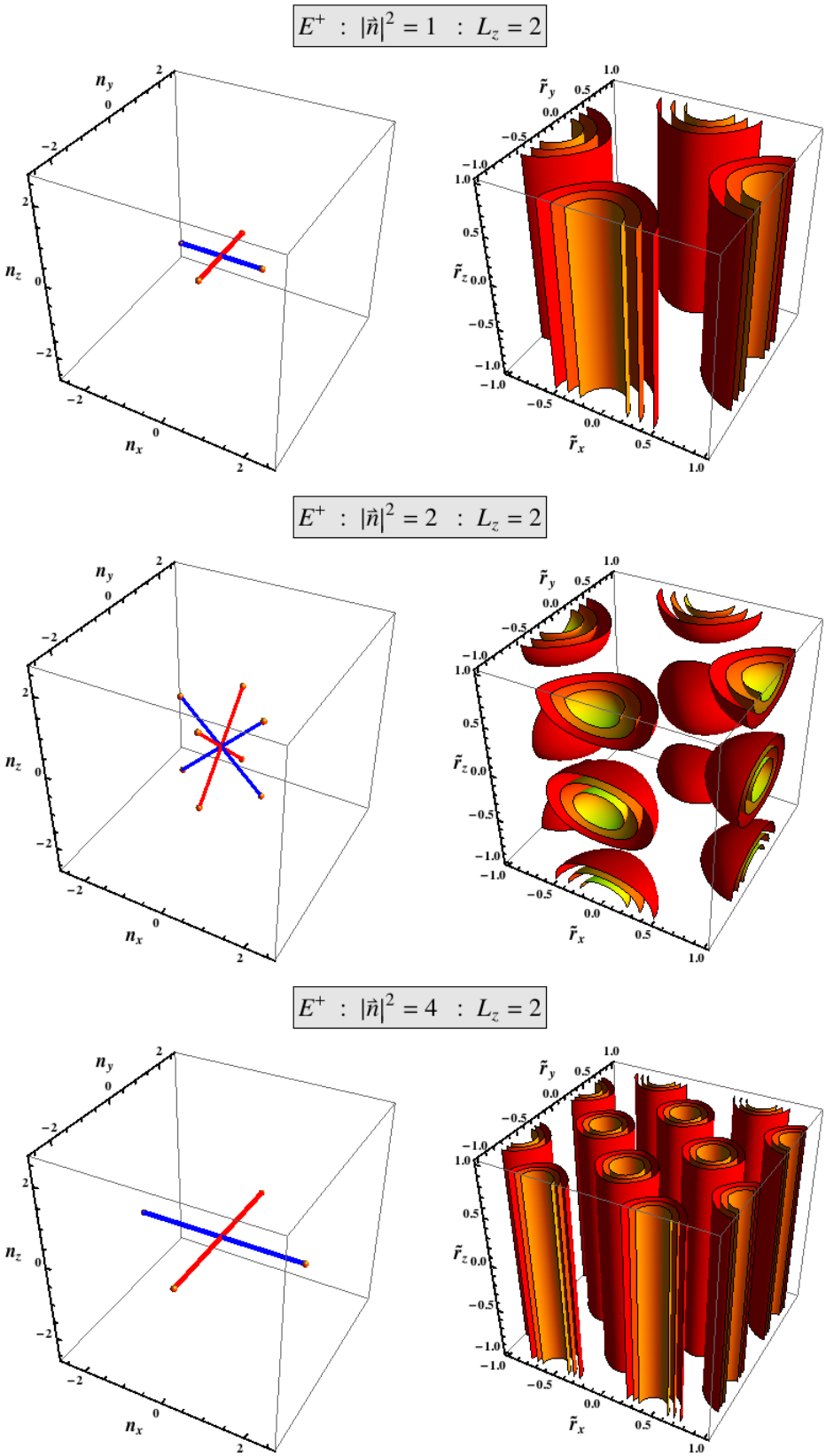

FIG. 8: The momentum-space representations (left) and position-space representations (right) of two-body relative states in the E^+ representation with $L_z = 2$ in the $|\mathbf{n}|^2$=1, 2, and 4 shells.

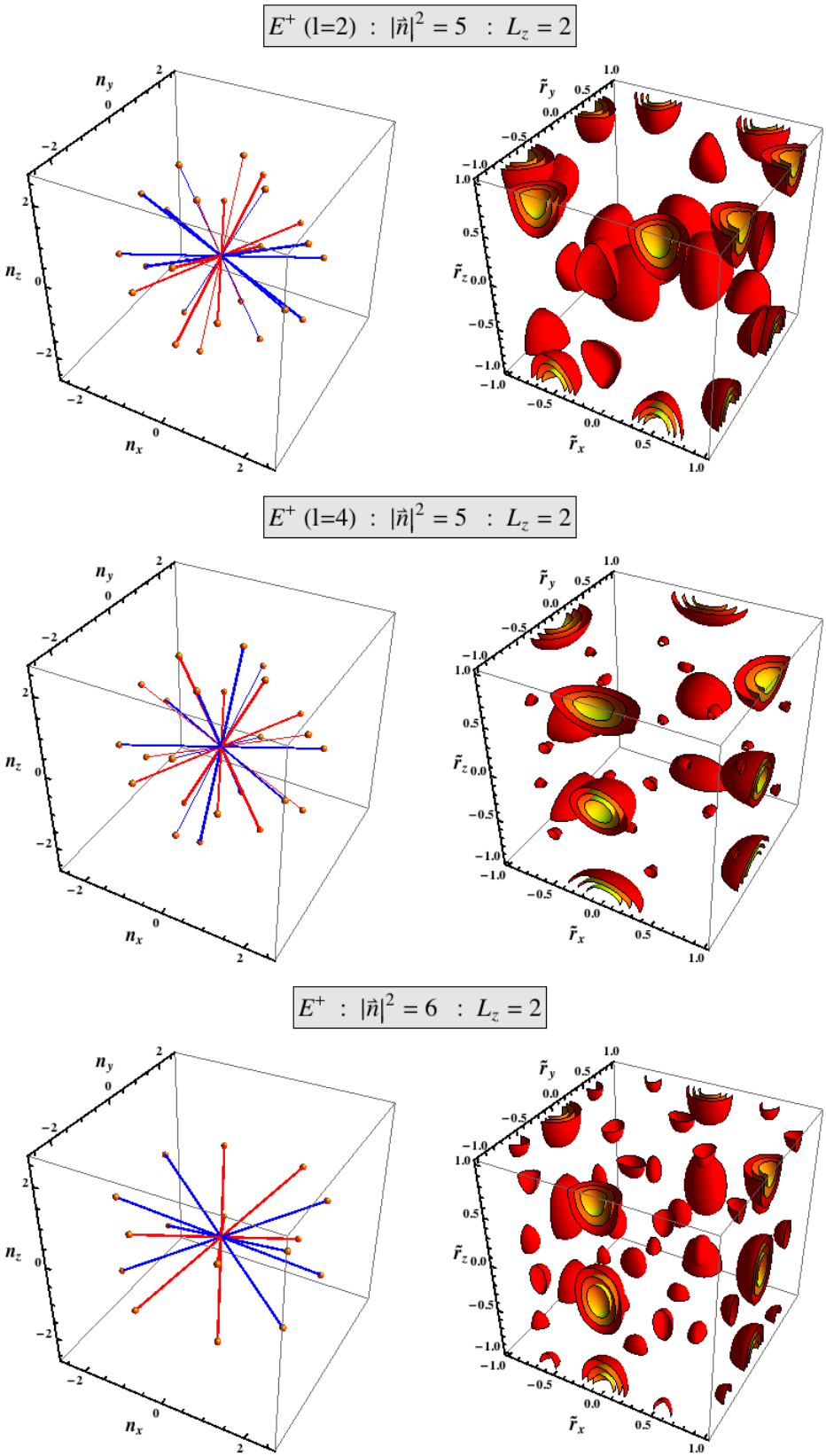

FIG. 9: The momentum-space representations (left) and position-space representations (right) of two-body relative states in the E^+ representation with $L_z = 2$ in the $|\mathbf{n}|^2$=5 and 6 shells.

TABLE VII: The momentum-space structure of E^+, $L_z = 0$ sources and sinks for $|\mathbf{n}|^2$=5 and 6.

$\|\mathbf{n}\|^2$=5$_{(l=2)}$		$\|\mathbf{n}\|^2$=5$_{(l=4)}$		$\|\mathbf{n}\|^2$=6	
$\|$(2,1,0) , +1$\rangle$	$\frac{5}{2\sqrt{78}}$	$\|$(2,1,0) , +1$\rangle$	$\frac{3}{2\sqrt{26}}$	$\|$(2,1,1) , +1$\rangle$	$-\frac{1}{2\sqrt{6}}$
$\|$(2,0,1) , +1$\rangle$	$\frac{1}{\sqrt{78}}$	$\|$(2,0,1) , +1$\rangle$	$-\sqrt{\frac{2}{13}}$	$\|$(2,1,-1) , +1$\rangle$	$-\frac{1}{2\sqrt{6}}$
$\|$(2,0,-1) , +1$\rangle$	$\frac{1}{\sqrt{78}}$	$\|$(2,0,-1) , +1$\rangle$	$-\sqrt{\frac{2}{13}}$	$\|$(2,-1,1) , +1$\rangle$	$-\frac{1}{2\sqrt{6}}$
$\|$(2,-1,0) , +1$\rangle$	$\frac{5}{2\sqrt{78}}$	$\|$(2,-1,0) , +1$\rangle$	$\frac{3}{2\sqrt{26}}$	$\|$(2,-1,-1) , +1$\rangle$	$-\frac{1}{2\sqrt{6}}$
$\|$(1,2,0) , +1$\rangle$	$\frac{5}{2\sqrt{78}}$	$\|$(1,2,0) , +1$\rangle$	$\frac{3}{2\sqrt{26}}$	$\|$(1,2,1) , +1$\rangle$	$-\frac{1}{2\sqrt{6}}$
$\|$(1,0,2) , +1$\rangle$	$-\frac{7}{2\sqrt{78}}$	$\|$(1,0,2) , +1$\rangle$	$\frac{1}{2\sqrt{26}}$	$\|$(1,2,-1) , +1$\rangle$	$-\frac{1}{2\sqrt{6}}$
$\|$(1,0,-2) , +1$\rangle$	$-\frac{7}{2\sqrt{78}}$	$\|$(1,0,-2) , +1$\rangle$	$\frac{1}{2\sqrt{26}}$	$\|$(1,1,2) , +1$\rangle$	$\frac{1}{\sqrt{6}}$
$\|$(1,-2,0) , +1$\rangle$	$\frac{5}{2\sqrt{78}}$	$\|$(1,-2,0) , +1$\rangle$	$\frac{3}{2\sqrt{26}}$	$\|$(1,1,-2) , +1$\rangle$	$\frac{1}{\sqrt{6}}$
$\|$(0,2,1) , +1$\rangle$	$\frac{1}{\sqrt{78}}$	$\|$(0,2,1) , +1$\rangle$	$-\sqrt{\frac{2}{13}}$	$\|$(1,-1,2) , +1$\rangle$	$\frac{1}{\sqrt{6}}$
$\|$(0,2,-1) , +1$\rangle$	$\frac{1}{\sqrt{78}}$	$\|$(0,2,-1) , +1$\rangle$	$-\sqrt{\frac{2}{13}}$	$\|$(1,-1,-2) , +1$\rangle$	$\frac{1}{\sqrt{6}}$
$\|$(0,1,2) , +1$\rangle$	$-\frac{7}{2\sqrt{78}}$	$\|$(0,1,2) , +1$\rangle$	$\frac{1}{2\sqrt{26}}$	$\|$(1,-2,1) , +1$\rangle$	$-\frac{1}{2\sqrt{6}}$
$\|$(0,1,-2) , +1$\rangle$	$-\frac{7}{2\sqrt{78}}$	$\|$(0,1,-2) , +1$\rangle$	$\frac{1}{2\sqrt{26}}$	$\|$(1,-2,-1) , +1$\rangle$	$-\frac{1}{2\sqrt{6}}$

TABLE VIII: The momentum-space structure of E^+, $L_z = 2$ sources and sinks for $|\mathbf{n}|^2$=1, 2, and 4. These are shown graphically in fig. 8.

$\|\mathbf{n}\|^2$=1		$\|\mathbf{n}\|^2$=2		$\|\mathbf{n}\|^2$=4	
		$\|$(1,0,1) , +1$\rangle$	$-\frac{1}{2}$		
$\|$(1,0,0) , +1$\rangle$	$-\frac{1}{\sqrt{2}}$	$\|$(1,0,-1) , +1$\rangle$	$-\frac{1}{2}$	$\|$(2,0,0) , +1$\rangle$	$-\frac{1}{\sqrt{2}}$
$\|$(0,1,0) , +1$\rangle$	$\frac{1}{\sqrt{2}}$	$\|$(0,1,1) , +1$\rangle$	$\frac{1}{2}$	$\|$(0,2,0) , +1$\rangle$	$\frac{1}{\sqrt{2}}$
		$\|$(0,1,-1) , +1$\rangle$	$\frac{1}{2}$		

4. T_1^+ Representation

The energy-eigenvalues of states transforming in the T_1^+ irrep receive contributions from interactions in the $l = 4, 6, ...$ partial-waves. The T_1^+ irrep is three-dimensional, with states identified by $L_z = 0, 1, 3$, and provides a contribution to the determinant in eq. (2) that results from a 6×6 matrix for $l \leq 6$. As the three L_z-states are degenerate, the analysis collapses down to that of a 2×2 matrix. The T_1^+ $L_z = 0$ states associated with the $\overline{F}^{(FV)}_{4;4}$ and $\overline{F}^{(FV)}_{6;6}$ blocks are

$$\begin{aligned} |T_1^+, 0; 4; 1\rangle &= \frac{1}{\sqrt{2}}|4, 4\rangle - \frac{1}{\sqrt{2}}|4, -4\rangle \\ |T_1^+, 0; 6; 1\rangle &= \frac{1}{\sqrt{2}}|6, 4\rangle - \frac{1}{\sqrt{2}}|6, -4\rangle \quad , \end{aligned} \tag{22}$$

TABLE IX: The momentum-space structure of E^+, $L_z = 2$ sources and sinks for $|\mathbf{n}|^2$=5 and 6. These are shown graphically in fig. 9.

$\|\mathbf{n}\|^2$=5$_{(l=2)}$		$\|\mathbf{n}\|^2$=5$_{(l=4)}$		$\|\mathbf{n}\|^2$=6	
$\|(2,1,0)\ ,+1\rangle$	$-\frac{3}{2\sqrt{26}}$	$\|(2,1,0)\ ,+1\rangle$	$-\frac{5}{2\sqrt{78}}$		
$\|(2,0,1)\ ,+1\rangle$	$-\sqrt{\frac{2}{13}}$	$\|(2,0,1)\ ,+1\rangle$	$\frac{1}{\sqrt{78}}$		
$\|(2,0,-1)\ ,+1\rangle$	$-\sqrt{\frac{2}{13}}$	$\|(2,0,-1)\ ,+1\rangle$	$\frac{1}{\sqrt{78}}$	$\|(2,1,1)\ ,+1\rangle$	$-\frac{1}{2\sqrt{2}}$
$\|(2,-1,0)\ ,+1\rangle$	$-\frac{3}{2\sqrt{26}}$	$\|(2,-1,0)\ ,+1\rangle$	$-\frac{5}{2\sqrt{78}}$	$\|(2,1,-1)\ ,+1\rangle$	$-\frac{1}{2\sqrt{2}}$
$\|(1,2,0)\ ,+1\rangle$	$\frac{3}{2\sqrt{26}}$	$\|(1,2,0)\ ,+1\rangle$	$\frac{5}{2\sqrt{78}}$	$\|(2,-1,1)\ ,+1\rangle$	$-\frac{1}{2\sqrt{2}}$
$\|(1,0,2)\ ,+1\rangle$	$-\frac{1}{2\sqrt{26}}$	$\|(1,0,2)\ ,+1\rangle$	$\frac{7}{2\sqrt{78}}$	$\|(2,-1,-1)\ ,+1\rangle$	$-\frac{1}{2\sqrt{2}}$
$\|(1,0,-2)\ ,+1\rangle$	$-\frac{1}{2\sqrt{26}}$	$\|(1,0,-2)\ ,+1\rangle$	$\frac{7}{2\sqrt{78}}$	$\|(1,2,1)\ ,+1\rangle$	$\frac{1}{2\sqrt{2}}$
$\|(1,-2,0)\ ,+1\rangle$	$\frac{3}{2\sqrt{26}}$	$\|(1,-2,0)\ ,+1\rangle$	$\frac{5}{2\sqrt{78}}$	$\|(1,2,-1)\ ,+1\rangle$	$\frac{1}{2\sqrt{2}}$
$\|(0,2,1)\ ,+1\rangle$	$\sqrt{\frac{2}{13}}$	$\|(0,2,1)\ ,+1\rangle$	$-\frac{1}{\sqrt{78}}$	$\|(1,-2,1)\ ,+1\rangle$	$\frac{1}{2\sqrt{2}}$
$\|(0,2,-1)\ ,+1\rangle$	$\sqrt{\frac{2}{13}}$	$\|(0,2,-1)\ ,+1\rangle$	$-\frac{1}{\sqrt{78}}$	$\|(1,-2,-1)\ ,+1\rangle$	$\frac{1}{2\sqrt{2}}$
$\|(0,1,2)\ ,+1\rangle$	$\frac{1}{2\sqrt{26}}$	$\|(0,1,2)\ ,+1\rangle$	$-\frac{7}{2\sqrt{78}}$		
$\|(0,1,-2)\ ,+1\rangle$	$\frac{1}{2\sqrt{26}}$	$\|(0,1,-2)\ ,+1\rangle$	$-\frac{7}{2\sqrt{78}}$		

and the contribution to eq. (2) is

$$\det\left[\begin{pmatrix}\cot\delta_4 & 0\\ 0 & \cot\delta_6\end{pmatrix} - \begin{pmatrix}\overline{F}^{(FV,T_1^+)}_{4;4} & \overline{F}^{(FV,T_1^+)}_{4;6}\\ \overline{F}^{(FV,T_1^+)}_{6;2} & \overline{F}^{(FV,T_1^+)}_{6;6}\end{pmatrix}\right] = 0 \quad , \tag{23}$$

where

$$\overline{F}^{(FV,T_1^+)}_{4;4} = \frac{\mathcal{Z}_{0,0}\left(1;\tilde{q}^2\right)}{\pi^{3/2}\tilde{q}} - \frac{448\mathcal{Z}_{8,0}\left(1;\tilde{q}^2\right)}{143\sqrt{17}\pi^{3/2}\tilde{q}^9} - \frac{4\mathcal{Z}_{6,0}\left(1;\tilde{q}^2\right)}{11\sqrt{13}\pi^{3/2}\tilde{q}^7} + \frac{54\mathcal{Z}_{4,0}\left(1;\tilde{q}^2\right)}{143\pi^{3/2}\tilde{q}^5}$$

$$\overline{F}^{(FV,T_1^+)}_{4;6} = \frac{576\sqrt{\frac{21}{65}}\mathcal{Z}_{10,0}\left(1;\tilde{q}^2\right)}{323\pi^{3/2}\tilde{q}^{11}} + \frac{112\sqrt{\frac{5}{221}}\mathcal{Z}_{8,0}\left(1;\tilde{q}^2\right)}{209\pi^{3/2}\tilde{q}^9} + \frac{42\sqrt{5}\mathcal{Z}_{6,0}\left(1;\tilde{q}^2\right)}{187\pi^{3/2}\tilde{q}^7} - \frac{12\sqrt{\frac{5}{13}}\mathcal{Z}_{4,0}\left(1;\tilde{q}^2\right)}{11\pi^{3/2}\tilde{q}^5}$$

$$\overline{F}^{(FV,T_1^+)}_{6;6} = \frac{\mathcal{Z}_{0,0}\left(1;\tilde{q}^2\right)}{\pi^{3/2}\tilde{q}} - \frac{26136\mathcal{Z}_{12,0}\left(1;\tilde{q}^2\right)}{37145\pi^{3/2}\tilde{q}^{13}} + \frac{1584\sqrt{1001}\mathcal{Z}_{12,4}\left(1;\tilde{q}^2\right)}{37145\pi^{3/2}\tilde{q}^{13}} + \frac{624\sqrt{21}\mathcal{Z}_{10,0}\left(1;\tilde{q}^2\right)}{7429\pi^{3/2}\tilde{q}^{11}}$$
$$+ \frac{120\mathcal{Z}_{8,0}\left(1;\tilde{q}^2\right)}{209\sqrt{17}\pi^{3/2}\tilde{q}^9} - \frac{80\sqrt{13}\mathcal{Z}_{6,0}\left(1;\tilde{q}^2\right)}{3553\pi^{3/2}\tilde{q}^7} - \frac{96\mathcal{Z}_{4,0}\left(1;\tilde{q}^2\right)}{187\pi^{3/2}\tilde{q}^5} \quad .$$

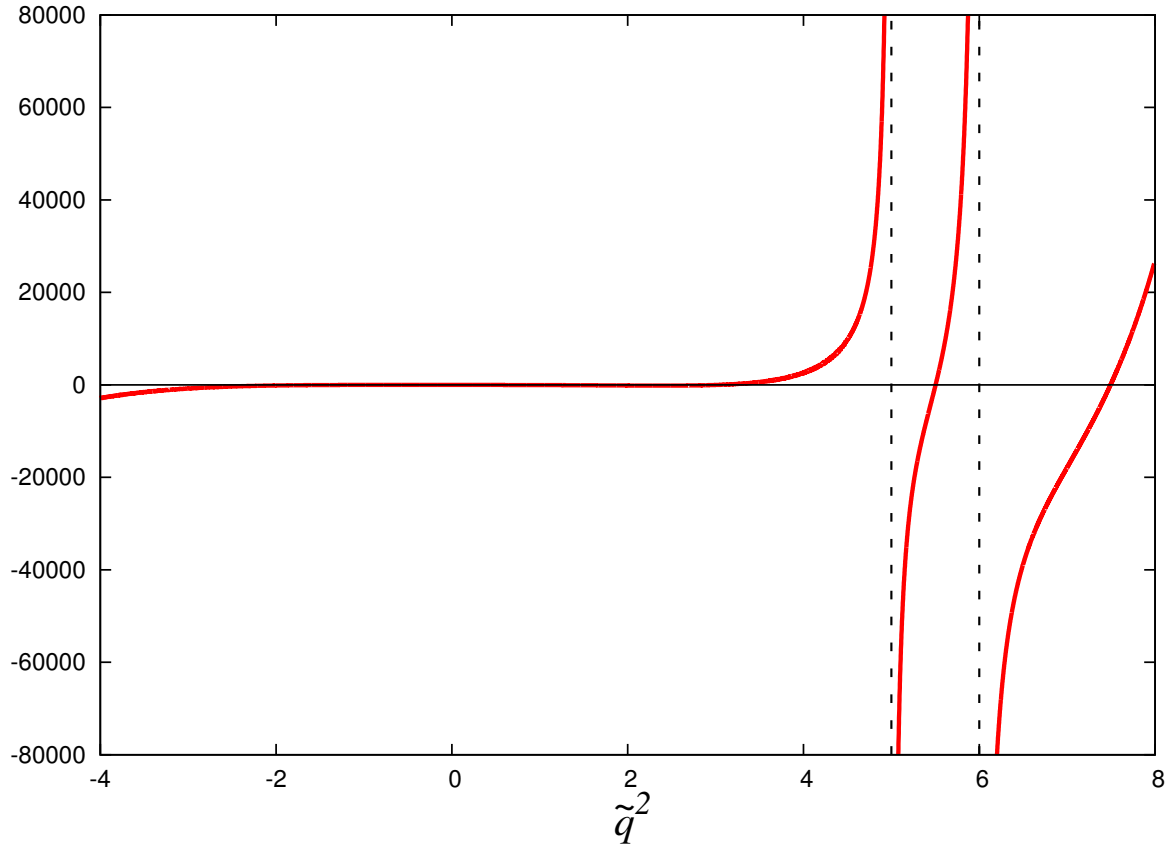

FIG. 10: The function $\mathcal{X}^{+}_{T_1}$, as defined in eq. (25), as a function of $\tilde{q}^2$. The vertical dashed lines denote the position of the poles of the function corresponding to the non-interacting energy-eigenvalues.

The solutions to eq. (23) are obtained from

$$\begin{aligned}
&\frac{\cot\delta_4}{2}+\frac{\cot\delta_6}{2}-\frac{312\sqrt{21}\mathcal{Z}_{10,0}\left(1;\tilde{q}^2\right)}{7429\pi^{3/2}\tilde{q}^{11}}+\frac{13068\mathcal{Z}_{12,0}\left(1;\tilde{q}^2\right)}{37145\pi^{3/2}\tilde{q}^{13}}-\frac{792\sqrt{1001}\mathcal{Z}_{12,4}\left(1;\tilde{q}^2\right)}{37145\pi^{3/2}\tilde{q}^{13}}\\
&\qquad-\frac{\mathcal{Z}_{0,0}\left(1;\tilde{q}^2\right)}{\pi^{3/2}\tilde{q}}+\frac{15\mathcal{Z}_{4,0}\left(1;\tilde{q}^2\right)}{221\pi^{3/2}\tilde{q}^{5}}+\frac{106\mathcal{Z}_{6,0}\left(1;\tilde{q}^2\right)}{323\sqrt{13}\pi^{3/2}\tilde{q}^{7}}+\frac{316\mathcal{Z}_{8,0}\left(1;\tilde{q}^2\right)}{247\sqrt{17}\pi^{3/2}\tilde{q}^{9}}=\\
&\pm\frac{1}{2}\left[\left(\frac{624\sqrt{21}\mathcal{Z}_{10,0}\left(1;\tilde{q}^2\right)}{7429\pi^{3/2}\tilde{q}^{11}}-\frac{26136\mathcal{Z}_{12,0}\left(1;\tilde{q}^2\right)}{37145\pi^{3/2}\tilde{q}^{13}}+\frac{1584\sqrt{1001}\mathcal{Z}_{12,4}\left(1;\tilde{q}^2\right)}{37145\pi^{3/2}\tilde{q}^{13}}-\frac{2166\mathcal{Z}_{4,0}\left(1;\tilde{q}^2\right)}{2431\pi^{3/2}\tilde{q}^{5}}\right.\right.\\
&\qquad\left.+\frac{252\mathcal{Z}_{6,0}\left(1;\tilde{q}^2\right)}{3553\sqrt{13}\pi^{3/2}\tilde{q}^{7}}+\frac{10072\mathcal{Z}_{8,0}\left(1;\tilde{q}^2\right)}{2717\sqrt{17}\pi^{3/2}\tilde{q}^{9}}+\cot\delta_4-\cot\delta_6\right)^2\\
&+\frac{4}{\pi^3}\left.\left(\frac{576\sqrt{\frac{21}{65}}\mathcal{Z}_{10,0}\left(1;\tilde{q}^2\right)}{323\tilde{q}^{11}}-\frac{12\sqrt{\frac{5}{13}}\mathcal{Z}_{4,0}\left(1;\tilde{q}^2\right)}{11\tilde{q}^{5}}+\frac{42\sqrt{5}\mathcal{Z}_{6,0}\left(1;\tilde{q}^2\right)}{187\tilde{q}^{7}}+\frac{112\sqrt{\frac{5}{221}}\mathcal{Z}_{8,0}\left(1;\tilde{q}^2\right)}{209\tilde{q}^{9}}\right)^2\right]^{1/2}.
\end{aligned}\tag{24}$$

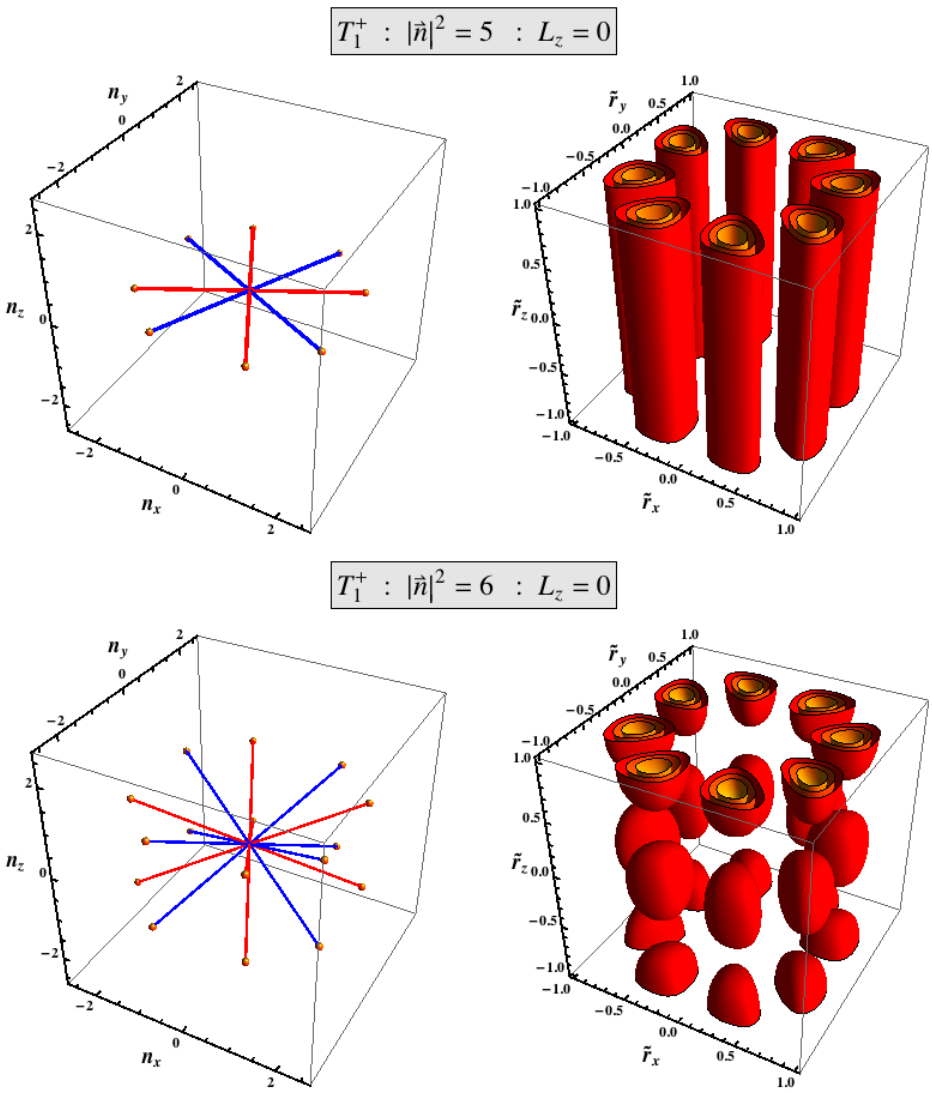

FIG. 11: The momentum-space representations (left) and position-space representations (right) of two-body relative states in the T_1^+ representation with $L_z = 0$ in the $|\mathbf{n}|^2$=5 and 6 shells.

In the situation where the interaction in the $l = 6$ (and higher) partial-wave vanishes, the energy-eigenvalues are sensitive to the $l = 4$ interaction alone, and can be found from

$$\begin{aligned} q^9 \cot\delta_4 &= \left(\frac{2\pi}{L}\right)^9 \frac{1}{\pi^{3/2}} \left(\tilde{q}^8 \mathcal{Z}_{0,0}\left(1;\tilde{q}^2\right) - \frac{448\mathcal{Z}_{8,0}\left(1;\tilde{q}^2\right)}{143\sqrt{17}} - \frac{4\tilde{q}^2\mathcal{Z}_{6,0}\left(1;\tilde{q}^2\right)}{11\sqrt{13}} + \frac{54\tilde{q}^4\mathcal{Z}_{4,0}\left(1;\tilde{q}^2\right)}{143}\right) \\ &\equiv \left(\frac{2\pi}{L}\right)^9 \frac{1}{\pi^{3/2}} \mathcal{X}_{T_1}^+\left(\tilde{q}^2\right) \quad , \end{aligned} \tag{25}$$

where the function $\mathcal{X}_{T_1}^+\left(\tilde{q}^2\right)$ is shown in fig. 10.

The graphical representations of the sources and sinks that generate the T_1^+ irrep for the low-lying $|\mathbf{n}|^2$-shells are shown in fig. 11, and the momentum-space structures for $L_z = 0$ are given explicitly in table X, and for $L_z = 1$ in table XI. The structures of the $L_z = 3$ sources and sinks are related to those with $L_z = 1$ by complex conjugation of the coefficients.

TABLE X: The momentum-space structure of T_1^+, $L_z = 0$ sources and sinks. These are shown graphically in fig. 11.

$\|\mathbf{n}\|^2$=5		$\|\mathbf{n}\|^2$=6			
$\|$(2,1,0) , +1$\rangle$	$\frac{1}{2}$	$\|$(2,1,1) , +1$\rangle$	$\frac{1}{2\sqrt{2}}$	$\|$(2,1,-1) , +1$\rangle$	$\frac{1}{2\sqrt{2}}$
$\|$(2,-1,0) , +1$\rangle$	$-\frac{1}{2}$	$\|$(2,-1,1) , +1$\rangle$	$-\frac{1}{2\sqrt{2}}$	$\|$(2,-1,-1) , +1$\rangle$	$-\frac{1}{2\sqrt{2}}$
$\|$(1,2,0) , +1$\rangle$	$-\frac{1}{2}$	$\|$(1,2,1) , +1$\rangle$	$-\frac{1}{2\sqrt{2}}$	$\|$(1,2,-1) , +1$\rangle$	$-\frac{1}{2\sqrt{2}}$
$\|$(1,-2,0) , +1$\rangle$	$\frac{1}{2}$	$\|$(1,-2,1) , +1$\rangle$	$\frac{1}{2\sqrt{2}}$	$\|$(1,-2,-1) , +1$\rangle$	$\frac{1}{2\sqrt{2}}$

TABLE XI: The momentum-space structure of T_1^+, $L_z = 1$ sources and sinks.

$\|\mathbf{n}\|^2$=5				$\|\mathbf{n}\|^2$=6			
				$\|$(2,1,1) , +1$\rangle$	$\frac{1}{4}$	$\|$(2,1,-1) , +1$\rangle$	$-\frac{1}{4}$
$\|$(2,0,1) , +1$\rangle$	$\frac{1}{2\sqrt{2}}$	$\|$(2,0,-1) , +1$\rangle$	$-\frac{1}{2\sqrt{2}}$	$\|$(2,-1,1) , +1$\rangle$	$\frac{1}{4}$	$\|$(2,-1,-1) , +1$\rangle$	$-\frac{1}{4}$
$\|$(1,0,2) , +1$\rangle$	$-\frac{1}{2\sqrt{2}}$	$\|$(1,0,-2) , +1$\rangle$	$\frac{1}{2\sqrt{2}}$	$\|$(1,2,1) , +1$\rangle$	$\frac{i}{4}$	$\|$(1,2,-1) , +1$\rangle$	$-\frac{i}{4}$
$\|$(0,2,1) , +1$\rangle$	$\frac{i}{2\sqrt{2}}$	$\|$(0,2,-1) , +1$\rangle$	$-\frac{i}{2\sqrt{2}}$	$\|$(1,1,2) , +1$\rangle$	$-\frac{1}{4}-\frac{i}{4}$	$\|$(1,1,-2) , +1$\rangle$	$\frac{1}{4}+\frac{i}{4}$
$\|$(0,1,2) , +1$\rangle$	$-\frac{i}{2\sqrt{2}}$	$\|$(0,1,-2) , +1$\rangle$	$\frac{i}{2\sqrt{2}}$	$\|$(1,-1,2) , +1$\rangle$	$-\frac{1}{4}+\frac{i}{4}$	$\|$(1,-1,-2) , +1$\rangle$	$\frac{1}{4}-\frac{i}{4}$
				$\|$(1,-2,1) , +1$\rangle$	$-\frac{i}{4}$	$\|$(1,-2,-1) , +1$\rangle$	$\frac{i}{4}$

5. T_2^+ *Representation*

The energy-eigenvalues of states transforming in the T_2^+ irrep receive contributions from interactions in the $l = 2, 4, 6, ...$ partial-waves. The T_2^+ irrep is three-dimensional, with states defined by $L_z = 1, 2, 3$, and provides a contribution to the determinant in eq. (2) that results from a 12×12 matrix for $l \leq 6$ (it is 12×12 and not 9×9 because there are two T_2^+'s in the decomposition of $l = 6$, see table I). As the three L_z-states are degenerate, the analysis collapses down to that of a 4×4 matrix. The T_2^+ $L_z = 2$ states associated with the $\overline{F}^{(FV)}_{2;2}$, $\overline{F}^{(FV)}_{4;4}$, and $\overline{F}^{(FV)}_{6,6}$ blocks are

$$
\begin{aligned}
|T_2^+, 2; 2; 1\rangle &= \frac{1}{\sqrt{2}}\left(|2,2\rangle \;-\; |2,-2\rangle\right) \\
|T_2^+, 2; 4; 1\rangle &= \frac{1}{\sqrt{2}}\left(|4,2\rangle \;-\; |4,-2\rangle\right) \\
|T_2^+, 2; 6; 1\rangle &= \frac{1}{\sqrt{2}}\left(|6,2\rangle \;-\; |6,-2\rangle\right) \\
|T_2^+, 2; 6; 2\rangle &= \frac{1}{\sqrt{2}}\left(|6,6\rangle \;-\; |6,-6\rangle\right)
\end{aligned}
\tag{26}
$$

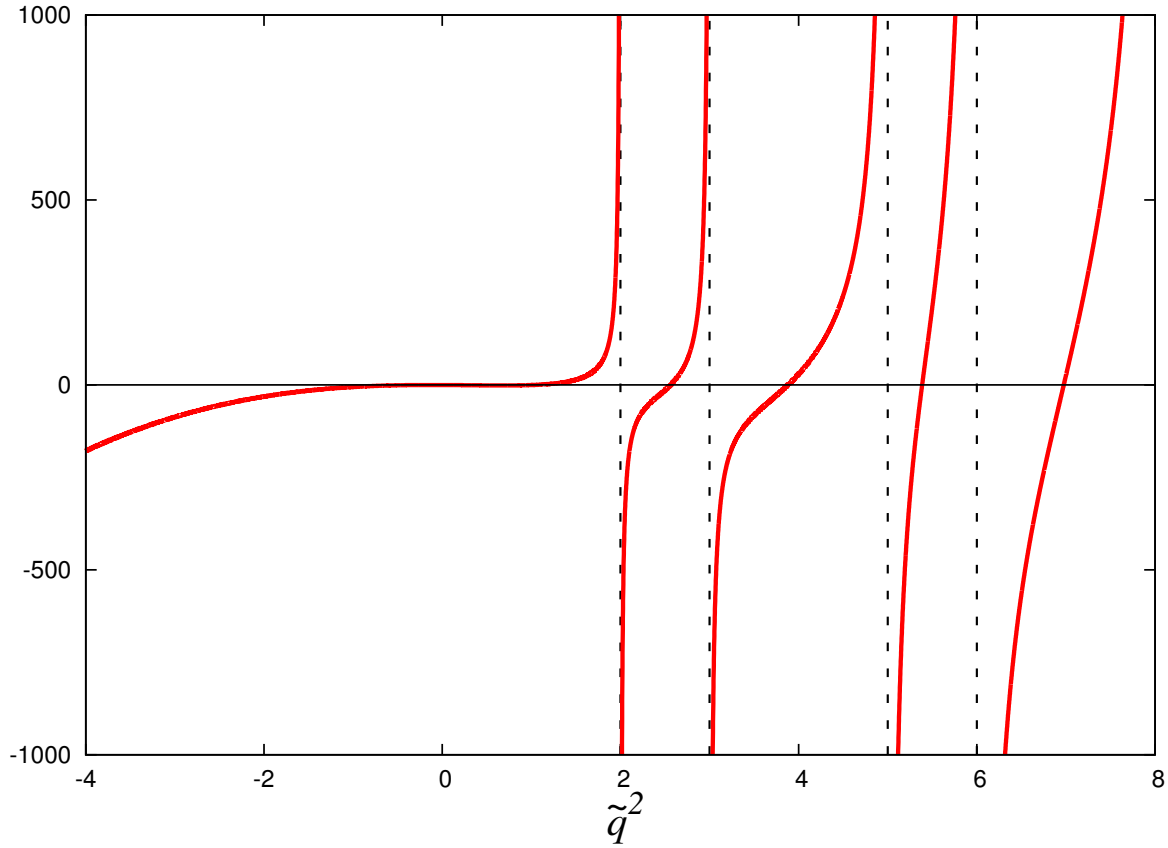

FIG. 12: The function $\mathcal{X}^{+}_{T_2}$, as defined in eq. (30), as a function of $\tilde{q}^2$. The vertical dashed lines denote the position of the poles of the function corresponding to the T_2^+ non-interacting energy-eigenvalues.

With these basis states, the contribution to the determinant in eq. (2) becomes

$$\det\left[\begin{pmatrix} \cot\delta_2 & 0 & 0 & 0 \\ 0 & \cot\delta_4 & 0 & 0 \\ 0 & 0 & \cot\delta_6 & 0 \\ 0 & 0 & 0 & \cot\delta_6 \end{pmatrix} - \begin{pmatrix} \overline{F}^{(FV,T_2^+)}_{2;2} & \overline{F}^{(FV,T_2^+)}_{2;4} & \overline{F}^{(FV,T_2^+)}_{2;6_1} & \overline{F}^{(FV,T_2^+)}_{2;6_2} \\ \overline{F}^{(FV,T_2^+)}_{4;2} & \overline{F}^{(FV,T_2^+)}_{4;4} & \overline{F}^{(FV,T_2^+)}_{4;6_1} & \overline{F}^{(FV,T_2^+)}_{4;6_2} \\ \overline{F}^{(FV,T_2^+)}_{6_1;2} & \overline{F}^{(FV,T_2^+)}_{6_1;4} & \overline{F}^{(FV,T_2^+)}_{6_1;6_1} & \overline{F}^{(FV,T_2^+)}_{6_1,6_2} \\ \overline{F}^{(FV,T_2^+)}_{6_2;2} & \overline{F}^{(FV,T_2^+)}_{6_2;4} & \overline{F}^{(FV,T_2^+)}_{6_2;6_1} & \overline{F}^{(FV,T_2^+)}_{6_2,6_2} \end{pmatrix}\right] = 0 \quad , \tag{27}$$

where

$$
\begin{aligned}
\overline{F}_{2,2}^{(FV,T_2^+)} &= \frac{\mathcal{Z}_{0,0}\left(1;\tilde{q}^2\right)}{\pi^{3/2}\tilde{q}} - \frac{4\mathcal{Z}_{4,0}\left(1;\tilde{q}^2\right)}{7\pi^{3/2}\tilde{q}^5} \\
\overline{F}_{2,4}^{(FV,T_2^+)} &= \frac{40\sqrt{\frac{3}{13}}\mathcal{Z}_{6,0}\left(1;\tilde{q}^2\right)}{11\pi^{3/2}\tilde{q}^7} - \frac{20\sqrt{3}\mathcal{Z}_{4,0}\left(1;\tilde{q}^2\right)}{77\pi^{3/2}\tilde{q}^5} \\
\overline{F}_{4,4}^{(FV,T_2^+)} &= \frac{\mathcal{Z}_{0,0}\left(1;\tilde{q}^2\right)}{\pi^{3/2}\tilde{q}} - \frac{54\mathcal{Z}_{4,0}\left(1;\tilde{q}^2\right)}{77\pi^{3/2}\tilde{q}^5} + \frac{20\mathcal{Z}_{6,0}\left(1;\tilde{q}^2\right)}{11\sqrt{13}\pi^{3/2}\tilde{q}^7} \\
\overline{F}_{2,6_1}^{(FV,T_2^+)} &= \frac{5\sqrt{\frac{13}{14}}\mathcal{Z}_{4,0}\left(1;\tilde{q}^2\right)}{11\pi^{3/2}\tilde{q}^5} - \frac{5\sqrt{14}\mathcal{Z}_{6,0}\left(1;\tilde{q}^2\right)}{11\pi^{3/2}\tilde{q}^7} \\
\overline{F}_{4,6_1}^{(FV,T_2^+)} &= -\frac{28\sqrt{\frac{42}{221}}\mathcal{Z}_{8,0}\left(1;\tilde{q}^2\right)}{19\pi^{3/2}\tilde{q}^9} + \frac{10\sqrt{\frac{6}{91}}\mathcal{Z}_{4,0}\left(1;\tilde{q}^2\right)}{11\pi^{3/2}\tilde{q}^5} + \frac{\sqrt{\frac{21}{2}}\mathcal{Z}_{6,0}\left(1;\tilde{q}^2\right)}{187\pi^{3/2}\tilde{q}^7} + \frac{1008\sqrt{\frac{2}{13}}\mathcal{Z}_{10,0}\left(1;\tilde{q}^2\right)}{323\pi^{3/2}\tilde{q}^{11}} \\
\overline{F}_{6_1,6_1}^{(FV,T_2^+)} &= -\frac{45\mathcal{Z}_{8,0}\left(1;\tilde{q}^2\right)}{19\sqrt{17}\pi^{3/2}\tilde{q}^9} + \frac{\mathcal{Z}_{0,0}\left(1;\tilde{q}^2\right)}{\pi^{3/2}\tilde{q}} - \frac{59\mathcal{Z}_{4,0}\left(1;\tilde{q}^2\right)}{187\pi^{3/2}\tilde{q}^5} + \frac{620\sqrt{13}\mathcal{Z}_{6,0}\left(1;\tilde{q}^2\right)}{3553\pi^{3/2}\tilde{q}^7} \\
&\quad + \frac{162\sqrt{21}\mathcal{Z}_{10,0}\left(1;\tilde{q}^2\right)}{7429\pi^{3/2}\tilde{q}^{11}} + \frac{3267\mathcal{Z}_{12,0}\left(1;\tilde{q}^2\right)}{7429\pi^{3/2}\tilde{q}^{13}} - \frac{198\sqrt{1001}\mathcal{Z}_{12,4}\left(1;\tilde{q}^2\right)}{7429\pi^{3/2}\tilde{q}^{13}}
\end{aligned}
$$

$$
\begin{aligned}
\overline{F}_{2,6_2}^{(FV,T_2^+)} &= \frac{15\sqrt{\frac{5}{2002}}\mathcal{Z}_{4,0}\left(1;\tilde{q}^2\right)}{\pi^{3/2}\tilde{q}^5} + \frac{\sqrt{\frac{14}{55}}\mathcal{Z}_{6,0}\left(1;\tilde{q}^2\right)}{\pi^{3/2}\tilde{q}^7} - \frac{64\sqrt{\frac{14}{12155}}\mathcal{Z}_{8,0}\left(1;\tilde{q}^2\right)}{3\pi^{3/2}\tilde{q}^9} \\
\overline{F}_{4,6_2}^{(FV,T_2^+)} &= -\frac{2\sqrt{\frac{30}{1001}}\mathcal{Z}_{4,0}\left(1;\tilde{q}^2\right)}{\pi^{3/2}\tilde{q}^5} - \frac{9\sqrt{\frac{105}{22}}\mathcal{Z}_{6,0}\left(1;\tilde{q}^2\right)}{17\pi^{3/2}\tilde{q}^7} + \frac{20\sqrt{\frac{210}{2431}}\mathcal{Z}_{8,0}\left(1;\tilde{q}^2\right)}{19\pi^{3/2}\tilde{q}^9} + \frac{336\sqrt{\frac{22}{65}}\mathcal{Z}_{10,0}\left(1;\tilde{q}^2\right)}{323\pi^{3/2}\tilde{q}^{11}} \\
\overline{F}_{6_1,6_2}^{(FV,T_2^+)} &= \frac{3\sqrt{\frac{5}{11}}\mathcal{Z}_{4,0}\left(1;\tilde{q}^2\right)}{17\pi^{3/2}\tilde{q}^5} + \frac{140\sqrt{\frac{65}{11}}\mathcal{Z}_{6,0}\left(1;\tilde{q}^2\right)}{323\pi^{3/2}\tilde{q}^7} + \frac{5\sqrt{\frac{5}{187}}\mathcal{Z}_{8,0}\left(1;\tilde{q}^2\right)}{57\pi^{3/2}\tilde{q}^9} - \frac{666\sqrt{\frac{231}{5}}\mathcal{Z}_{10,0}\left(1;\tilde{q}^2\right)}{7429\pi^{3/2}\tilde{q}^{11}} \\
&\quad - \frac{1287\sqrt{\frac{11}{5}}\mathcal{Z}_{12,0}\left(1;\tilde{q}^2\right)}{7429\pi^{3/2}\tilde{q}^{13}} + \frac{858\sqrt{\frac{91}{5}}\mathcal{Z}_{12,4}\left(1;\tilde{q}^2\right)}{7429\pi^{3/2}\tilde{q}^{13}} \\
\overline{F}_{6_2,6_2}^{(FV,T_2^+)} &= \frac{\mathcal{Z}_{0,0}\left(1;\tilde{q}^2\right)}{\pi^{3/2}\tilde{q}} + \frac{9\mathcal{Z}_{4,0}\left(1;\tilde{q}^2\right)}{17\pi^{3/2}\tilde{q}^5} - \frac{20\sqrt{13}\mathcal{Z}_{6,0}\left(1;\tilde{q}^2\right)}{323\pi^{3/2}\tilde{q}^7} + \frac{5\mathcal{Z}_{8,0}\left(1;\tilde{q}^2\right)}{19\sqrt{17}\pi^{3/2}\tilde{q}^9} - \frac{18\sqrt{21}\mathcal{Z}_{10,0}\left(1;\tilde{q}^2\right)}{7429\pi^{3/2}\tilde{q}^{11}} \\
&\quad - \frac{23991\mathcal{Z}_{12,0}\left(1;\tilde{q}^2\right)}{37145\pi^{3/2}\tilde{q}^{13}} - \frac{594\sqrt{1001}\mathcal{Z}_{12,4}\left(1;\tilde{q}^2\right)}{37145\pi^{3/2}\tilde{q}^{13}} \quad .
\end{aligned}
\tag{28}
$$

The solutions to eq. (27) must be determined numerically and will, in general, depend upon the interactions in the $l = 2$, 4, and 6 partial-waves. In the limit where the interactions in the $l = 6$ and higher partial-waves vanish, leaving contributions only from interactions in the $l = 2, 4$ partial-waves, the contribution to the determinant in eq. (27) collapses down to

TABLE XII: The momentum-space structure of T_2^+, $L_z = 2$ sources and sinks for $|\mathbf{n}|^2$=2, 3, and 5. These are shown graphically in figs. 13.

$\|\mathbf{n}\|^2$=2		$\|\mathbf{n}\|^2$=3		$\|\mathbf{n}\|^2$=5	
$\|(1,1,0)\ ,+1\rangle$	$-\frac{1}{\sqrt{2}}$	$\|(1,1,1)\ ,+1\rangle$	$\frac{1}{2}$	$\|(2,1,0)\ ,+1\rangle$	$-\frac{1}{2}$
$\|(1,-1,0)\ ,+1\rangle$	$\frac{1}{\sqrt{2}}$	$\|(1,1,-1)\ ,+1\rangle$	$\frac{1}{2}$	$\|(2,-1,0)\ ,+1\rangle$	$\frac{1}{2}$
		$\|(1,-1,1)\ ,+1\rangle$	$-\frac{1}{2}$	$\|(1,2,0)\ ,+1\rangle$	$-\frac{1}{2}$
		$\|(1,-1,-1)\ ,+1\rangle$	$-\frac{1}{2}$	$\|(1,-2,0)\ ,+1\rangle$	$\frac{1}{2}$

TABLE XIII: The momentum-space structure of T_2^+, $L_z = 2$ sources and sinks for $|\mathbf{n}|^2$=6. These are shown graphically in figs. 14.

$\|\mathbf{n}\|^2=6_{(l=2)}$				$\|\mathbf{n}\|^2=6_{(l=4)}$			
$\|(2,1,1)\ ,+1\rangle$	$\frac{1}{3}$	$\|(2,1,-1)\ ,+1\rangle$	$\frac{1}{3}$	$\|(2,1,1)\ ,+1\rangle$	$-\frac{1}{6\sqrt{2}}$	$\|(2,1,-1)\ ,+1\rangle$	$-\frac{1}{6\sqrt{2}}$
$\|(2,-1,1)\ ,+1\rangle$	$-\frac{1}{3}$	$\|(2,-1,-1)\ ,+1\rangle$	$-\frac{1}{3}$	$\|(2,-1,1)\ ,+1\rangle$	$\frac{1}{6\sqrt{2}}$	$\|(2,-1,-1)\ ,+1\rangle$	$\frac{1}{6\sqrt{2}}$
$\|(1,2,1)\ ,+1\rangle$	$\frac{1}{3}$	$\|(1,2,-1)\ ,+1\rangle$	$\frac{1}{3}$	$\|(1,2,1)\ ,+1\rangle$	$-\frac{1}{6\sqrt{2}}$	$\|(1,2,-1)\ ,+1\rangle$	$-\frac{1}{6\sqrt{2}}$
$\|(1,1,2)\ ,+1\rangle$	$\frac{1}{6}$	$\|(1,1,-2)\ ,+1\rangle$	$\frac{1}{6}$	$\|(1,1,2)\ ,+1\rangle$	$\frac{\sqrt{2}}{3}$	$\|(1,1,-2)\ ,+1\rangle$	$\frac{\sqrt{2}}{3}$
$\|(1,-1,2)\ ,+1\rangle$	$-\frac{1}{6}$	$\|(1,-1,-2)\ ,+1\rangle$	$-\frac{1}{6}$	$\|(1,-1,2)\ ,+1\rangle$	$-\frac{\sqrt{2}}{3}$	$\|(1,-1,-2)\ ,+1\rangle$	$-\frac{\sqrt{2}}{3}$
$\|(1,-2,1)\ ,+1\rangle$	$-\frac{1}{3}$	$\|(1,-2,-1)\ ,+1\rangle$	$-\frac{1}{3}$	$\|(1,-2,1)\ ,+1\rangle$	$\frac{1}{6\sqrt{2}}$	$\|(1,-2,-1)\ ,+1\rangle$	$\frac{1}{6\sqrt{2}}$

that of a 2×2 matrix, which has solutions

$$\frac{\cot\delta_2}{2} + \frac{\cot\delta_4}{2} - \frac{\mathcal{Z}_{0,0}\left(1;\tilde{q}^2\right)}{\pi^{3/2}\tilde{q}} + \frac{7\mathcal{Z}_{4,0}\left(1;\tilde{q}^2\right)}{11\pi^{3/2}\tilde{q}^5} - \frac{10\mathcal{Z}_{6,0}\left(1;\tilde{q}^2\right)}{11\sqrt{13}\pi^{3/2}\tilde{q}^7}$$
$$= \pm\frac{1}{2}\left[\left(-\frac{10\mathcal{Z}_{4,0}\left(1;\tilde{q}^2\right)}{77\pi^{3/2}\tilde{q}^5} + \frac{20\mathcal{Z}_{6,0}\left(1;\tilde{q}^2\right)}{11\sqrt{13}\pi^{3/2}\tilde{q}^7} + \cot\delta_2 - \cot\delta_4\right)^2\right.$$
$$\left. + 4\left(\frac{20\sqrt{3}\mathcal{Z}_{4,0}\left(1;\tilde{q}^2\right)}{77\pi^{3/2}\tilde{q}^5} - \frac{40\sqrt{\frac{3}{13}}\mathcal{Z}_{6,0}\left(1;\tilde{q}^2\right)}{11\pi^{3/2}\tilde{q}^7}\right)^2\right]^{1/2} . \quad (29)$$

In the limit that $\tan\delta_4 << \tan\delta_2$ the energy-eigenvalues are the solutions to

$$q^5\cot\delta_2 = \left(\frac{2\pi}{L}\right)^5 \frac{1}{\pi^{3/2}}\left(\tilde{q}^4\mathcal{Z}_{0,0}\left(1;\tilde{q}^2\right) - \frac{4}{7}\mathcal{Z}_{4,0}\left(1;\tilde{q}^2\right)\right) = \left(\frac{2\pi}{L}\right)^5 \frac{1}{\pi^{3/2}}\mathcal{X}_{T_2}^+\left(\tilde{q}^2\right) \quad , \quad (30)$$

where $\mathcal{X}_{T_2}^+$ is shown as a function of $\tilde{q}^2$ in fig. 12. The T_2^+ irrep first appears in the $|\mathbf{n}|^2 = 2$-shell, as can be seen in fig. 12. The graphical representations of the sources and sinks that generate the T_2^+ irrep for the low-lying $|\mathbf{n}|^2$-shells are shown in fig. 13 and fig. 14, and the momentum-space structures for $L_z = 2$ and $L_z = 1$ are given explicitly in table XII and table XV, respectively. The structures of the $L_z = 3$ sources and sinks are related to those with $L_z = 1$ by complex conjugation of the coefficients.

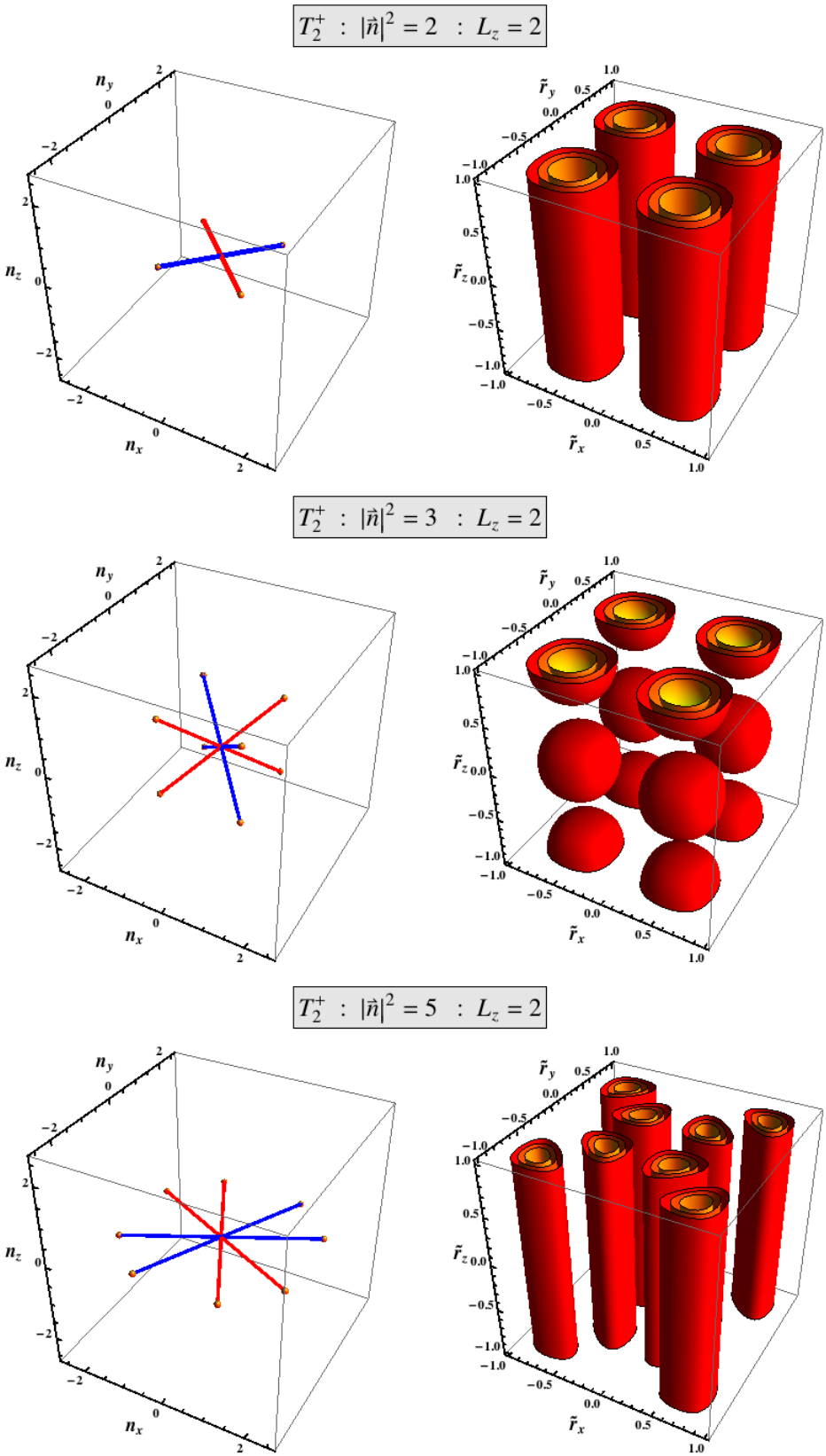

FIG. 13: The momentum-space representations (left) and position-space representations (right) of two-body relative states in the T_2^+ representation with $L_z = 2$ for $|\mathbf{n}|^2$=2, 3, and 5 shells.

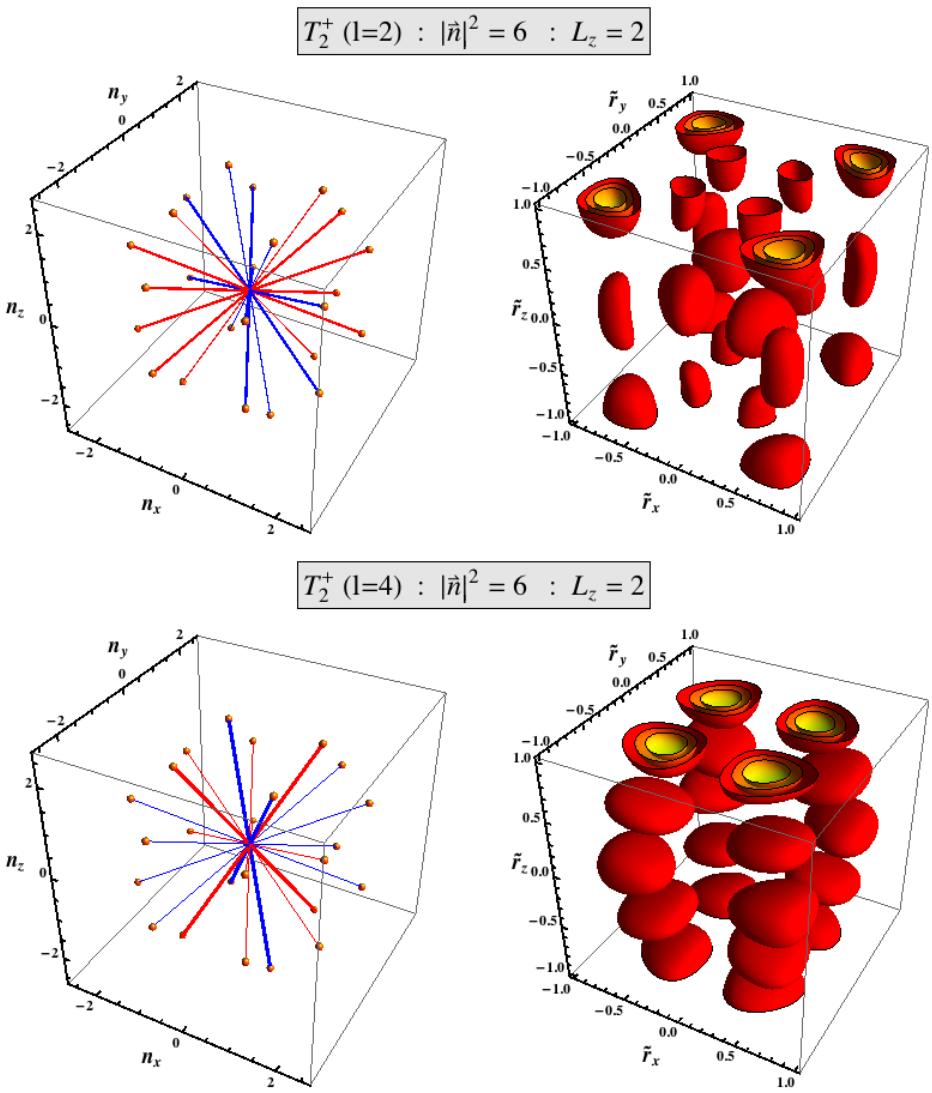

FIG. 14: The momentum-space representations (left) and position-space representations (right) of two-body relative states in the T_2^+ representation with $L_z = 2$ for the $|\mathbf{n}|^2$=6-shells.

TABLE XIV: The momentum-space structure of T_2^+, $L_z = 1$ sources and sinks for $|\mathbf{n}|^2$=2, 3, and 5.

$\|\mathbf{n}\|^2$=2		$\|\mathbf{n}\|^2$=3		$\|\mathbf{n}\|^2$=5			
$\|(1,0,1)\ ,\ +1\rangle$	$-\frac{1}{2}$	$\|(1,1,1)\ ,\ +1\rangle$	$-\frac{1}{2}$	$\|(2,0,1)\ ,\ +1\rangle$	$-\frac{1}{2\sqrt{2}}$	$\|(2,0,-1)\ ,\ +1\rangle$	$\frac{1}{2\sqrt{2}}$
$\|(1,0,-1)\ ,\ +1\rangle$	$\frac{1}{2}$	$\|(1,1,-1)\ ,\ +1\rangle$	$\frac{1}{2}$	$\|(1,0,2)\ ,\ +1\rangle$	$-\frac{1}{2\sqrt{2}}$	$\|(1,0,-2)\ ,\ +1\rangle$	$\frac{1}{2\sqrt{2}}$
$\|(0,1,1)\ ,\ +1\rangle$	$-\frac{i}{2}$	$\|(1,-1,1)\ ,\ +1\rangle$	$\frac{i}{2}$	$\|(0,2,1)\ ,\ +1\rangle$	$-\frac{i}{2\sqrt{2}}$	$\|(0,2,-1)\ ,\ +1\rangle$	$\frac{i}{2\sqrt{2}}$
$\|(0,1,-1)\ ,\ +1\rangle$	$\frac{i}{2}$	$\|(1,-1,-1)\ ,\ +1\rangle$	$-\frac{i}{2}$	$\|(0,1,2)\ ,\ +1\rangle$	$-\frac{i}{2\sqrt{2}}$	$\|(0,1,-2)\ ,\ +1\rangle$	$\frac{i}{2\sqrt{2}}$

TABLE XV: The momentum-space structure of T_2^+, $L_z = 1$ sources and sinks for $|\mathbf{n}|^2$=6.

$\|\mathbf{n}\|^2$=6$_{(l=2)}$				$\|\mathbf{n}\|^2$=6$_{(l=4)}$			
$\|(2,1,1)\ ,+1\rangle$	$\frac{\sqrt{\frac{5}{2}}}{6}$	$\|(2,1,-1)\ ,+1\rangle$	$-\frac{\sqrt{\frac{5}{2}}}{6}$	$\|(2,1,1)\ ,+1\rangle$	$\frac{\frac{23}{12}-2i}{\sqrt{65}}$	$\|(2,1,-1)\ ,+1\rangle$	$-\frac{\frac{23}{12}-2i}{\sqrt{65}}$
$\|(2,-1,1)\ ,+1\rangle$	$\frac{\frac{1}{2}-\frac{2i}{3}}{\sqrt{10}}$	$\|(2,-1,-1)\ ,+1\rangle$	$-\frac{\frac{1}{2}-\frac{2i}{3}}{\sqrt{10}}$	$\|(2,-1,1)\ ,+1\rangle$	$-\frac{\frac{3}{4}-\frac{8i}{3}}{\sqrt{65}}$	$\|(2,-1,-1)\ ,+1\rangle$	$\frac{\frac{3}{4}-\frac{8i}{3}}{\sqrt{65}}$
$\|(1,2,1)\ ,+1\rangle$	$\frac{\frac{2}{3}+\frac{i}{2}}{\sqrt{10}}$	$\|(1,2,-1)\ ,+1\rangle$	$-\frac{\frac{2}{3}+\frac{i}{2}}{\sqrt{10}}$	$\|(1,2,1)\ ,+1\rangle$	$-\frac{\frac{8}{3}+\frac{3i}{4}}{\sqrt{65}}$	$\|(1,2,-1)\ ,+1\rangle$	$\frac{\frac{8}{3}+\frac{3i}{4}}{\sqrt{65}}$
$\|(1,1,2)\ ,+1\rangle$	$\frac{1}{3}\sqrt{\frac{4}{5}+\frac{3i}{5}}$	$\|(1,1,-2)\ ,+1\rangle$	$-\frac{1+\frac{i}{3}}{\sqrt{10}}$	$\|(1,1,2)\ ,+1\rangle$	$\frac{\frac{1}{4}+\frac{11i}{12}}{\sqrt{65}}$	$\|(1,1,-2)\ ,+1\rangle$	$-\frac{\frac{1}{4}+\frac{11i}{12}}{\sqrt{65}}$
$\|(1,-1,2)\ ,+1\rangle$	$\frac{\frac{1}{3}-i}{\sqrt{10}}$	$\|(1,-1,-2)\ ,+1\rangle$	$-\frac{\frac{1}{3}-i}{\sqrt{10}}$	$\|(1,-1,2)\ ,+1\rangle$	$\frac{\frac{11}{12}-\frac{i}{4}}{\sqrt{65}}$	$\|(1,-1,-2)\ ,+1\rangle$	$-\frac{\frac{11}{12}-\frac{i}{4}}{\sqrt{65}}$
$\|(1,-2,1)\ ,+1\rangle$	$-\frac{1}{6}i\sqrt{\frac{5}{2}}$	$\|(1,-2,-1)\ ,+1\rangle$	$\frac{1}{6}i\sqrt{\frac{5}{2}}$	$\|(1,-2,1)\ ,+1\rangle$	$-\frac{2+\frac{23i}{12}}{\sqrt{65}}$	$\|(1,-2,-1)\ ,+1\rangle$	$\frac{2+\frac{23i}{12}}{\sqrt{65}}$

The $l = 2$ phase-shift was calculated from the energies of states in both the E^+ and T_2^+ irreps in recent work by Dudek *et al* [20]. Two states in each irrep were calculated below the $2\pi \to 4\pi$ inelastic threshold at the pion mass of the calculation. The contamination in the extraction of δ_2 from the higher partial-waves was estimated to be small.

B. Negative Parity Systems

The analysis of the odd-parity energy-levels, and their associated sources and sinks, parallels that of the even-parity states. There are five negative parity irreps of the cubic group, A_1^-, A_2^-, E^-, T_1^-, and T_2^- with dimensions $1, 1, 2, 3$, and 3 respectively. The energy-eigenvalues, sources and sinks for the negative-parity states are presented in the following sections: III B 1, III B 2, III B 3, III B 4 and III B 5. As discussed previously, the A_1^- irrep first appears relatively high in the spectrum, in the $|\mathbf{n}|^2 = 14$ shell, and is sensitive to the $l = 9$ and higher partial-waves.

1. A_2^- Representation

The energy-eigenvalues of states transforming in the A_2^- irrep ($L_z = 2$) receive contributions only from interactions in the $l = 3$ partial-wave for $l \leq 6$, as presented in table I. The A_2^- state associated with the $\overline{F}_{3;3}^{(FV)}$ block is (in the $|l, m\rangle$ basis)

$$|A_2^-, 2; 3; 1\rangle \;=\; \frac{1}{\sqrt{2}}|3, 2\rangle \;-\; \frac{1}{\sqrt{2}}|3, -2\rangle \quad ,$$

and the solutions to eq. (2) from this irrep result from

$$\begin{aligned} q^7 \cot\delta_3 &= \left(\frac{2\pi}{L}\right)^7 \frac{1}{\pi^{3/2}} \left(\tilde{q}^6 \mathcal{Z}_{0,0}\left(1; \tilde{q}^2\right) - \frac{12}{11}\tilde{q}^2 \mathcal{Z}_{4,0}\left(1; \tilde{q}^2\right) + \frac{80}{11\sqrt{13}} \mathcal{Z}_{6,0}\left(1; \tilde{q}^2\right)\right) \\ &\equiv \left(\frac{2\pi}{L}\right)^7 \frac{1}{\pi^{3/2}}\, \mathcal{X}_{A_2}^-\left(\tilde{q}^2\right) \quad , \end{aligned} \tag{31}$$

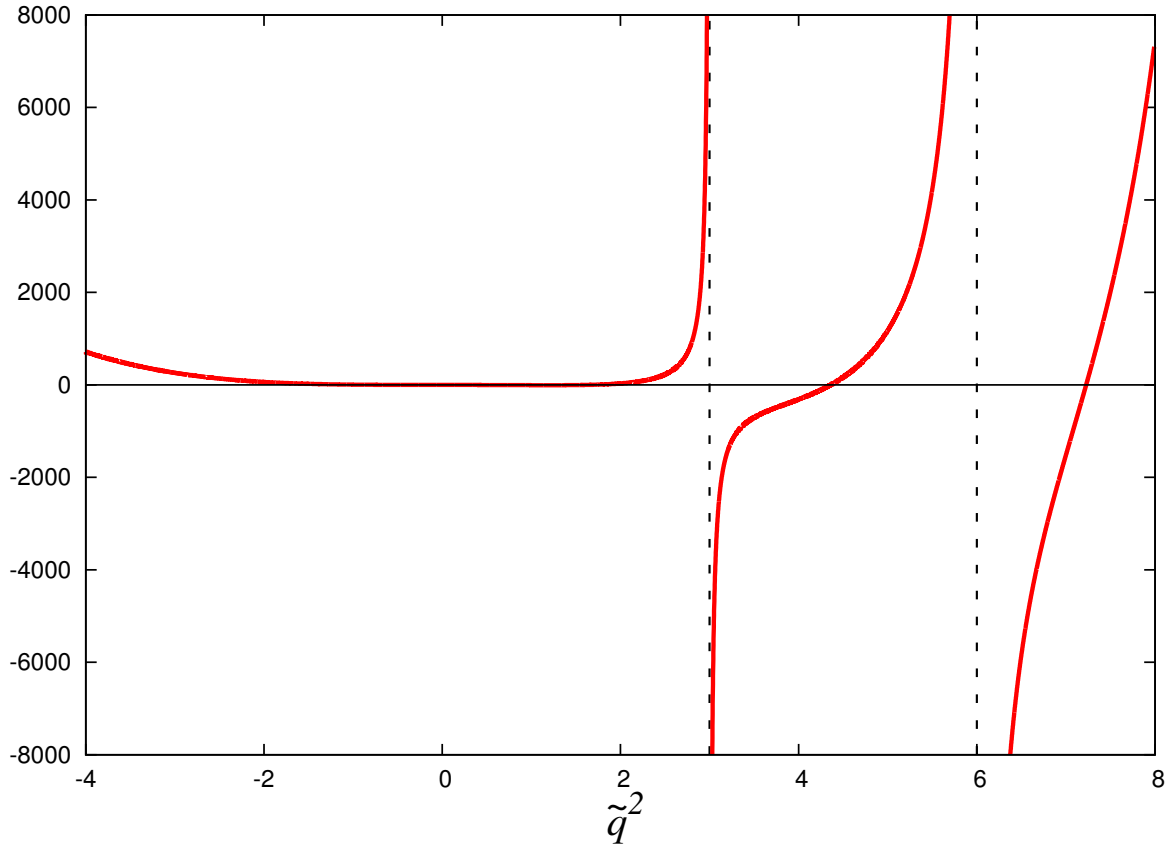

FIG. 15: The function $\mathcal{X}^{-}_{A_2}$, as defined in eq. (31), as a function of $\tilde{q}^2$. The vertical dashed lines denote the position of the poles of the function corresponding to the non-interacting energy-eigenvalues.

TABLE XVI: The momentum-space structure of A_2^- sources and sinks. These are shown graphically in fig. 16.

$\|\mathbf{n}\|^2$=3		$\|\mathbf{n}\|^2$=6			
		$\|(2,1,1)\ ,\ -1\rangle$	$\frac{1}{2\sqrt{3}}$	$\|(2,1,-1)\ ,\ -1\rangle$	$-\frac{1}{2\sqrt{3}}$
$\|(1,1,1)\ ,\ -1\rangle$	$\frac{1}{2}$	$\|(2,-1,1)\ ,\ -1\rangle$	$-\frac{1}{2\sqrt{3}}$	$\|(2,-1,-1)\ ,\ -1\rangle$	$\frac{1}{2\sqrt{3}}$
$\|(1,1,-1)\ ,\ -1\rangle$	$-\frac{1}{2}$	$\|(1,2,1)\ ,\ -1\rangle$	$\frac{1}{2\sqrt{3}}$	$\|(1,2,-1)\ ,\ -1\rangle$	$-\frac{1}{2\sqrt{3}}$
$\|(1,-1,1)\ ,\ -1\rangle$	$-\frac{1}{2}$	$\|(1,1,2)\ ,\ -1\rangle$	$\frac{1}{2\sqrt{3}}$	$\|(1,1,-2)\ ,\ -1\rangle$	$-\frac{1}{2\sqrt{3}}$
$\|(1,-1,-1)\ ,\ -1\rangle$	$\frac{1}{2}$	$\|(1,-1,2)\ ,\ -1\rangle$	$-\frac{1}{2\sqrt{3}}$	$\|(1,-1,-2)\ ,\ -1\rangle$	$\frac{1}{2\sqrt{3}}$
		$\|(1,-2,1)\ ,\ -1\rangle$	$-\frac{1}{2\sqrt{3}}$	$\|(1,-2,-1)\ ,\ -1\rangle$	$\frac{1}{2\sqrt{3}}$

where the function $\mathcal{X}^{-}_{A_2}(\tilde{q}^2)$ is shown in fig. 15. The graphical representations of the sources and sinks that generate the A_2^- irrep in the low-lying $|\mathbf{n}|^2$-shells ($|\mathbf{n}|^2 = 3$ and $|\mathbf{n}|^2 = 6$) are shown in fig. 16, and the momentum-space structures are given explicitly in table XVI.

The A_2^- irrep first appears in the $|\mathbf{n}|^2 = 3$-shell and $l = 3$ is the lowest contributing partial-wave. LQCD calculations of correlation functions from sources and sinks transforming as

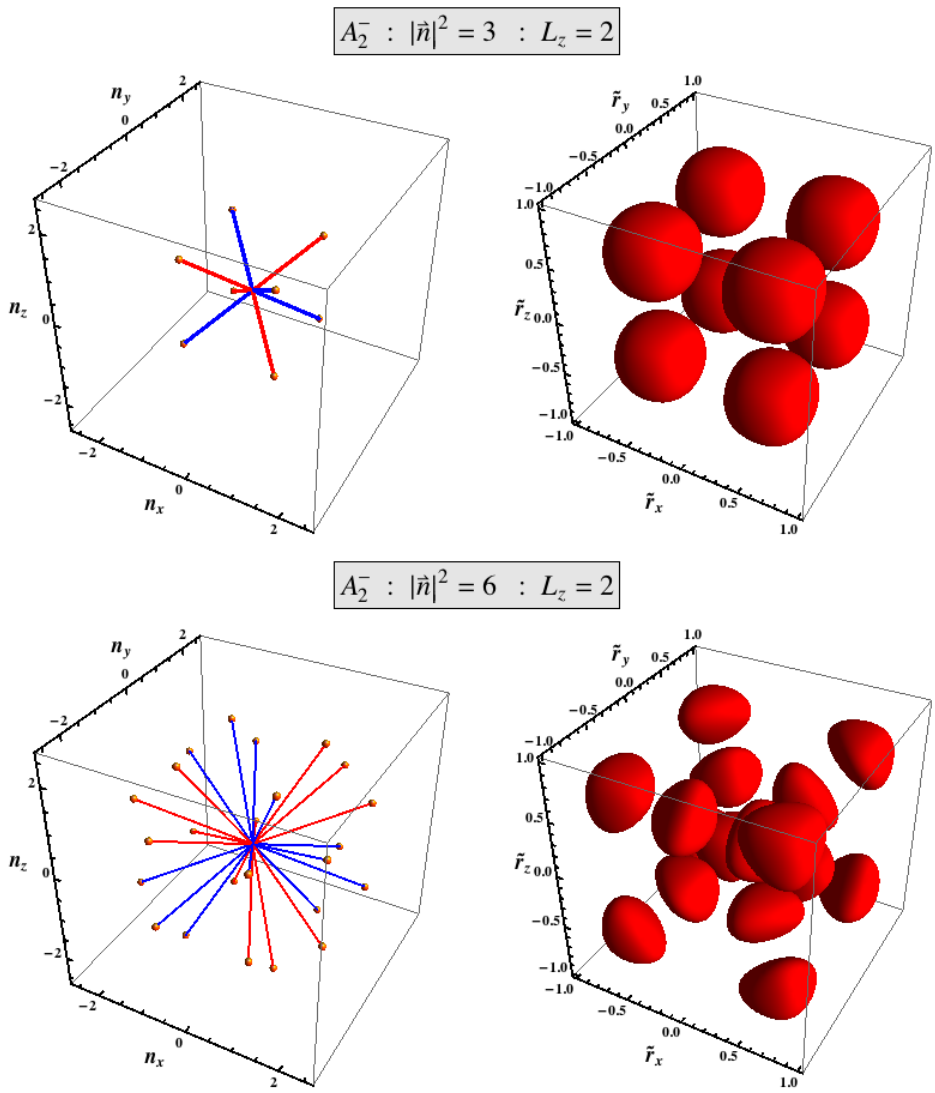

FIG. 16: The momentum-space representations (left) and position-space representations (right) of two-body relative states in the A_2^- representation for the lowest-lying $|\mathbf{n}|^2$-shells.

A_2^- will provide determinations of δ_3 with contamination from partial-waves with $l \geq 7$, i.e. the energy of the A_2^- states receive contributions from $l = 3, 7, \ldots$. This is in contrast to states in the T_2^- irrep, which will be considered subsequently, whose energy-eigenvalues receive contributions from partial-waves with $l = 3, 5, \ldots$. This suggests that the A_2^- irrep is optimal for determining δ_3.

2. E^- Representation

The energy-eigenvalues of E^- states receive contributions only from interactions in the $l = 5$ partial-wave for $l \leq 6$, as presented in table I. As the E^- irrep is two-dimensional, the contribution to the determinant in eq. (2) results from a 2×2 matrix for $l \leq 6$, which collapses down to a one-dimensional factor as the $L_z = 0$ and $L_z = 2$ states are degenerate.

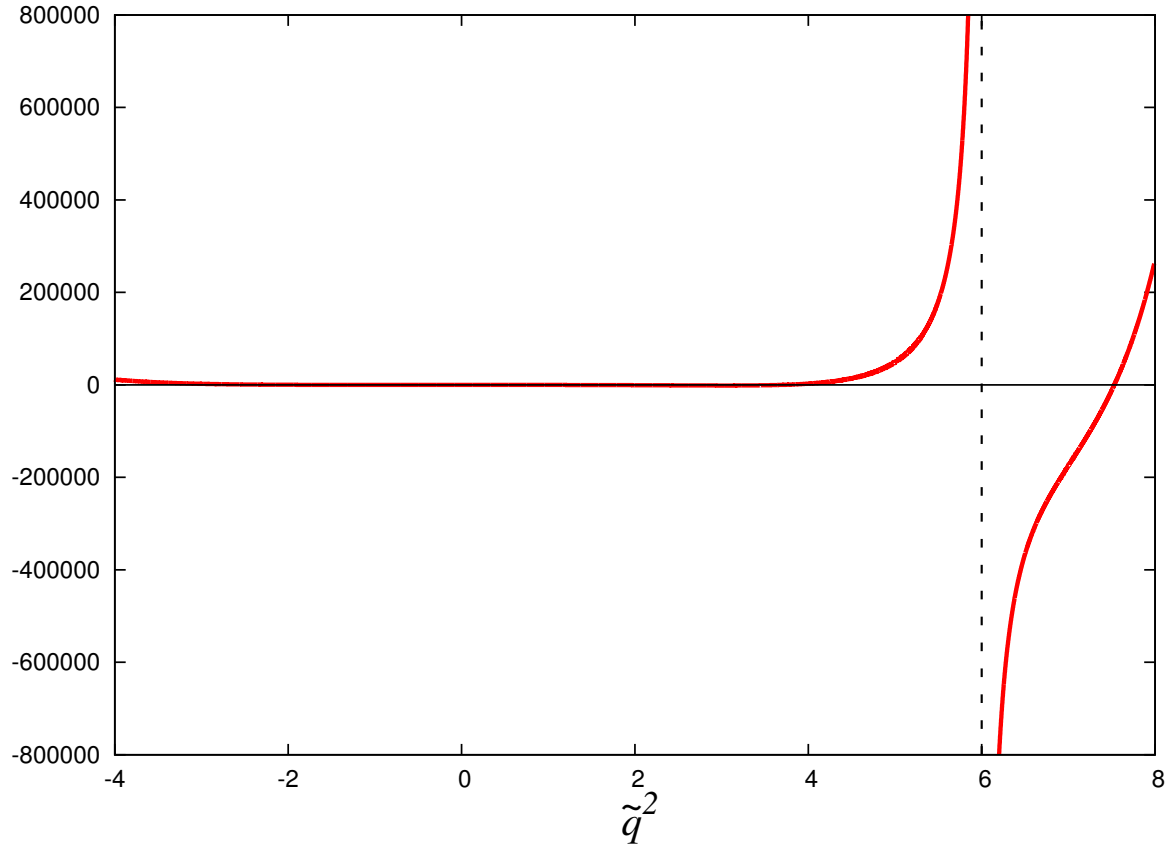

FIG. 17: The function $\mathcal{X}_E^-$, as defined in eq. (32), as a function of $\tilde{q}^2$. The vertical dashed lines denote the position of the poles of the function corresponding to the non-interacting energy-eigenvalues.

The E^- $L_z = 0$ state associated with the $\overline{F}_{5,5}^{(FV)}$ block is

$$|E^-, 0; 5; 1\rangle \;=\; \frac{1}{\sqrt{2}}|5,4\rangle \;-\; \frac{1}{\sqrt{2}}|5,-4\rangle \quad .$$

The solution to eq. (2) from the E^- irrep results from

$$\begin{aligned} q^{11}\cot\delta_5 \;&=\; \left(\frac{2\pi}{L}\right)^{11} \frac{1}{\pi^{3/2}} \;\times \\ &\left(\tilde{q}^{10}\mathcal{Z}_{0,0}\left(1;\tilde{q}^2\right) - \frac{6\tilde{q}^6\mathcal{Z}_{4,0}\left(1;\tilde{q}^2\right)}{13} + \frac{32\tilde{q}^4\mathcal{Z}_{6,0}\left(1;\tilde{q}^2\right)}{17\sqrt{13}} - \frac{672\tilde{q}^2\mathcal{Z}_{8,0}\left(1;\tilde{q}^2\right)}{247\sqrt{17}} + \frac{1152\sqrt{21}\mathcal{Z}_{10,0}\left(1;\tilde{q}^2\right)}{4199}\right) \\ &\equiv\; \left(\frac{2\pi}{L}\right)^{11} \frac{1}{\pi^{3/2}}\mathcal{X}_E^-\left(\tilde{q}^2\right) \quad . \end{aligned} \tag{32}$$

where the function $\mathcal{X}_E^-(\tilde{q}^2)$ is shown in fig. 17. The graphical representations of the source and sink that generate the E^- irrep in the $|\mathbf{n}|^2 = 6$-shell are shown in fig. 18, and the momentum-space structure is given explicitly in table XVII.

The E^- irrep first appears in the $|\mathbf{n}|^2 = 6$-shell and $l = 5$ is the lowest contributing partial-wave. LQCD calculations of correlation functions from sources and sinks transforming as

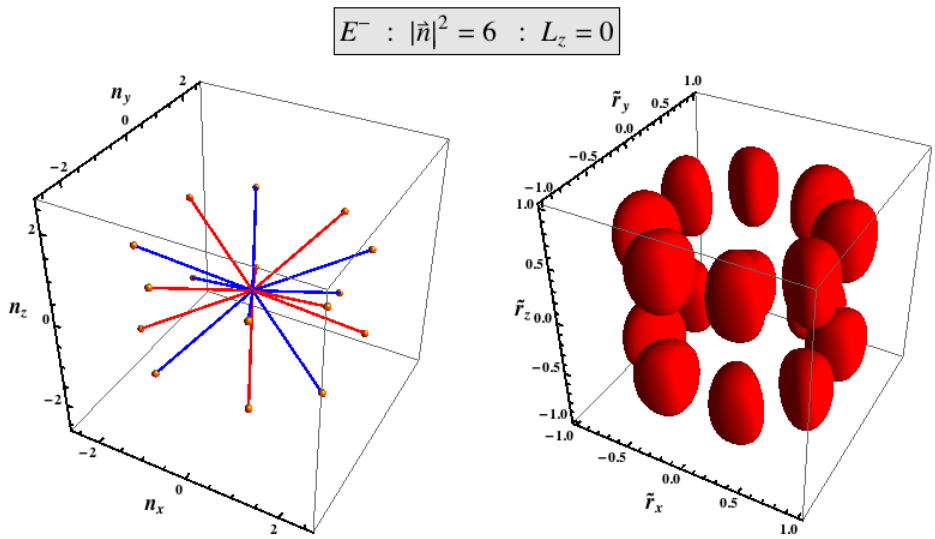

FIG. 18: The momentum-space representations (left) and position-space representations (right) of two-body relative states in the E^- representation with $L_z = 0$ for the $|\mathbf{n}|^2 = 6$ shell.

TABLE XVII: The momentum-space structure of E^-, $L_z = 0$, 2 sources and sinks. The $L_z = 0$ case is shown graphically in fig. 18.

$\|\mathbf{n}\|^2$=6 $L_z = 0$				$\|\mathbf{n}\|^2$=6 $L_z = 2$			
$\|(2,1,1)\ ,\ -1\rangle$	$-\frac{1}{2\sqrt{2}}$	$\|(2,1,-1)\ ,\ -1\rangle$	$\frac{1}{2\sqrt{2}}$	$\|(2,1,1)\ ,\ -1\rangle$	$-\frac{1}{2\sqrt{6}}$	$\|(2,1,-1)\ ,\ -1\rangle$	$\frac{1}{2\sqrt{6}}$
$\|(2,-1,1)\ ,\ -1\rangle$	$\frac{1}{2\sqrt{2}}$	$\|(2,-1,-1)\ ,\ -1\rangle$	$-\frac{1}{2\sqrt{2}}$	$\|(2,-1,1)\ ,\ -1\rangle$	$\frac{1}{2\sqrt{6}}$	$\|(2,-1,-1)\ ,\ -1\rangle$	$-\frac{1}{2\sqrt{6}}$
$\|(1,2,1)\ ,\ -1\rangle$	$\frac{1}{2\sqrt{2}}$	$\|(1,2,-1)\ ,\ -1\rangle$	$-\frac{1}{2\sqrt{2}}$	$\|(1,2,1)\ ,\ -1\rangle$	$-\frac{1}{2\sqrt{6}}$	$\|(1,2,-1)\ ,\ -1\rangle$	$\frac{1}{2\sqrt{6}}$
$\|(1,-2,1)\ ,\ -1\rangle$	$-\frac{1}{2\sqrt{2}}$	$\|(1,-2,-1)\ ,\ -1\rangle$	$\frac{1}{2\sqrt{2}}$	$\|(1,1,2)\ ,\ -1\rangle$	$\frac{1}{\sqrt{6}}$	$\|(1,1,-2)\ ,\ -1\rangle$	$-\frac{1}{\sqrt{6}}$
				$\|(1,-1,2)\ ,\ -1\rangle$	$-\frac{1}{\sqrt{6}}$	$\|(1,-1,-2)\ ,\ -1\rangle$	$\frac{1}{\sqrt{6}}$
				$\|(1,-2,1)\ ,\ -1\rangle$	$\frac{1}{2\sqrt{6}}$	$\|(1,-2,-1)\ ,\ -1\rangle$	$-\frac{1}{2\sqrt{6}}$

E^- will provide determinations of δ_5 with contamination from partial-waves with $l \geq 7$, i.e. the energy of the E^- states receive contributions from $l = 5, 7, ...$ The LQCD calculations will need to be performed in relatively large volumes, as we discuss later, in order for the $|\mathbf{n}|^2 = 6$ shell to lie below the inelastic threshold.

3. T_1^- Representation

The energy-eigenvalues of states transforming in the T_1^- irrep receive contributions from interactions in the $l = 1, 3, 5, ...$ partial-waves, as presented in table I. As the T_1^- irrep is three-dimensional, the contribution to eq. (2) is the determinant of a 12×12 matrix for $l \leq 6$ (there are two T_1^-'s in the decomposition of $l = 5$), which collapses down to the determinant of a 4×4 matrix as the $L_z = 0$, $L_z = 1$ and $L_z = 3$ states are degenerate. The T_1^- $L_z = 0$

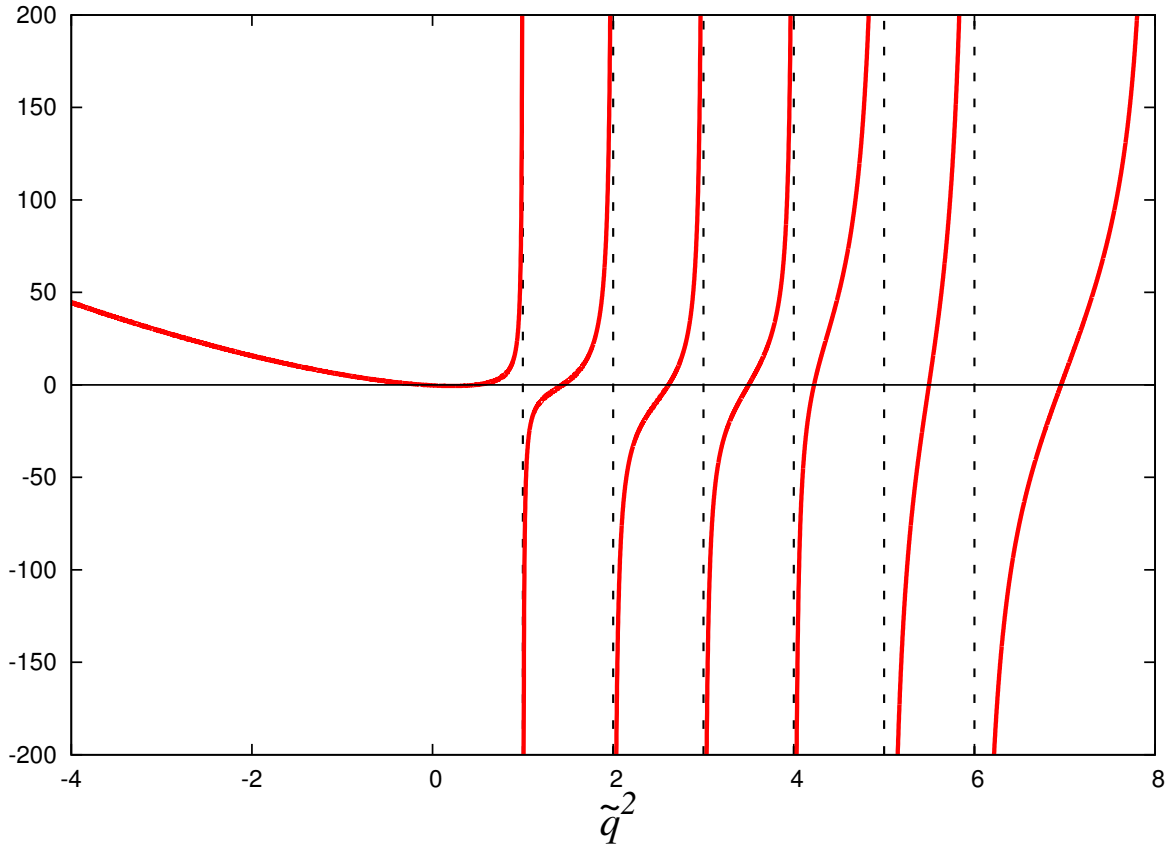

FIG. 19: The function $\mathcal{X}^-_{T_1}$, as defined in eq. (36), as a function of $\tilde{q}^2$. The vertical dashed lines denote the position of the poles of the function corresponding to the non-interacting energy-eigenvalues.

states associated with the $\overline{F}^{(FV)}_{1;1}$, $\overline{F}^{(FV)}_{3;3}$, and $\overline{F}^{(FV)}_{5;5}$ blocks are

$$\begin{aligned}
|T_1^-, 0; 1; 1\rangle &= |1, 0\rangle \\
|T_1^-, 0; 3; 1\rangle &= |3, 0\rangle \\
|T_1^-, 0; 5; 1\rangle &= |5, 0\rangle \\
|T_1^-, 0; 5; 2\rangle &= \frac{1}{\sqrt{2}} \left(\, |5, 4\rangle \; + \; |5, -4\rangle \, \right) \quad .
\end{aligned}$$

With these four basis states, the T_1^- contribution to eq. (2) becomes

$$\det \left[\begin{pmatrix} \cot\delta_1 & 0 & 0 & 0 \\ 0 & \cot\delta_3 & 0 & 0 \\ 0 & 0 & \cot\delta_5 & 0 \\ 0 & 0 & 0 & \cot\delta_5 \end{pmatrix} - \begin{pmatrix} \overline{F}^{(FV,T_1^-)}_{1;1} & \overline{F}^{(FV,T_1^-)}_{1;3} & \overline{F}^{(FV,T_1^-)}_{1;5_1} & \overline{F}^{(FV,T_1^-)}_{1;5_2} \\ \overline{F}^{(FV,T_1^-)}_{3;1} & \overline{F}^{(FV,T_1^-)}_{3;3} & \overline{F}^{(FV,T_1^-)}_{3;5_1} & \overline{F}^{(FV,T_1^-)}_{3;5_2} \\ \overline{F}^{(FV,T_1^-)}_{5_1;1} & \overline{F}^{(FV,T_1^-)}_{5_1;3} & \overline{F}^{(FV,T_1^-)}_{5_1;5_1} & \overline{F}^{(FV,T_1^-)}_{5_1,5_2} \\ \overline{F}^{(FV,T_1^-)}_{5_2;1} & \overline{F}^{(FV,T_1^-)}_{5_2;3} & \overline{F}^{(FV,T_1^-)}_{5_2,5_1} & \overline{F}^{(FV,T_1^-)}_{5_2,5_2} \end{pmatrix} \right] = 0 \quad , \tag{33}$$

where

$$
\begin{aligned}
\overline{F}^{(FV,T_1^-)}_{1,1} &= \frac{\mathcal{Z}_{0,0}\left(1;\tilde{q}^2\right)}{\pi^{3/2}\tilde{q}} \\
\overline{F}^{(FV,T_1^-)}_{1,3} &= \frac{4\mathcal{Z}_{4,0}\left(1;\tilde{q}^2\right)}{\sqrt{21}\pi^{3/2}\tilde{q}^5} \\
\overline{F}^{(FV,T_1^-)}_{1,5_1} &= \frac{5\mathcal{Z}_{4,0}\left(1;\tilde{q}^2\right)}{\sqrt{33}\pi^{3/2}\tilde{q}^5} + \frac{6\sqrt{\frac{3}{143}}\mathcal{Z}_{6,0}\left(1;\tilde{q}^2\right)}{\pi^{3/2}\tilde{q}^7} \\
\overline{F}^{(FV,T_1^-)}_{1,5_2} &= \frac{\sqrt{\frac{15}{77}}\mathcal{Z}_{4,0}\left(1;\tilde{q}^2\right)}{\pi^{3/2}\tilde{q}^5} - \frac{2\sqrt{\frac{105}{143}}\mathcal{Z}_{6,0}\left(1;\tilde{q}^2\right)}{\pi^{3/2}\tilde{q}^7} \\
\overline{F}^{(FV,T_1^-)}_{3,3} &= \frac{\mathcal{Z}_{0,0}\left(1;\tilde{q}^2\right)}{\pi^{3/2}\tilde{q}} + \frac{100\mathcal{Z}_{6,0}\left(1;\tilde{q}^2\right)}{33\sqrt{13}\pi^{3/2}\tilde{q}^7} + \frac{6\mathcal{Z}_{4,0}\left(1;\tilde{q}^2\right)}{11\pi^{3/2}\tilde{q}^5} \\
\overline{F}^{(FV,T_1^-)}_{3,5_1} &= \frac{60\mathcal{Z}_{4,0}\left(1;\tilde{q}^2\right)}{13\sqrt{77}\pi^{3/2}\tilde{q}^5} + \frac{7\sqrt{\frac{7}{143}}\mathcal{Z}_{6,0}\left(1;\tilde{q}^2\right)}{3\pi^{3/2}\tilde{q}^7} + \frac{56\sqrt{\frac{7}{187}}\mathcal{Z}_{8,0}\left(1;\tilde{q}^2\right)}{13\pi^{3/2}\tilde{q}^9} \\
\overline{F}^{(FV,T_1^-)}_{3,5_2} &= -\frac{12\sqrt{\frac{5}{11}}\mathcal{Z}_{4,0}\left(1;\tilde{q}^2\right)}{13\pi^{3/2}\tilde{q}^5} + \frac{7\sqrt{\frac{5}{143}}\mathcal{Z}_{6,0}\left(1;\tilde{q}^2\right)}{\pi^{3/2}\tilde{q}^7} + \frac{56\sqrt{\frac{5}{187}}\mathcal{Z}_{8,0}\left(1;\tilde{q}^2\right)}{39\pi^{3/2}\tilde{q}^9} \\
\overline{F}^{(FV,T_1^-)}_{5_1,5_1} &= \frac{\mathcal{Z}_{0,0}\left(1;\tilde{q}^2\right)}{\pi^{3/2}\tilde{q}} + \frac{6\mathcal{Z}_{4,0}\left(1;\tilde{q}^2\right)}{13\pi^{3/2}\tilde{q}^5} + \frac{80\mathcal{Z}_{6,0}\left(1;\tilde{q}^2\right)}{51\sqrt{13}\pi^{3/2}\tilde{q}^7} + \frac{490\mathcal{Z}_{8,0}\left(1;\tilde{q}^2\right)}{247\sqrt{17}\pi^{3/2}\tilde{q}^9} + \frac{756\sqrt{21}\mathcal{Z}_{10,0}\left(1;\tilde{q}^2\right)}{4199\pi^{3/2}\tilde{q}^{11}} \\
\overline{F}^{(FV,T_1^-)}_{5_1,5_2} &= \frac{6\sqrt{\frac{5}{7}}\mathcal{Z}_{4,0}\left(1;\tilde{q}^2\right)}{13\pi^{3/2}\tilde{q}^5} + \frac{8\sqrt{\frac{35}{13}}\mathcal{Z}_{6,0}\left(1;\tilde{q}^2\right)}{17\pi^{3/2}\tilde{q}^7} - \frac{154\sqrt{\frac{35}{17}}\mathcal{Z}_{8,0}\left(1;\tilde{q}^2\right)}{741\pi^{3/2}\tilde{q}^9} - \frac{2772\sqrt{\frac{3}{5}}\mathcal{Z}_{10,0}\left(1;\tilde{q}^2\right)}{4199\pi^{3/2}\tilde{q}^{11}} \\
\overline{F}^{(FV,T_1^-)}_{5_2,5_2} &= \frac{\mathcal{Z}_{0,0}\left(1;\tilde{q}^2\right)}{\pi^{3/2}\tilde{q}} - \frac{6\mathcal{Z}_{4,0}\left(1;\tilde{q}^2\right)}{13\pi^{3/2}\tilde{q}^5} + \frac{32\mathcal{Z}_{6,0}\left(1;\tilde{q}^2\right)}{17\sqrt{13}\pi^{3/2}\tilde{q}^7} + \frac{14\sqrt{17}\mathcal{Z}_{8,0}\left(1;\tilde{q}^2\right)}{247\pi^{3/2}\tilde{q}^9} - \frac{84\sqrt{21}\mathcal{Z}_{10,0}\left(1;\tilde{q}^2\right)}{323\pi^{3/2}\tilde{q}^{11}} \quad .
\end{aligned}
\tag{34}
$$

In the limit of vanishing interactions in the $l = 5$ partial-wave, eq. (33) collapses down to the determinant of a 2×2 matrix, which has solutions

$$
\begin{aligned}
&\frac{\cot\delta_1}{2} + \frac{\cot\delta_3}{2} - \frac{\mathcal{Z}_{0,0}\left(1;\tilde{q}^2\right)}{\pi^{3/2}\tilde{q}} - \frac{3\mathcal{Z}_{4,0}\left(1;\tilde{q}^2\right)}{11\pi^{3/2}\tilde{q}^5} - \frac{50\mathcal{Z}_{6,0}\left(1;\tilde{q}^2\right)}{33\sqrt{13}\pi^{3/2}\tilde{q}^7} \\
&\qquad = \pm\frac{1}{2}\sqrt{\left(\frac{6\mathcal{Z}_{4,0}\left(1;\tilde{q}^2\right)}{11\pi^{3/2}\tilde{q}^5} + \frac{100\mathcal{Z}_{6,0}\left(1;\tilde{q}^2\right)}{33\sqrt{13}\pi^{3/2}\tilde{q}^7} + \cot\delta_1 - \cot\delta_3\right)^2 + \frac{64\mathcal{Z}_{4,0}\left(1;\tilde{q}^2\right)^2}{21\pi^3\tilde{q}^{10}}} \quad .
\end{aligned}
\tag{35}
$$

In the situation where $\tan\delta_3 << \tan\delta_1$, eq. (35) can be perturbatively expanded to give the $l = 1$ dominant solution

$$
q^3\cot\delta_1 = \left(\frac{2\pi}{L}\right)^3 \frac{1}{\pi^{3/2}}\tilde{q}^2\mathcal{Z}_{0,0}\left(1;\tilde{q}^2\right) \quad \equiv \quad \left(\frac{2\pi}{L}\right)^3 \frac{1}{\pi^{3/2}}\mathcal{X}^-_{T_1}\left(\tilde{q}^2\right) \quad , \tag{36}
$$

where the function $\mathcal{X}^-_{T_1}\left(\tilde{q}^2\right)$ is shown in fig. 19. The graphical representations of the source and sink that generate the T_1^- irrep for the lowest-lying $|\mathbf{n}|^2$-shell are shown in fig. 20, fig. 21 and fig. 22, and the momentum-space structure is given explicitly in table XVIII and

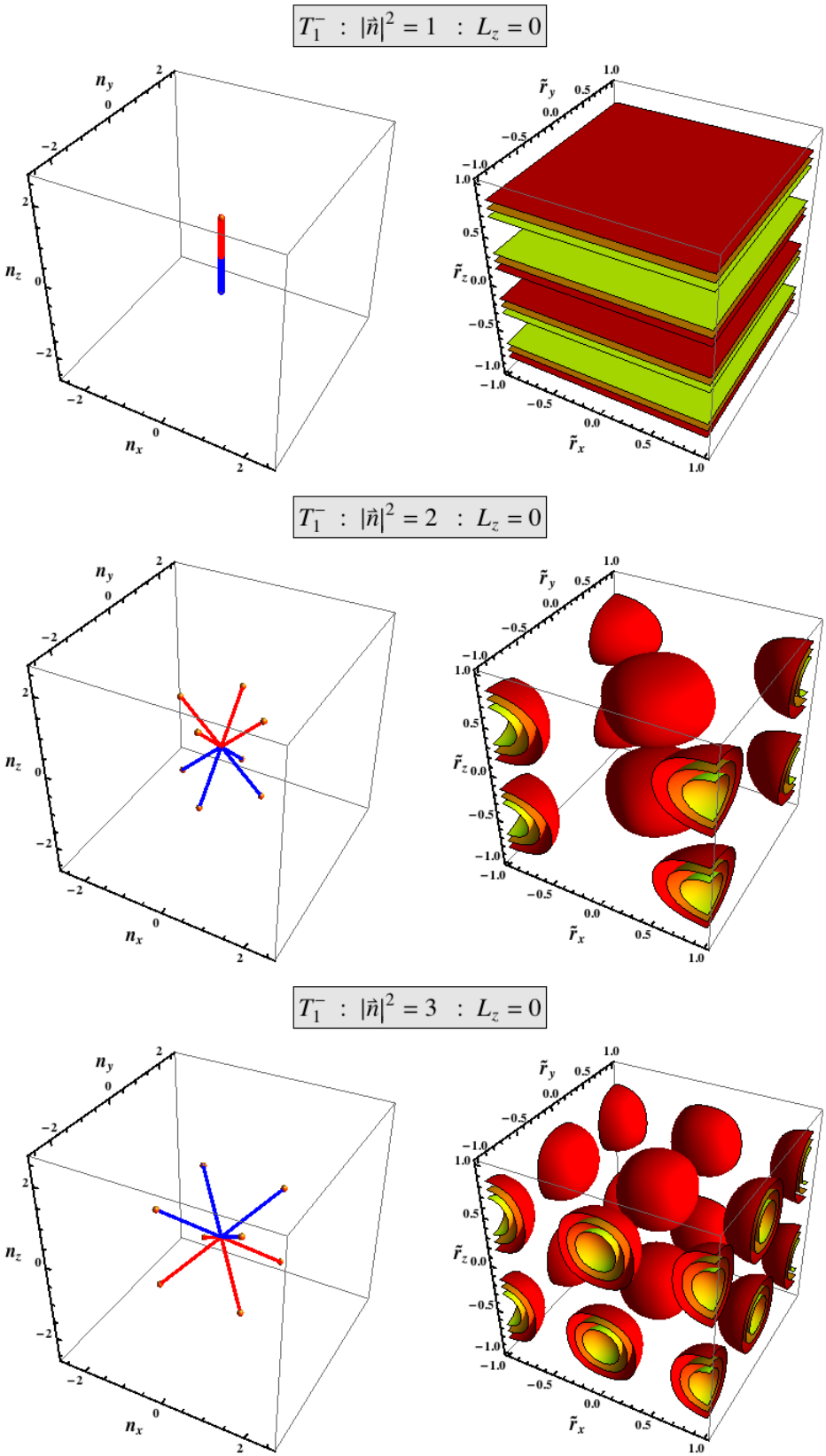

FIG. 20: The momentum-space representations (left) and position-space representations (right) of two-body relative states in the T_1^- representation with $L_z = 0$ for the $|\mathbf{n}|^2 = 1, 2, 3$-shells.

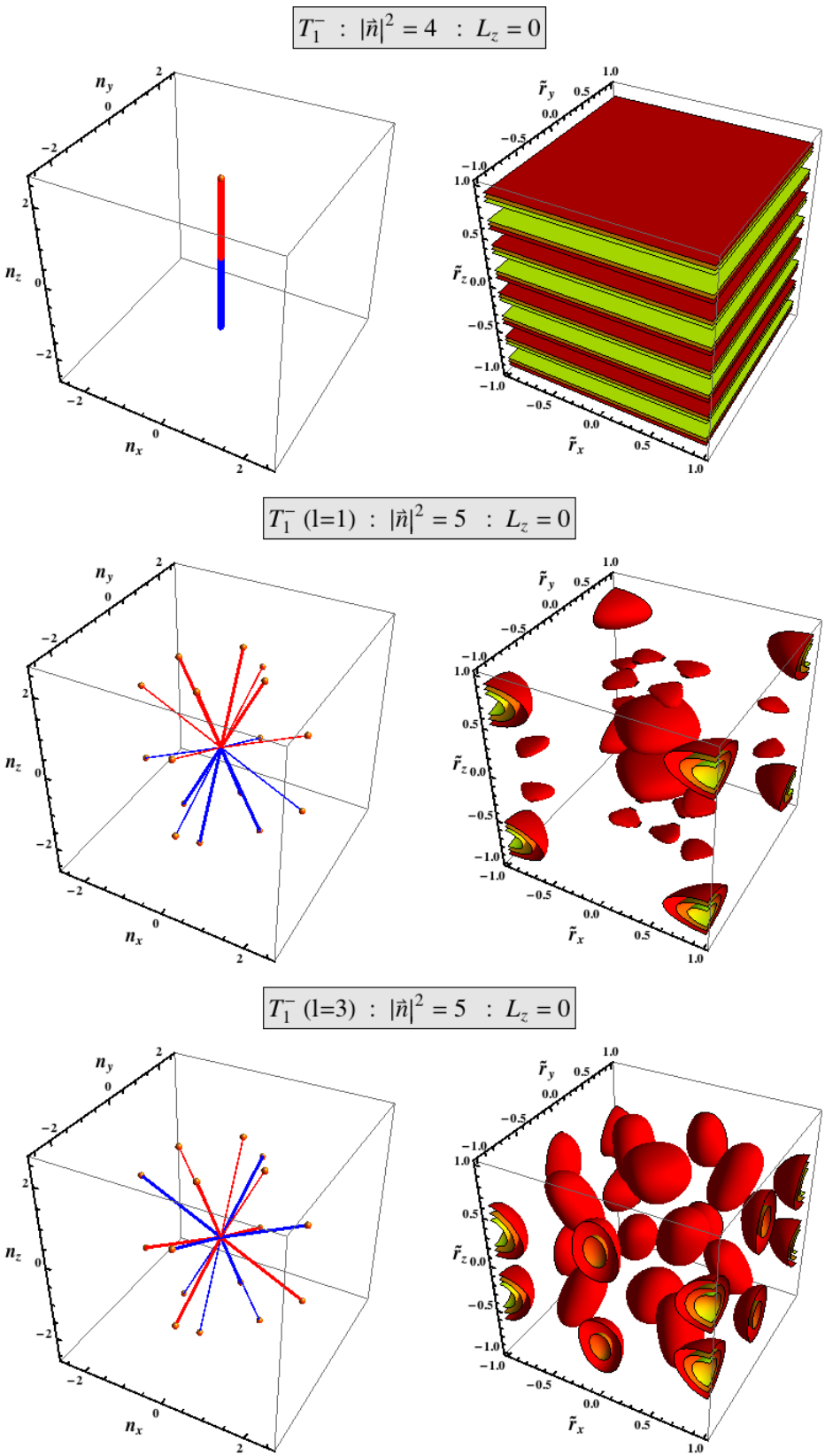

FIG. 21: The momentum-space representations (left) and position-space representations (right) of two-body relative states in the T_1^- representation with $L_z = 0$ for the $|\mathbf{n}|^2 = 4, 5$-shells.

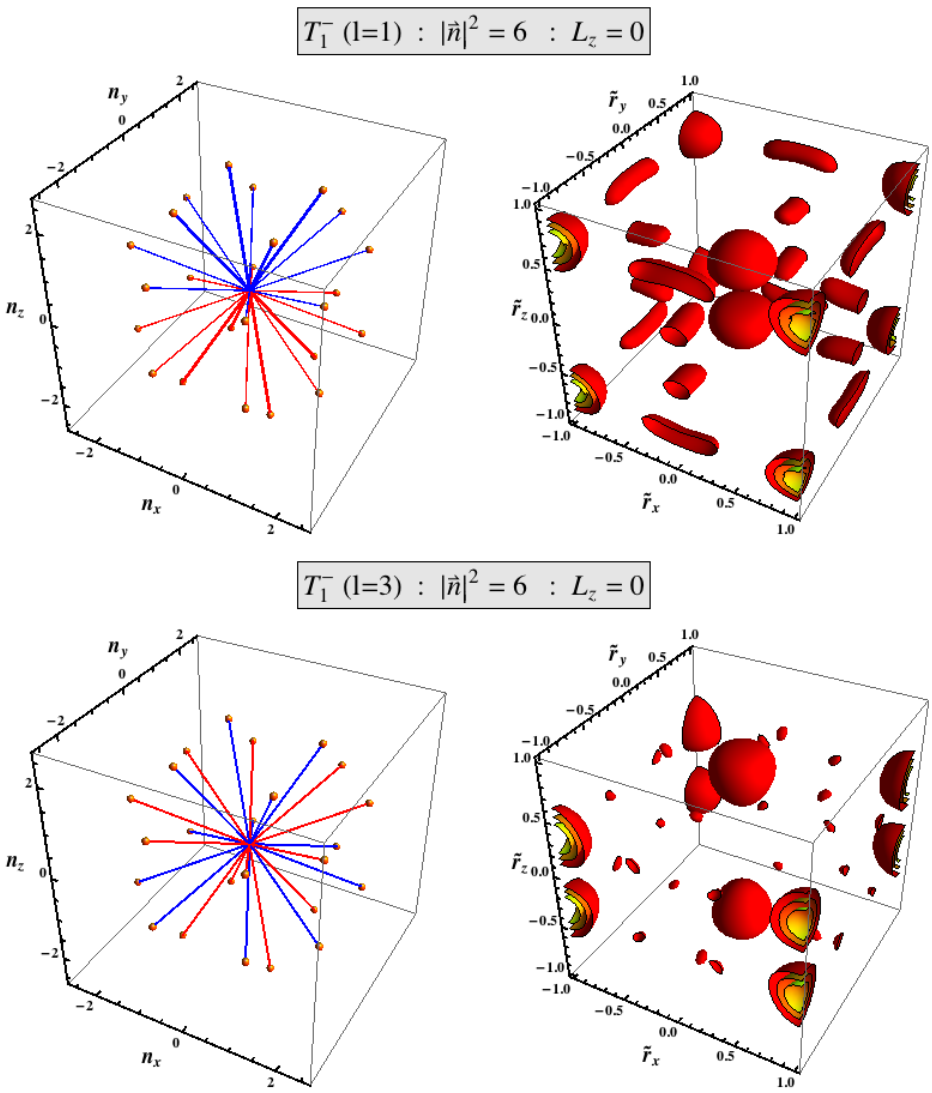

FIG. 22: The momentum-space representations (left) and position-space representations (right) of two-body relative states in the T_1^- representation with $L_z = 0$ for the $|\mathbf{n}|^2 = 6$-shells.

TABLE XVIII: The momentum-space structure of T_1^-, $L_z = 0$ sources and sinks for $|\mathbf{n}|^2$=1-4. These are shown graphically in figs. 20 and 21.

$\|\mathbf{n}\|^2$=1	$\|\mathbf{n}\|^2$=2	$\|\mathbf{n}\|^2$=3	$\|\mathbf{n}\|^2$=4
$\|(0,0,1)\ ,\ -1\rangle$ 1	$\|(1,0,1)\ ,\ -1\rangle$ $\frac{1}{2}$ $\|(1,0,-1)\ ,\ -1\rangle$ $-\frac{1}{2}$ $\|(0,1,1)\ ,\ -1\rangle$ $\frac{1}{2}$ $\|(0,1,-1)\ ,\ -1\rangle$ $-\frac{1}{2}$	$\|(1,1,1)\ ,\ -1\rangle$ $-\frac{1}{2}$ $\|(1,1,-1)\ ,\ -1\rangle$ $\frac{1}{2}$ $\|(1,-1,1)\ ,\ -1\rangle$ $-\frac{1}{2}$ $\|(1,-1,-1)\ ,\ -1\rangle$ $\frac{1}{2}$	$\|(0,0,2)\ ,\ -1\rangle$ 1

TABLE XIX: The momentum-space structure of T_1^-, $L_z = 0$ sources and sinks for $|\mathbf{n}|^2$=5 and 6. These are shown graphically in figs. 21 and 22.

$\|\mathbf{n}\|^2$=5$_{(l=1)}$	$\|\mathbf{n}\|^2$=5$_{(l=3)}$	$\|\mathbf{n}\|^2$=6$_{(l=1)}$	$\|\mathbf{n}\|^2$=6$_{(l=3)}$
		$\|(2,1,1)\ ,\ -1\rangle$ $-\frac{1}{2\sqrt{6}}$	$\|(2,1,1)\ ,\ -1\rangle$ $\frac{1}{2\sqrt{3}}$
		$\|(2,1,-1)\ ,\ -1\rangle$ $\frac{1}{2\sqrt{6}}$	$\|(2,1,-1)\ ,\ -1\rangle$ $-\frac{1}{2\sqrt{3}}$
$\|(2,0,1)\ ,\ -1\rangle$ $\frac{1}{2\sqrt{5}}$	$\|(2,0,1)\ ,\ -1\rangle$ $-\frac{1}{\sqrt{5}}$	$\|(2,-1,1)\ ,\ -1\rangle$ $-\frac{1}{2\sqrt{6}}$	$\|(2,-1,1)\ ,\ -1\rangle$ $\frac{1}{2\sqrt{3}}$
$\|(2,0,-1)\ ,\ -1\rangle$ $-\frac{1}{2\sqrt{5}}$	$\|(2,0,-1)\ ,\ -1\rangle$ $\frac{1}{\sqrt{5}}$	$\|(2,-1,-1)\ ,\ -1\rangle$ $\frac{1}{2\sqrt{6}}$	$\|(2,-1,-1)\ ,\ -1\rangle$ $-\frac{1}{2\sqrt{3}}$
$\|(1,0,2)\ ,\ -1\rangle$ $\frac{1}{\sqrt{5}}$	$\|(1,0,2)\ ,\ -1\rangle$ $\frac{1}{2\sqrt{5}}$	$\|(1,2,1)\ ,\ -1\rangle$ $-\frac{1}{2\sqrt{6}}$	$\|(1,2,1)\ ,\ -1\rangle$ $\frac{1}{2\sqrt{3}}$
$\|(1,0,-2)\ ,\ -1\rangle$ $-\frac{1}{\sqrt{5}}$	$\|(1,0,-2)\ ,\ -1\rangle$ $-\frac{1}{2\sqrt{5}}$	$\|(1,2,-1)\ ,\ -1\rangle$ $\frac{1}{2\sqrt{6}}$	$\|(1,2,-1)\ ,\ -1\rangle$ $-\frac{1}{2\sqrt{3}}$
$\|(0,2,1)\ ,\ -1\rangle$ $\frac{1}{2\sqrt{5}}$	$\|(0,2,1)\ ,\ -1\rangle$ $-\frac{1}{\sqrt{5}}$	$\|(1,1,2)\ ,\ -1\rangle$ $-\frac{1}{\sqrt{6}}$	$\|(1,1,2)\ ,\ -1\rangle$ $-\frac{1}{2\sqrt{3}}$
$\|(0,2,-1)\ ,\ -1\rangle$ $-\frac{1}{2\sqrt{5}}$	$\|(0,2,-1)\ ,\ -1\rangle$ $\frac{1}{\sqrt{5}}$	$\|(1,1,-2)\ ,\ -1\rangle$ $\frac{1}{\sqrt{6}}$	$\|(1,1,-2)\ ,\ -1\rangle$ $\frac{1}{2\sqrt{3}}$
$\|(0,1,2)\ ,\ -1\rangle$ $\frac{1}{\sqrt{5}}$	$\|(0,1,2)\ ,\ -1\rangle$ $\frac{1}{2\sqrt{5}}$	$\|(1,-1,2)\ ,\ -1\rangle$ $-\frac{1}{\sqrt{6}}$	$\|(1,-1,2)\ ,\ -1\rangle$ $-\frac{1}{2\sqrt{3}}$
$\|(0,1,-2)\ ,\ -1\rangle$ $-\frac{1}{\sqrt{5}}$	$\|(0,1,-2)\ ,\ -1\rangle$ $-\frac{1}{2\sqrt{5}}$	$\|(1,-1,-2)\ ,\ -1\rangle$ $\frac{1}{\sqrt{6}}$	$\|(1,-1,-2)\ ,\ -1\rangle$ $\frac{1}{2\sqrt{3}}$
		$\|(1,-2,1)\ ,\ -1\rangle$ $-\frac{1}{2\sqrt{6}}$	$\|(1,-2,1)\ ,\ -1\rangle$ $\frac{1}{2\sqrt{3}}$
		$\|(1,-2,-1)\ ,\ -1\rangle$ $\frac{1}{2\sqrt{6}}$	$\|(1,-2,-1)\ ,\ -1\rangle$ $-\frac{1}{2\sqrt{3}}$

TABLE XX: The momentum-space structure of T_1^-, $L_z = 1$ sources and sinks for $|\mathbf{n}|^2$=1-4.

$\|\mathbf{n}\|^2$=1	$\|\mathbf{n}\|^2$=2	$\|\mathbf{n}\|^2$=3	$\|\mathbf{n}\|^2$=4
	$\|(1,1,0)\ ,\ -1\rangle$ $\frac{i}{2}$		
	$\|(1,0,1)\ ,\ -1\rangle$ $\frac{1}{4}+\frac{i}{4}$	$\|(1,1,1)\ ,\ -1\rangle$ $\frac{1}{2}$	
$\|(1,0,0)\ ,\ -1\rangle$ $\frac{1}{\sqrt{2}}$	$\|(1,0,-1)\ ,\ -1\rangle$ $\frac{1}{4}+\frac{i}{4}$	$\|(1,1,-1)\ ,\ -1\rangle$ $\frac{1}{2}$	$\|(2,0,0)\ ,\ -1\rangle$ $\frac{1}{\sqrt{2}}$
$\|(0,1,0)\ ,\ -1\rangle$ $\frac{i}{\sqrt{2}}$	$\|(1,-1,0)\ ,\ -1\rangle$ $\frac{1}{2}$	$\|(1,-1,1)\ ,\ -1\rangle$ $-\frac{i}{2}$	$\|(0,2,0)\ ,\ -1\rangle$ $\frac{i}{\sqrt{2}}$
	$\|(0,1,1)\ ,\ -1\rangle$ $-\frac{1}{4}+\frac{i}{4}$	$\|(1,-1,-1)\ ,\ -1\rangle$ $-\frac{i}{2}$	
	$\|(0,1,-1)\ ,\ -1\rangle$ $-\frac{1}{4}+\frac{i}{4}$		

table XX. The structures of the $L_z = 3$ sources and sinks are related to those with $L_z = 1$ by complex conjugation of the coefficients.

The T_1^- irrep first appears in the $|\mathbf{n}|^2 = 1$-shell and $l = 1$ is the lowest contributing partial-wave. LQCD calculations of correlation functions from sources and sinks transforming as T_1^- will provide determinations of δ_1 with contamination from partial-waves with $l \geq 3$. LQCD calculations of the phase-shift in this partial-wave are presently being performed, and the ρ-resonance is beginning to be mapped out, e.g. Ref. [48].

4. T_2^- Representation

The energy-eigenvalues of states transforming in the T_2^- irrep receive contributions from interactions in the $l = 3, 5, ...$ partial-waves, as presented in table I. As the T_2^- irrep is three-dimensional, the contribution to the determinant in eq. (2) results from a 6×6 matrix

TABLE XXI: The momentum-space structure of T_1^-, $L_z = 1$ sources and sinks for $|\mathbf{n}|^2$=5 and 6.

$\|\mathbf{n}\|^2$=5$_{(l=1)}$		$\|\mathbf{n}\|^2$=5$_{(l=3)}$		$\|\mathbf{n}\|^2$=6$_{(l=1)}$		$\|\mathbf{n}\|^2$=6$_{(l=3)}$	
$\|(2,1,0)\ ,\ -1\rangle$	$\frac{1}{2\sqrt{2}}$	$\|(2,1,0)\ ,\ -1\rangle$	$\frac{1}{2\sqrt{2}}$	$\|(2,1,1)\ ,\ -1\rangle$	$\frac{\sqrt{\frac{5}{3}}}{4}$	$\|(2,1,1)\ ,\ -1\rangle$	$\frac{i}{2\sqrt{3}}$
$\|(2,0,1)\ ,\ -1\rangle$	$\frac{\frac{2}{5}-\frac{i}{5}}{\sqrt{2}}$	$\|(2,0,1)\ ,\ -1\rangle$	$\frac{\frac{1}{10}+\frac{i}{5}}{\sqrt{2}}$	$\|(2,1,-1)\ ,\ -1\rangle$	$\frac{\sqrt{\frac{5}{3}}}{4}$	$\|(2,1,-1)\ ,\ -1\rangle$	$\frac{i}{2\sqrt{3}}$
$\|(2,0,-1)\ ,\ -1\rangle$	$\frac{\frac{2}{5}-\frac{i}{5}}{\sqrt{2}}$	$\|(2,0,-1)\ ,\ -1\rangle$	$\frac{\frac{1}{10}+\frac{i}{5}}{\sqrt{2}}$	$\|(2,-1,1)\ ,\ -1\rangle$	$\frac{\frac{3}{4}-i}{\sqrt{15}}$	$\|(2,-1,1)\ ,\ -1\rangle$	$-\frac{1}{2\sqrt{3}}$
$\|(2,-1,0)\ ,\ -1\rangle$	$\frac{\frac{3}{10}-\frac{2i}{5}}{\sqrt{2}}$	$\|(2,-1,0)\ ,\ -1\rangle$	$-\frac{\frac{3}{10}-\frac{2i}{5}}{\sqrt{2}}$	$\|(2,-1,-1)\ ,\ -1\rangle$	$\frac{\frac{3}{4}-i}{\sqrt{15}}$	$\|(2,-1,-1)\ ,\ -1\rangle$	$-\frac{1}{2\sqrt{3}}$
$\|(1,2,0)\ ,\ -1\rangle$	$\frac{\frac{2}{5}+\frac{3i}{10}}{\sqrt{2}}$	$\|(1,2,0)\ ,\ -1\rangle$	$-\frac{\frac{2}{5}+\frac{3i}{10}}{\sqrt{2}}$	$\|(1,2,1)\ ,\ -1\rangle$	$\frac{1+\frac{3i}{4}}{\sqrt{15}}$	$\|(1,2,1)\ ,\ -1\rangle$	$-\frac{i}{2\sqrt{3}}$
$\|(1,0,2)\ ,\ -1\rangle$	$\frac{\frac{1}{5}-\frac{i}{10}}{\sqrt{2}}$	$\|(1,0,2)\ ,\ -1\rangle$	$-\frac{\frac{1}{5}+\frac{2i}{5}}{\sqrt{2}}$	$\|(1,2,-1)\ ,\ -1\rangle$	$\frac{1+\frac{3i}{4}}{\sqrt{15}}$	$\|(1,2,-1)\ ,\ -1\rangle$	$-\frac{i}{2\sqrt{3}}$
$\|(1,0,-2)\ ,\ -1\rangle$	$\frac{\frac{1}{5}-\frac{i}{10}}{\sqrt{2}}$	$\|(1,0,-2)\ ,\ -1\rangle$	$-\frac{\frac{1}{5}+\frac{2i}{5}}{\sqrt{2}}$	$\|(1,1,2)\ ,\ -1\rangle$	$\frac{1}{2}\sqrt{\frac{2}{15}+\frac{i}{10}}$	$\|(1,1,2)\ ,\ -1\rangle$	$\frac{1}{2\sqrt{3}}$
$\|(1,-2,0)\ ,\ -1\rangle$	$-\frac{i}{2\sqrt{2}}$	$\|(1,-2,0)\ ,\ -1\rangle$	$-\frac{i}{2\sqrt{2}}$	$\|(1,1,-2)\ ,\ -1\rangle$	$\frac{1}{2}\sqrt{\frac{2}{15}+\frac{i}{10}}$	$\|(1,1,-2)\ ,\ -1\rangle$	$\frac{1}{2\sqrt{3}}$
$\|(0,2,1)\ ,\ -1\rangle$	$\frac{\frac{1}{5}+\frac{2i}{5}}{\sqrt{2}}$	$\|(0,2,1)\ ,\ -1\rangle$	$-\frac{\frac{1}{5}-\frac{i}{10}}{\sqrt{2}}$	$\|(1,-1,2)\ ,\ -1\rangle$	$\frac{1}{2}\sqrt{-\frac{2}{15}-\frac{i}{10}}$	$\|(1,-1,2)\ ,\ -1\rangle$	$-\frac{i}{2\sqrt{3}}$
$\|(0,2,-1)\ ,\ -1\rangle$	$\frac{\frac{1}{5}+\frac{2i}{5}}{\sqrt{2}}$	$\|(0,2,-1)\ ,\ -1\rangle$	$-\frac{\frac{1}{5}-\frac{i}{10}}{\sqrt{2}}$	$\|(1,-1,-2)\ ,\ -1\rangle$	$\frac{1}{2}\sqrt{-\frac{2}{15}-\frac{i}{10}}$	$\|(1,-1,-2)\ ,\ -1\rangle$	$-\frac{i}{2\sqrt{3}}$
$\|(0,1,2)\ ,\ -1\rangle$	$\frac{\frac{1}{10}+\frac{i}{5}}{\sqrt{2}}$	$\|(0,1,2)\ ,\ -1\rangle$	$\frac{\frac{2}{5}-\frac{i}{5}}{\sqrt{2}}$	$\|(1,-2,1)\ ,\ -1\rangle$	$-\frac{1}{4}i\sqrt{\frac{5}{3}}$	$\|(1,-2,1)\ ,\ -1\rangle$	$\frac{1}{2\sqrt{3}}$
$\|(0,1,-2)\ ,\ -1\rangle$	$\frac{\frac{1}{10}+\frac{i}{5}}{\sqrt{2}}$	$\|(0,1,-2)\ ,\ -1\rangle$	$\frac{\frac{2}{5}-\frac{i}{5}}{\sqrt{2}}$	$\|(1,-2,-1)\ ,\ -1\rangle$	$-\frac{1}{4}i\sqrt{\frac{5}{3}}$	$\|(1,-2,-1)\ ,\ -1\rangle$	$\frac{1}{2\sqrt{3}}$

for $l \leq 6$, which collapses down to the determinant of a 2×2 matrix as the $L_z = 1$, $L_z = 2$ and $L_z = 3$ states are degenerate. The T_2^- $L_z = 2$ states associated with the $\overline{F}_{3;3}^{(FV)}$ and $F_{5;5}^{(FV)}$ blocks are

$$
\begin{aligned}
|T_2^-, 2; 3; 1\rangle &= \frac{1}{\sqrt{2}}|3, 2\rangle + \frac{1}{\sqrt{2}}|3, -2\rangle \\
|T_2^-, 2; 5; 1\rangle &= \frac{1}{\sqrt{2}}|5, 2\rangle + \frac{1}{\sqrt{2}}|5, -2\rangle \quad ,
\end{aligned}
$$

in terms of which, the T_2^- contribution to eq. (2) becomes

$$
\det\left[\begin{pmatrix} \cot\delta_3 & 0 \\ 0 & \cot\delta_5 \end{pmatrix} - \begin{pmatrix} \overline{F}_{3;3}^{(FV,T_2^-)} & \overline{F}_{3;5}^{(FV,T_2^-)} \\ \overline{F}_{5;3}^{(FV,T_2^-)} & \overline{F}_{5;5}^{(FV,T_2^-)} \end{pmatrix}\right] = 0 \quad , \tag{37}
$$

where

$$
\begin{aligned}
\overline{F}_{3;3}^{(FV,T_2^-)} &= \frac{\mathcal{Z}_{0,0}\left(1;\tilde{q}^2\right)}{\pi^{3/2}\tilde{q}} - \frac{2\mathcal{Z}_{4,0}\left(1;\tilde{q}^2\right)}{11\pi^{3/2}\tilde{q}^5} - \frac{60\mathcal{Z}_{6,0}\left(1;\tilde{q}^2\right)}{11\sqrt{13}\pi^{3/2}\tilde{q}^7} \\
\overline{F}_{3;5}^{(FV,T_2^-)} &= -\frac{20\mathcal{Z}_{4,0}\left(1;\tilde{q}^2\right)}{13\sqrt{11}\pi^{3/2}\tilde{q}^5} - \frac{14\mathcal{Z}_{6,0}\left(1;\tilde{q}^2\right)}{\sqrt{143}\pi^{3/2}\tilde{q}^7} + \frac{112\mathcal{Z}_{8,0}\left(1;\tilde{q}^2\right)}{13\sqrt{187}\pi^{3/2}\tilde{q}^9} \\
\overline{F}_{5;5}^{(FV,T_2^-)} &= \frac{\mathcal{Z}_{0,0}\left(1;\tilde{q}^2\right)}{\pi^{3/2}\tilde{q}} + \frac{4\mathcal{Z}_{4,0}\left(1;\tilde{q}^2\right)}{13\pi^{3/2}\tilde{q}^5} - \frac{80\mathcal{Z}_{6,0}\left(1;\tilde{q}^2\right)}{17\sqrt{13}\pi^{3/2}\tilde{q}^7} - \frac{280\mathcal{Z}_{8,0}\left(1;\tilde{q}^2\right)}{247\sqrt{17}\pi^{3/2}\tilde{q}^9} - \frac{432\sqrt{21}\mathcal{Z}_{10,0}\left(1;\tilde{q}^2\right)}{4199\pi^{3/2}\tilde{q}^{11}} \quad .
\end{aligned}
$$

TABLE XXII: The momentum-space structure of T_2^-, $L_z = 2$ sources and sinks. These are shown graphically in figs. 24 and 25.

$\|\mathbf{n}\|^2$=2	$\|\mathbf{n}\|^2$=5$_{(l=3)}$	$\|\mathbf{n}\|^2$=5$_{(l=5)}$	$\|\mathbf{n}\|^2$=6
	$\|(2,0,1)\ ,\ -1\rangle\ \ -\frac{1}{\sqrt{5}}$	$\|(2,0,1)\ ,\ -1\rangle\ \ \frac{1}{2\sqrt{5}}$	$\|(2,1,1)\ ,\ -1\rangle\ \ -\frac{1}{2\sqrt{2}}$
	$\|(2,0,-1)\ ,\ -1\rangle\ \ \frac{1}{\sqrt{5}}$	$\|(2,0,-1)\ ,\ -1\rangle\ \ -\frac{1}{2\sqrt{5}}$	$\|(2,1,-1)\ ,\ -1\rangle\ \ \frac{1}{2\sqrt{2}}$
$\|(1,0,1)\ ,\ -1\rangle\ \ -\frac{1}{2}$	$\|(1,0,2)\ ,\ -1\rangle\ \ -\frac{1}{2\sqrt{5}}$	$\|(1,0,2)\ ,\ -1\rangle\ \ -\frac{1}{\sqrt{5}}$	$\|(2,-1,1)\ ,\ -1\rangle\ \ -\frac{1}{2\sqrt{2}}$
$\|(1,0,-1)\ ,\ -1\rangle\ \ \frac{1}{2}$	$\|(1,0,-2)\ ,\ -1\rangle\ \ \frac{1}{2\sqrt{5}}$	$\|(1,0,-2)\ ,\ -1\rangle\ \ \frac{1}{\sqrt{5}}$	$\|(2,-1,-1)\ ,\ -1\rangle\ \ \frac{1}{2\sqrt{2}}$
$\|(0,1,1)\ ,\ -1\rangle\ \ \frac{1}{2}$	$\|(0,2,1)\ ,\ -1\rangle\ \ \frac{1}{\sqrt{5}}$	$\|(0,2,1)\ ,\ -1\rangle\ \ -\frac{1}{2\sqrt{5}}$	$\|(1,2,1)\ ,\ -1\rangle\ \ \frac{1}{2\sqrt{2}}$
$\|(0,1,-1)\ ,\ -1\rangle\ \ -\frac{1}{2}$	$\|(0,2,-1)\ ,\ -1\rangle\ \ -\frac{1}{\sqrt{5}}$	$\|(0,2,-1)\ ,\ -1\rangle\ \ \frac{1}{2\sqrt{5}}$	$\|(1,2,-1)\ ,\ -1\rangle\ \ -\frac{1}{2\sqrt{2}}$
	$\|(0,1,2)\ ,\ -1\rangle\ \ \frac{1}{2\sqrt{5}}$	$\|(0,1,2)\ ,\ -1\rangle\ \ \frac{1}{\sqrt{5}}$	$\|(1,-2,1)\ ,\ -1\rangle\ \ \frac{1}{2\sqrt{2}}$
	$\|(0,1,-2)\ ,\ -1\rangle\ \ -\frac{1}{2\sqrt{5}}$	$\|(0,1,-2)\ ,\ -1\rangle\ \ -\frac{1}{\sqrt{5}}$	$\|(1,-2,-1)\ ,\ -1\rangle\ \ -\frac{1}{2\sqrt{2}}$

The solutions to this equation result from

$$\frac{\cot\delta_3}{2}+\frac{\cot\delta_5}{2}-\frac{\mathcal{Z}_{0,0}\left(1;\tilde{q}^2\right)}{\pi^{3/2}\tilde{q}}-\frac{9\mathcal{Z}_{4,0}\left(1;\tilde{q}^2\right)}{143\pi^{3/2}\tilde{q}^5}+\frac{950\mathcal{Z}_{6,0}\left(1;\tilde{q}^2\right)}{187\sqrt{13}\pi^{3/2}\tilde{q}^7}+\frac{140\mathcal{Z}_{8,0}\left(1;\tilde{q}^2\right)}{247\sqrt{17}\pi^{3/2}\tilde{q}^9}+\frac{216\sqrt{21}\mathcal{Z}_{10,0}\left(1;\tilde{q}^2\right)}{4199\pi^{3/2}\tilde{q}^{11}}=$$
$$\pm\frac{1}{2}\left[\left(-\frac{432\sqrt{21}\mathcal{Z}_{10,0}\left(1;\tilde{q}^2\right)}{4199\pi^{3/2}\tilde{q}^{11}}+\frac{70\mathcal{Z}_{4,0}\left(1;\tilde{q}^2\right)}{143\pi^{3/2}\tilde{q}^5}+\frac{140\mathcal{Z}_{6,0}\left(1;\tilde{q}^2\right)}{187\sqrt{13}\pi^{3/2}\tilde{q}^7}-\frac{280\mathcal{Z}_{8,0}\left(1;\tilde{q}^2\right)}{247\sqrt{17}\pi^{3/2}\tilde{q}^9}+\cot\delta_3-\cot\delta_5\right)^2\right.$$
$$\left.+\frac{4}{\pi^3}\left(\frac{20\mathcal{Z}_{4,0}\left(1;\tilde{q}^2\right)}{13\sqrt{11}\tilde{q}^5}+\frac{14\mathcal{Z}_{6,0}\left(1;\tilde{q}^2\right)}{\sqrt{143}\tilde{q}^7}-\frac{112\mathcal{Z}_{8,0}\left(1;\tilde{q}^2\right)}{13\sqrt{187}\tilde{q}^9}\right)^2\right]^{1/2}\quad . \tag{38}$$

In the limit of vanishing interactions in the $l = 5$ partial-wave, eq. (37) collapses down to

$$\begin{aligned} q^7\cot\delta_3 &= \left(\frac{2\pi}{L}\right)^7\frac{1}{\pi^{3/2}}\left(\tilde{q}^6\mathcal{Z}_{0,0}\left(1;\tilde{q}^2\right)-\frac{2\tilde{q}^2\mathcal{Z}_{4,0}\left(1;\tilde{q}^2\right)}{11}-\frac{60\mathcal{Z}_{6,0}\left(1;\tilde{q}^2\right)}{11\sqrt{13}}\right) \\ &\equiv \left(\frac{2\pi}{L}\right)^7\frac{1}{\pi^{3/2}}\ \mathcal{X}_{T_2}^-\left(\tilde{q}^2\right)\quad , \end{aligned} \tag{39}$$

where the function $\mathcal{X}_{T_2}^-\left(\tilde{q}^2\right)$ is shown in fig. 23. The graphical representations of the source and sink that generate the T_2^- irrep for the lowest-lying $|\mathbf{n}|^2$-shell are shown in fig. 24 and fig. 25, and the momentum-space structure is given explicitly in tables XXII and table XXIII. The structures of the $L_z = 3$ sources and sinks are related to those with $L_z = 1$ by complex conjugation of the coefficients.

The T_2^- irrep first appears in the $|\mathbf{n}|^2 = 2$-shell and $l = 3$ is the lowest contributing partial-wave. LQCD calculations of correlation functions from sources and sinks transforming as T_2^- will provide determinations of δ_3 with contamination from partial-waves with $l \geq 5$.

5. A_1^- *Representation*

The lowest-lying state transforming in the A_1^- irrep is in the $|\mathbf{n}|^2 = 14$-shell. The energy-eigenvalues are sensitive to interactions in odd partial-waves with $l \geq 9$, and the energy-

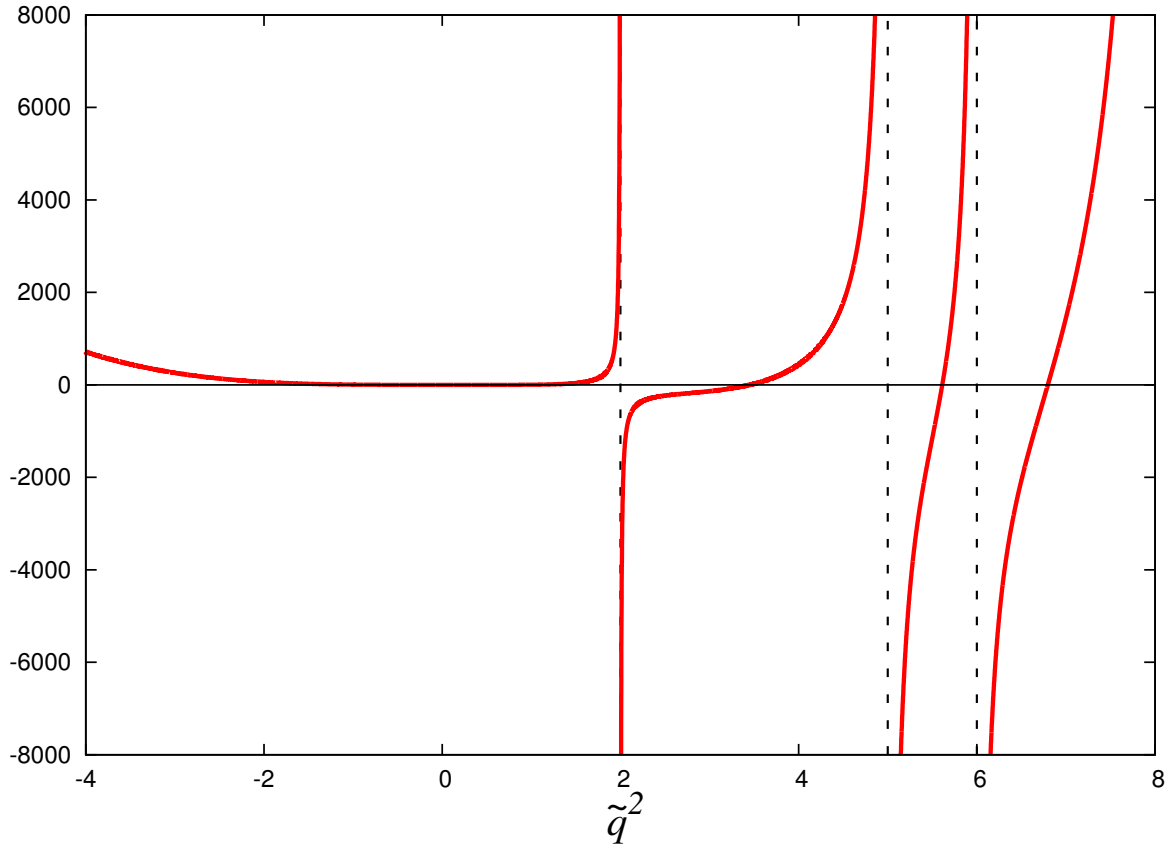

FIG. 23: The function $\mathcal{X}^{-}_{T_2}$, as defined in eq. (39), as a function of $\tilde{q}^2$. The vertical dashed lines denote the position of the poles of the function corresponding to the non-interacting energy-eigenvalues.

splitting in the large volume limit is dominated by the $l = 9$ partial-wave. Using the methods of the previous section to isolate the state and determine the appropriate energy-eigenvalue equation is tedious as $F^{(FV)}_{9;9}$ is a 19×19 matrix. Using the following spherical basis state,

$$|A_1^-, 0; 9; 1\rangle = \frac{1}{4}\sqrt{\frac{7}{3}}\left(|9,8\rangle - |9,-8\rangle\right) - \frac{1}{4}\sqrt{\frac{17}{3}}\left(|9,4\rangle - |9,-4\rangle\right) \ , \tag{40}$$

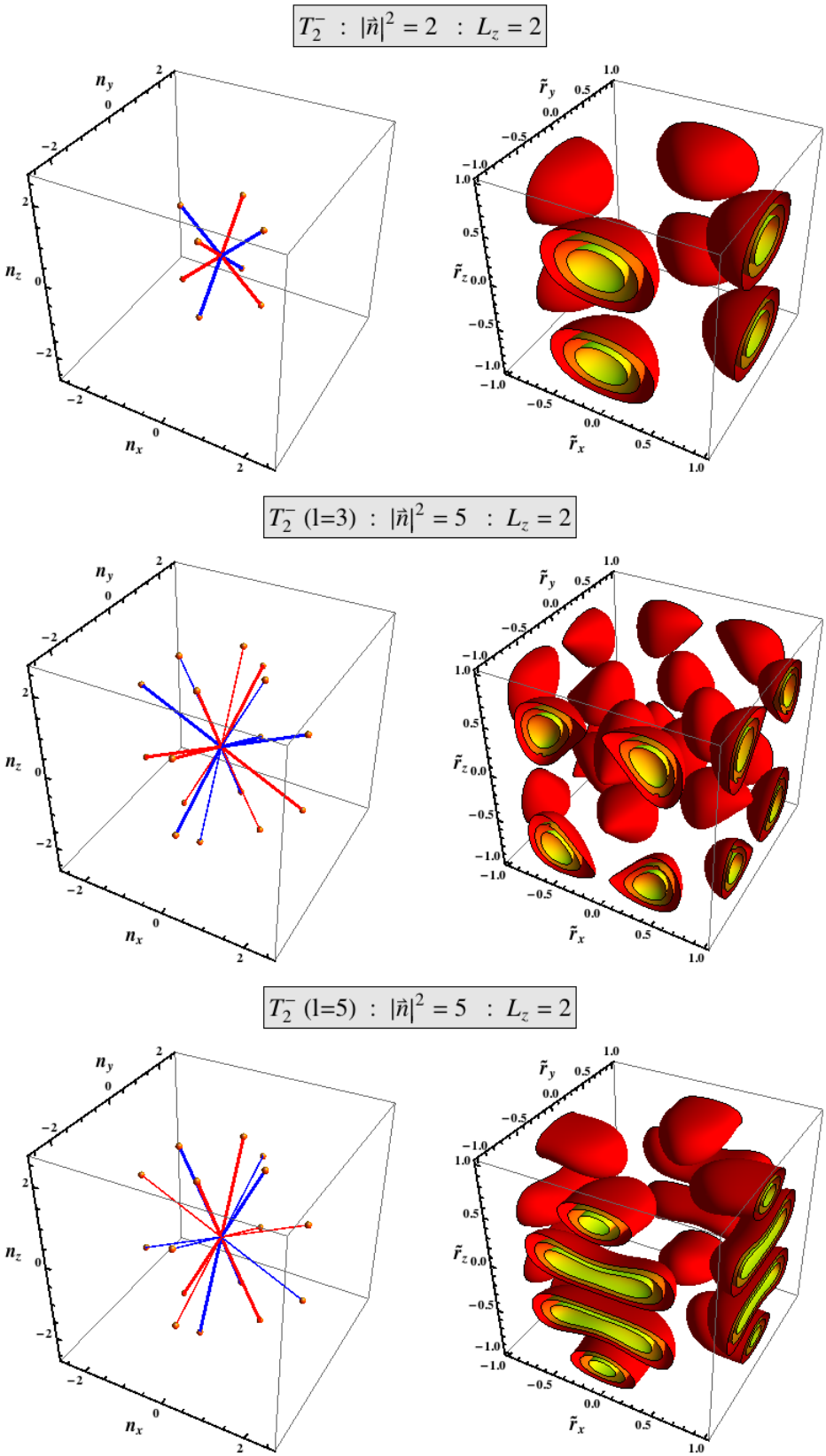

FIG. 24: The momentum-space representations (left) and position-space representations (right) of two-body relative states in the T_2^- representation with $L_z = 2$ for select $|\mathbf{n}|^2$-shells.

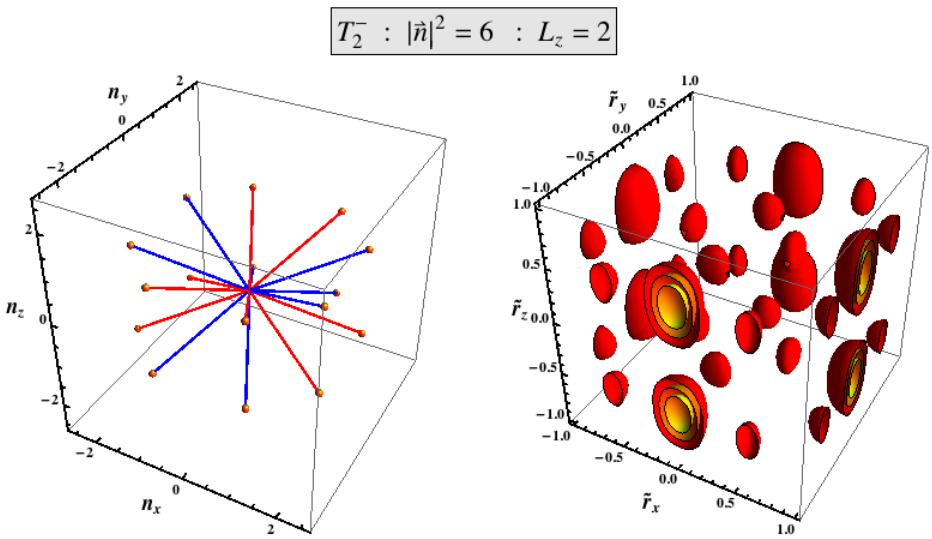

FIG. 25: The momentum space representations (left) and position-space representations (right) of two-body relative states in the T_2^- representation with $L_z = 2$ for the $|\mathbf{n}|^2 = 6$-shell.

TABLE XXIII: The momentum-space structure of T_2^-, $L_z = 1$ sources and sinks.

$\|\mathbf{n}\|^2$=2		$\|\mathbf{n}\|^2$=$5_{(l=3)}$		$\|\mathbf{n}\|^2$=$5_{(l=5)}$		$\|\mathbf{n}\|^2$=6	
		$\|(2,1,0)\ ,\ -1\rangle$	$\frac{1}{2\sqrt{2}}$	$\|(2,1,0)\ ,\ -1\rangle$	$\frac{1}{2\sqrt{2}}$		
		$\|(2,0,1)\ ,\ -1\rangle$	$-\frac{\frac{1}{10}-\frac{i}{5}}{\sqrt{2}}$	$\|(2,0,1)\ ,\ -1\rangle$	$-\frac{\frac{2}{5}+\frac{i}{5}}{\sqrt{2}}$	$\|(2,1,1)\ ,\ -1\rangle$	$\frac{1}{4}$
		$\|(2,0,-1)\ ,\ -1\rangle$	$-\frac{\frac{1}{10}-\frac{i}{5}}{\sqrt{2}}$	$\|(2,0,-1)\ ,\ -1\rangle$	$-\frac{\frac{2}{5}+\frac{i}{5}}{\sqrt{2}}$	$\|(2,1,-1)\ ,\ -1\rangle$	$\frac{1}{4}$
		$\|(2,-1,0)\ ,\ -1\rangle$	$-\frac{\frac{3}{10}+\frac{2i}{5}}{\sqrt{2}}$	$\|(2,-1,0)\ ,\ -1\rangle$	$\frac{\frac{3}{10}+\frac{2i}{5}}{\sqrt{2}}$	$\|(2,-1,1)\ ,\ -1\rangle$	$-\frac{1}{4}$
$\|(1,1,0)\ ,\ -1\rangle$	$\frac{1}{2}$	$\|(1,2,0)\ ,\ -1\rangle$	$\frac{\frac{2}{5}-\frac{3i}{10}}{\sqrt{2}}$	$\|(1,2,0)\ ,\ -1\rangle$	$-\frac{\frac{2}{5}-\frac{3i}{10}}{\sqrt{2}}$	$\|(2,-1,-1)\ ,\ -1\rangle$	$-\frac{1}{4}$
$\|(1,0,1)\ ,\ -1\rangle$	$-\frac{1}{4}+\frac{i}{4}$	$\|(1,0,2)\ ,\ -1\rangle$	$-\frac{\frac{1}{5}-\frac{2i}{5}}{\sqrt{2}}$	$\|(1,0,2)\ ,\ -1\rangle$	$\frac{\frac{1}{5}+\frac{i}{10}}{\sqrt{2}}$	$\|(1,2,1)\ ,\ -1\rangle$	$-\frac{i}{4}$
$\|(1,0,-1)\ ,\ -1\rangle$	$-\frac{1}{4}+\frac{i}{4}$	$\|(1,0,-2)\ ,\ -1\rangle$	$-\frac{\frac{1}{5}-\frac{2i}{5}}{\sqrt{2}}$	$\|(1,0,-2)\ ,\ -1\rangle$	$\frac{\frac{1}{5}+\frac{i}{10}}{\sqrt{2}}$	$\|(1,2,-1)\ ,\ -1\rangle$	$-\frac{i}{4}$
$\|(1,-1,0)\ ,\ -1\rangle$	$-\frac{i}{2}$	$\|(1,-2,0)\ ,\ -1\rangle$	$-\frac{i}{2\sqrt{2}}$	$\|(1,-2,0)\ ,\ -1\rangle$	$-\frac{i}{2\sqrt{2}}$	$\|(1,1,2)\ ,\ -1\rangle$	$-\frac{1}{4}+\frac{i}{4}$
$\|(0,1,1)\ ,\ -1\rangle$	$-\frac{1}{4}-\frac{i}{4}$	$\|(0,2,1)\ ,\ -1\rangle$	$-\frac{\frac{1}{5}+\frac{i}{10}}{\sqrt{2}}$	$\|(0,2,1)\ ,\ -1\rangle$	$\frac{\frac{1}{5}-\frac{2i}{5}}{\sqrt{2}}$	$\|(1,1,-2)\ ,\ -1\rangle$	$-\frac{1}{4}+\frac{i}{4}$
$\|(0,1,-1)\ ,\ -1\rangle$	$-\frac{1}{4}-\frac{i}{4}$	$\|(0,2,-1)\ ,\ -1\rangle$	$-\frac{\frac{1}{5}+\frac{i}{10}}{\sqrt{2}}$	$\|(0,2,-1)\ ,\ -1\rangle$	$\frac{\frac{1}{5}-\frac{2i}{5}}{\sqrt{2}}$	$\|(1,-1,2)\ ,\ -1\rangle$	$\frac{1}{4}+\frac{i}{4}$
		$\|(0,1,2)\ ,\ -1\rangle$	$-\frac{\frac{2}{5}+\frac{i}{5}}{\sqrt{2}}$	$\|(0,1,2)\ ,\ -1\rangle$	$-\frac{\frac{1}{10}-\frac{i}{5}}{\sqrt{2}}$	$\|(1,-1,-2)\ ,\ -1\rangle$	$\frac{1}{4}+\frac{i}{4}$
		$\|(0,1,-2)\ ,\ -1\rangle$	$-\frac{\frac{2}{5}+\frac{i}{5}}{\sqrt{2}}$	$\|(0,1,-2)\ ,\ -1\rangle$	$-\frac{\frac{1}{10}-\frac{i}{5}}{\sqrt{2}}$	$\|(1,-2,1)\ ,\ -1\rangle$	$-\frac{i}{4}$
						$\|(1,-2,-1)\ ,\ -1\rangle$	$-\frac{i}{4}$

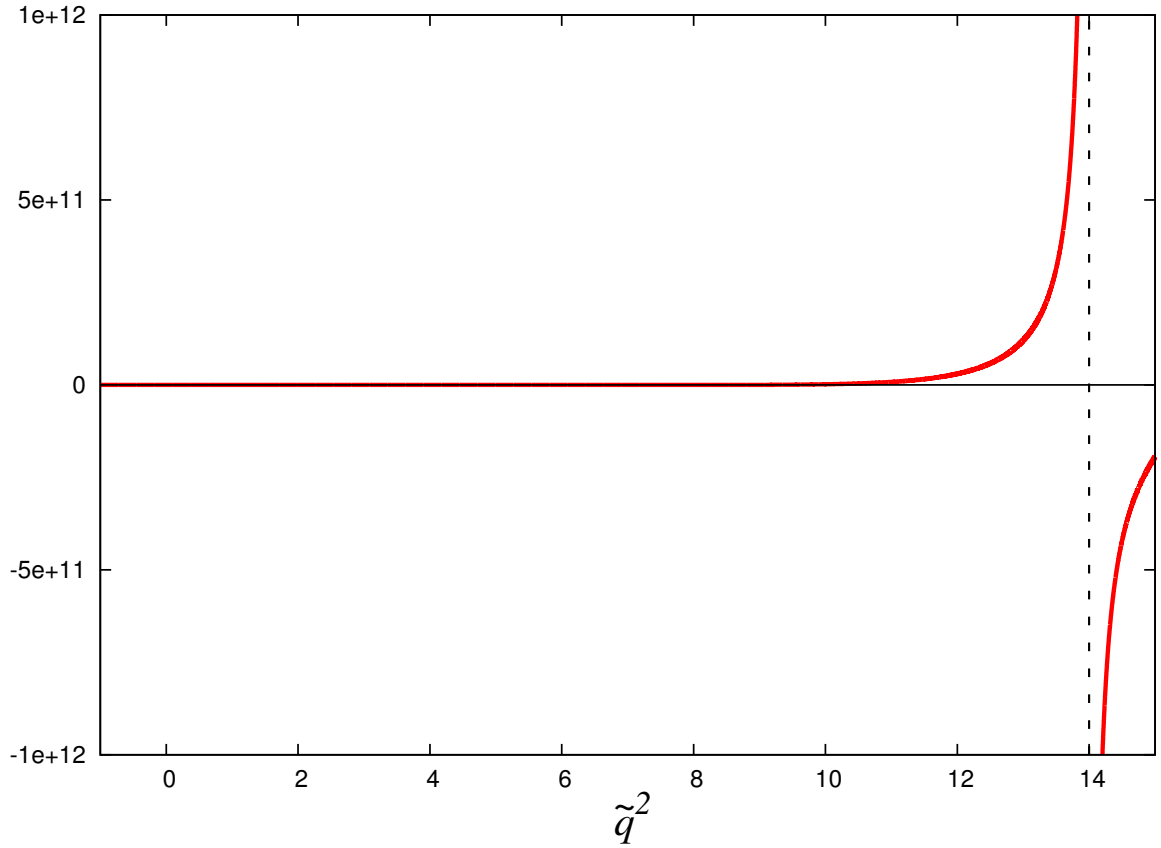

FIG. 26: The function $\mathcal{X}^-_{A_1}$, as defined in eq. (41), as a function of $\tilde{q}^2$. The vertical dashed line denotes the position of the first pole of the function corresponding to the non-interacting energy-eigenvalue.

the eigenvalue-equation for the interaction in the $l = 9$ partial-wave is

$$
\begin{aligned}
q^{19}\cot\delta_9 \;=\; & \left(\frac{2\pi}{L}\right)^{19} \frac{1}{\pi^{3/2}} \left(\tilde{q}^{18}\mathcal{Z}_{0,0}(1;\tilde{q}^2) - \frac{6\tilde{q}^{14}\mathcal{Z}_{4,0}(1;\tilde{q}^2)}{23} - \frac{32\sqrt{13}\tilde{q}^{12}\mathcal{Z}_{6,0}(1;\tilde{q}^2)}{115}\right. \\
& - \frac{56\sqrt{17}\tilde{q}^{10}\mathcal{Z}_{8,0}(1;\tilde{q}^2)}{345} + \frac{1568\sqrt{7}\tilde{q}^{8}\mathcal{Z}_{10,0}(1;\tilde{q}^2)}{3335\sqrt{3}} + \frac{308\tilde{q}^{6}\mathcal{Z}_{12,0}(1;\tilde{q}^2)}{2139} \\
& + \frac{616\sqrt{1001}\tilde{q}^{6}\mathcal{Z}_{12,4}(1;\tilde{q}^2)}{20677} + \frac{53248\tilde{q}^{4}\mathcal{Z}_{14,0}(1;\tilde{q}^2)}{10695\sqrt{29}} - \frac{1664\sqrt{11}\tilde{q}^{2}\mathcal{Z}_{16,0}(1;\tilde{q}^2)}{3565\sqrt{3}} \\
& \left. + \frac{832\sqrt{46189}\tilde{q}^{2}\mathcal{Z}_{16,4}(1;\tilde{q}^2)}{103385\sqrt{7}} + \frac{2206464\tilde{\mathcal{Z}}_{18,0}(1;\tilde{q}^2)}{103385\sqrt{37}} + \frac{28288\sqrt{3553}\mathcal{Z}_{18,4}(1;\tilde{q}^2)}{20677\sqrt{259}}\right) \\
= \; & \left(\frac{2\pi}{L}\right)^{19} \frac{1}{\pi^{3/2}} \; \mathcal{X}^-_{A_1}\left(\tilde{q}^2\right) \quad , \qquad (41)
\end{aligned}
$$

where the function $\mathcal{X}^-_{A_1}(\tilde{q}^2)$ is shown in fig. 26. The graphical representations of the source and sink that generate the A_1^- irrep for the $|\mathbf{n}|^2 = 14$-shell are shown in fig. 27, and the momentum-space structure is given explicitly in table XXIV. It is interesting to note that these odd-parity singlet states require the integers comprising the integer triplet to differ

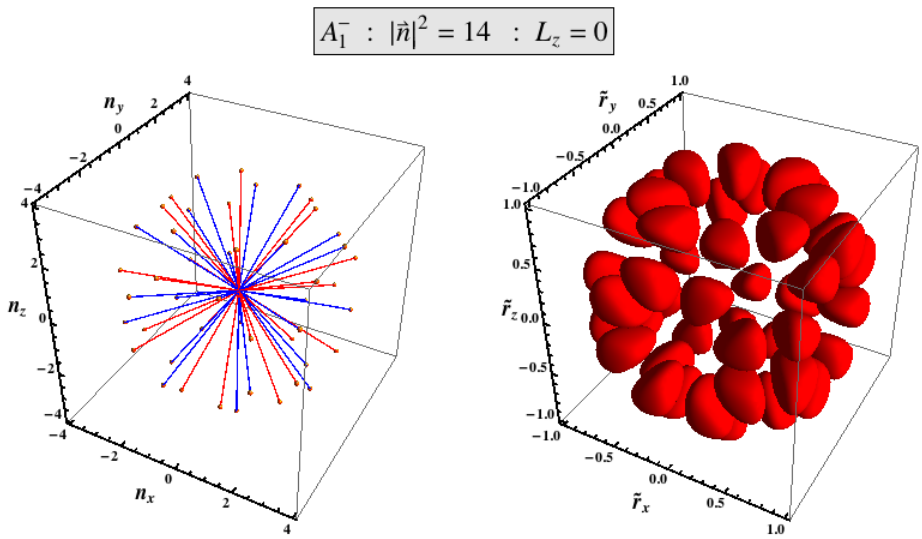

FIG. 27: The momentum space representations (left) and position-space representations (right) of two-body relative states in the A_1^- representation with $L_z = 0$ for the $|\mathbf{n}^2| = 14$-shell.

TABLE XXIV: The momentum-space structure of A_1^-, $L_z = 0$ sources and sinks. These are shown graphically in fig. 27. The coefficients of the state vectors are of the form $c_i \sim \varepsilon^{|n_x|,|n_y|,|n_z|}\mathrm{sgn}(n_x)\mathrm{sgn}(n_y)\mathrm{sgn}(n_z)$.

$\|\mathbf{n}\|^2$=14					
$\|(1,2,3)\ ,\ -1\rangle$	$\frac{1}{\sqrt{24}}$	$\|(1,2,-3)\ ,\ -1\rangle$	$-\frac{1}{\sqrt{24}}$	$\|(1,-2,3)\ ,\ -1\rangle$	$-\frac{1}{\sqrt{24}}$
$\|(1,-2,-3)\ ,\ -1\rangle$	$\frac{1}{\sqrt{24}}$	$\|(1,3,2)\ ,\ -1\rangle$	$-\frac{1}{\sqrt{24}}$	$\|(1,3,-2)\ ,\ -1\rangle$	$\frac{1}{\sqrt{24}}$
$\|(1,-3,2)\ ,\ -1\rangle$	$\frac{1}{\sqrt{24}}$	$\|(1,-3,-2)\ ,\ -1\rangle$	$-\frac{1}{\sqrt{24}}$	$\|(2,1,3)\ ,\ -1\rangle$	$-\frac{1}{\sqrt{24}}$
$\|(2,1,-3)\ ,\ -1\rangle$	$\frac{1}{\sqrt{24}}$	$\|(2,-1,3)\ ,\ -1\rangle$	$\frac{1}{\sqrt{24}}$	$\|(2,-1,-3)\ ,\ -1\rangle$	$-\frac{1}{\sqrt{24}}$
$\|(2,3,1)\ ,\ -1\rangle$	$\frac{1}{\sqrt{24}}$	$\|(2,3,-1)\ ,\ -1\rangle$	$-\frac{1}{\sqrt{24}}$	$\|(2,-3,1)\ ,\ -1\rangle$	$-\frac{1}{\sqrt{24}}$
$\|(2,-3,-1)\ ,\ -1\rangle$	$\frac{1}{\sqrt{24}}$	$\|(3,2,1)\ ,\ -1\rangle$	$-\frac{1}{\sqrt{24}}$	$\|(3,2,-1)\ ,\ -1\rangle$	$\frac{1}{\sqrt{24}}$
$\|(3,-2,1)\ ,\ -1\rangle$	$\frac{1}{\sqrt{24}}$	$\|(3,-2,-1)\ ,\ -1\rangle$	$-\frac{1}{\sqrt{24}}$	$\|(3,1,2)\ ,\ -1\rangle$	$\frac{1}{\sqrt{24}}$
$\|(3,1,-2)\ ,\ -1\rangle$	$-\frac{1}{\sqrt{24}}$	$\|(3,-1,2)\ ,\ -1\rangle$	$-\frac{1}{\sqrt{24}}$	$\|(3,-1,-2)\ ,\ -1\rangle$	$\frac{1}{\sqrt{24}}$

from each other. The first $|\mathbf{n}|^2$-shell for which this is possible has $|\mathbf{n}|^2 = 14$, and the next has $|\mathbf{n}|^2 = 21$. Given the first appearance of this irrep is high in the spectrum, a LQCD calculation of the $l = 9$ phase-shift will require enormous lattice volumes in order for the state to lie below inelastic thresholds. Thus, this calculation cannot be expected to be performed in the near future.

TABLE XXV: The $|\mathbf{n}|^2$-shell of the lowest-lying energy-eigenstate transforming as $\Gamma^{(i)}$, and the angular-momentum of the dominant interaction in the large-volume limit.

$\|\mathbf{n}\|^2$	Γ	l
0	A_1^+	0
1	T_1^-	1
1	E^+	2
2	T_2^+	2
2	T_2^-	3
3	A_2^-	3
5	T_1^+	4
5	A_2^+	6
6	E^-	5
14	A_1^-	9

IV. DISCUSSION

A. Strategy for Extracting Phase-Shifts from Lattice QCD

In Lattice QCD calculations, sources and sinks with the quantum numbers of the hadronic states of interest generate correlation functions, which in general are sums of exponentials with arguments that depend upon the energy of the eigenstates in the lattice volume. One path for LQCD calculations to follow is to form sources and/or sinks that transform as irreps of the cubic group from the eigenstates of linear-momentum (generated by the Fourier-transform of single-hadron objects). Clearly, such sources are not the energy-eigenstates in the lattice-volume due to the interactions between the particles, and as such these sources and sinks will couple, in principle, to all states in the lattice-volume with the appropriate quantum numbers. At large times, the correlation function will depend exponentially upon the energy of the lowest eigenstate. For instance, the correlation function resulting from an A_1^+ source constructed from eigenstates with $|\mathbf{n}|^2 \gg 0$ will depend upon the energy of the lowest-lying A_1^+ irrep at large times. Of course, the overlap onto the lowest-lying A_1^+ irrep may be small, in which case the ground-state dominates only after a large number of time-slices. It is then clear that the optimal way to extract the δ_l for $l \leq 6$ is to determine the lowest energy-eigenvalue of the cubic irrep that is dominated by each δ_l. These irreps are shown in table XXV, along with the $|\mathbf{n}|^2$-shell of the lowest-lying energy-eigenstate that contributes to the corresponding correlation functions. Table XXV shows that with just the lowest two $|\mathbf{n}|^2$-shells, $|\mathbf{n}|^2 = 0, 1$, the phase-shifts in the lowest three partial-waves, $\delta_{0,1,2}$, can be determined. In order to determine the phase-shifts in all partial-waves with $l \leq 6$, correlation functions must be formed for states that have ground-states in the shells up to $|\mathbf{n}|^2 = 6$. Determining the phase-shift for $l \geq 7$ can be seen to be decidedly more difficult than for $l \leq 6$ as there is only one further irrep of the cubic group, the A_1^- which first occurs in the $|\mathbf{n}|^2 = 14$ and is dominated by the interactions in the $l = 9$ partial-wave in the large volume limit.

For shells in which there are multiple occurrences of a given $\Gamma^{(i)}$, the partial-diagonalization of the states in the infinite-volume limit in terms of the angular-momentum

of the interactions is possible. However, sources cannot be constructed to isolate these states due to interactions, and in general, closely spaced-states will be encountered in the spectrum.

B. Expectations for the $\pi\pi$ Energy-Eigenvalues

In order to estimate the computational resources required to extract the $\pi\pi$ phase-shifts in higher partial-waves, the experimentally determined (and parameterized) phase-shifts can be used to determine the energy-eigenvalues for a range of lattice volumes. The $\pi\pi$ phase-shifts

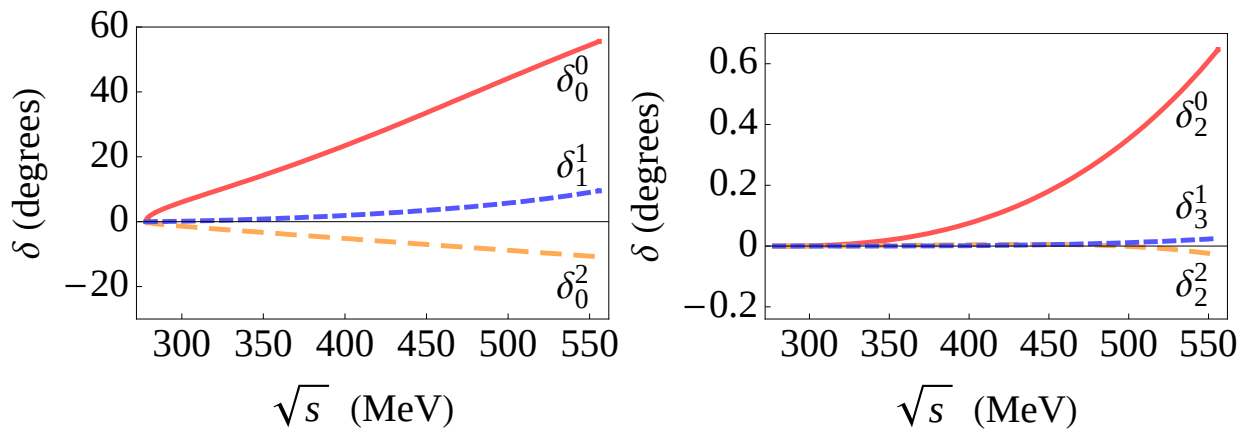

FIG. 28: The $\pi\pi$ phase-shifts, δ_l^I, as a function of $\sqrt{s} < 4m_\pi$ for $l = 0, 1, 2, 3$, as parameterized in Ref. [57].

for $l = 0, 1, 2$, and 3 partial-waves extracted from experimental data and parameterized with functions that satisfy unitarity and analyticity, and specifically incorporate any lowest-lying resonances in the channel [57] [7] are shown in fig. 28. The central values of the parameters describing each partial-wave provided in Ref. [57] are used in the analysis, but, as only estimates of the energy-eigenvalues are being explored, a systematic propagation of the uncertainties has not been performed. Further, we assume isospin symmetry in our analysis. As Lüscher's formalism is valid below inelastic thresholds, only the phase-shifts in the kinematic regime $\sqrt{s} < 4m_\pi$ (at the physical pion mass) are considered.

Figure 29 shows the energy-eigenvalues associated with two non-interacting pions with vanishing total momentum in the lattice volume (also shown in fig. 1 of Ref. [1]). At the physical pion mass, LQCD calculations in volumes with $L \gtrsim 6$ fm are highly desirable in order to suppress the exponential corrections that are not included in the formalism of Lüscher [55]. The energy-shift between the non-interacting state and the interacting $I = 0$ A_1^+ and $I = 2$ A_1^+ states in the $|\mathbf{n}|^2 = 0$ shell are shown in fig. 30. The energy-shifts for the eigenstates in the $|\mathbf{n}|^2 = 1, 2, 3, 4$ shells are shown in figs. 31-34, respectively. The energy-shifts for the $|\mathbf{n}|^2 = 0$ A_1^+ states and the $|\mathbf{n}|^2 = 1$ T_1^- state can also be found in fig. 7 of Ref. [1]. The energy-shifts of the states due to the s-wave and p-wave interactions are of comparable size. As the s-wave interactions are currently being calculated in volumes with $L \sim 3.5$ fm, we do not anticipate significant difficulty in performing these calculations at the

[7] The real-part of the inverse scattering amplitude, $\cot\delta_l^I$, is expanded as a power-series in the function $w(s) = \frac{\sqrt{s}-\sqrt{s_i-s}}{\sqrt{s}+\sqrt{s_i-s}}$, where s_i is the energy above which inelastic processes cannot be neglected.

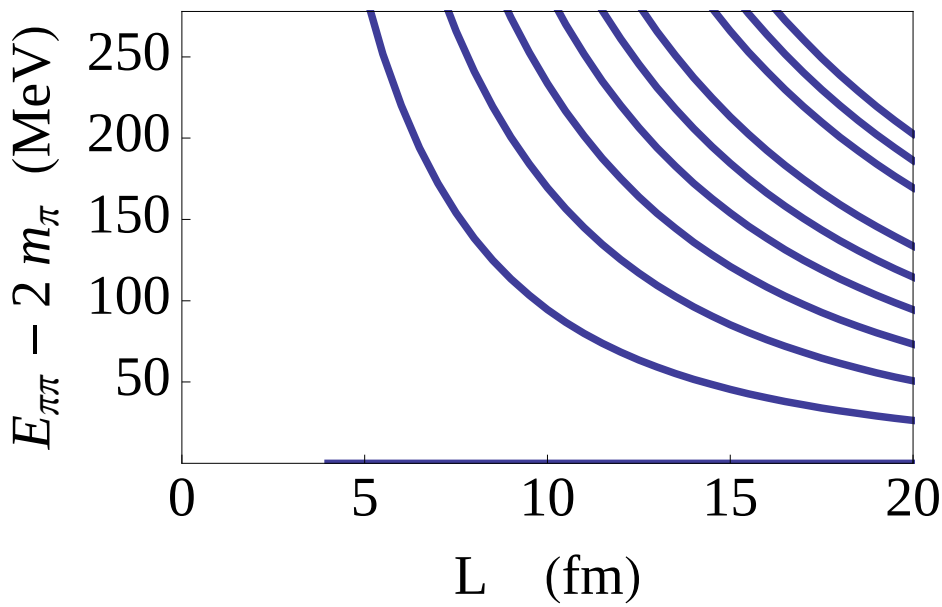

FIG. 29: The energy-eigenvalues associated with two non-interacting pions as a function of the spatial-extent of the lattice volume, L. The spectrum results from the momentum of each pion being restricted to $\mathbf{q} = \frac{2\pi}{L}\mathbf{n}$ for all possible triplets of integers, $\mathbf{n}$, due to the periodic boundary conditions imposed on the quark and gluon fields. The maximum value shown on the vertical-axis corresponds to the inelastic threshold $\sqrt{s} = 4m_\pi$. For reference, a spatial-extent of $L = 6$ fm corresponds to $m_\pi L \sim 4.2$.

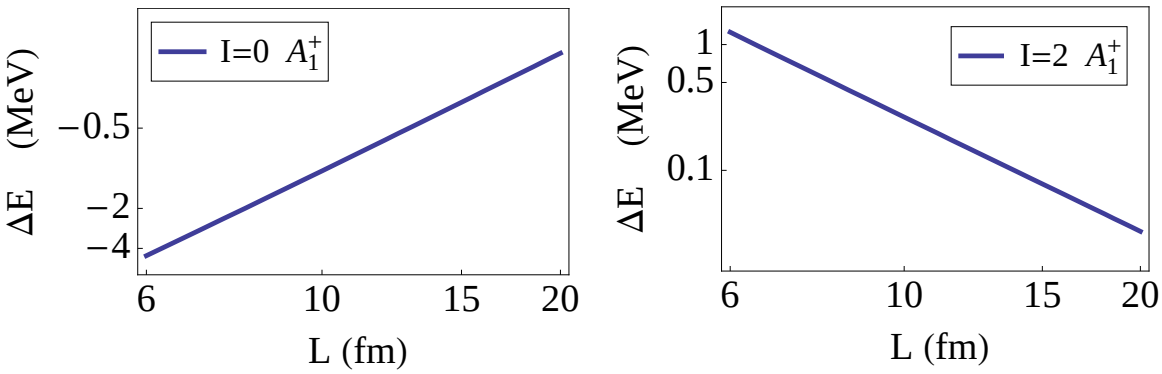

FIG. 30: The expected $\pi\pi$ energy-shifts in the $|\mathbf{n}|^2 = 0$ shell due to strong interactions. The left panel shows the shift in the $I = 0$ A_1^+ irrep (dominated by δ_0^0), while the right panel shows the shift in the $I = 2$ A_1^+ irrep (dominated by δ_0^2). Both the L-axis and the ΔE-axis are scaled logarithmically ($\log_{10}$).

physical pion mass in lattices with $L \gtrsim 6$ fm. In contrast, the energy-shifts of states due to the d-wave ($l = 2$) and f-wave ($l = 3$) interactions are more than an order of magnitude smaller than those of the A_1^+ irrep. Significantly more computational resources will be required to extract the phase-shifts beyond the s-wave and p-wave. It is difficult to make estimates for the energy-shifts due to interactions beyond the f-wave as the experimental measurements of these phase-shifts have large uncertainties or are absent. Given the results obtained for

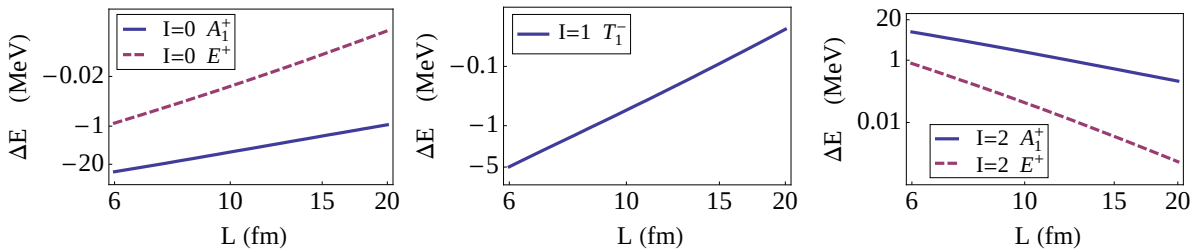

FIG. 31: The expected $\pi\pi$ energy-shifts in the $|\mathbf{n}|^2 = 1$ shell due to strong interactions. The left panel shows the shift in the $I = 0$ A_1^+, E^+ irreps (dominated by δ_0^0 and δ_2^0, respectively), the center panel shows the shift in the $I = 1$ T_1^- irrep (dominated by δ_1^1) and the right panel shows the shift in the $I = 2$ A_1^+, E^+ irreps (dominated by δ_0^2 and δ_2^2, respectively). Both the L-axis and the ΔE-axis are scaled logarithmically ($\log_{10}$).

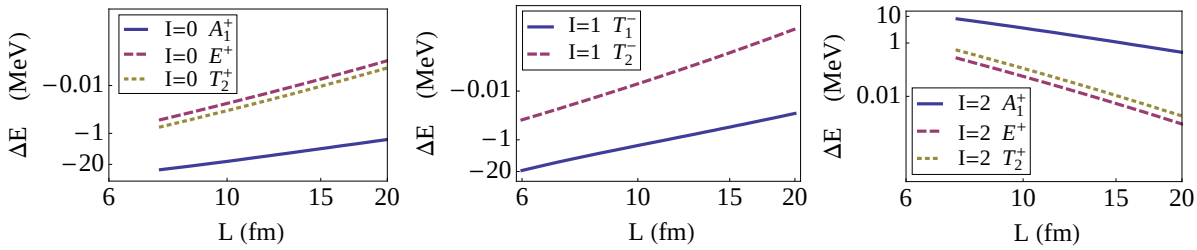

FIG. 32: The expected $\pi\pi$ energy-shifts in the $|\mathbf{n}|^2 = 2$ shell due to strong interactions. The left panel shows the shift in the $I = 0$ A_1^+, E^+, T_2^+ irreps (dominated by δ_0^0, δ_2^0 and δ_2^0, respectively), the center panel shows the shift in the $I = 1$ T_1^-, T_2^- irrep (dominated by δ_1^1 and δ_3^1) and the right panel shows the shift in the $I = 2$ A_1^+, E^+, T_2^+ irreps (dominated by δ_0^2, δ_2^2 and δ_2^2, respectively). Both the L-axis and the ΔE-axis are scaled logarithmically ($\log_{10}$).

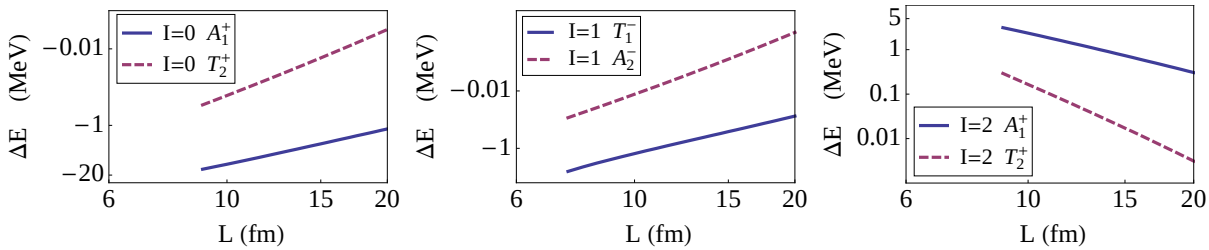

FIG. 33: The expected $\pi\pi$ energy-shifts in the $|\mathbf{n}|^2 = 3$ shell due to strong interactions. The left panel shows the shift in the $I = 0$ A_1^+, T_2^+ irreps (dominated by δ_0^0 and δ_2^0, respectively), the center panel shows the shift in the $I = 1$ T_1^-, A_2^- irreps (dominated by δ_1^1 and δ_3^1, respectively) and the right panel shows the shift in the $I = 2$ A_1^+, T_2^+ irreps (dominated by δ_0^2 and δ_2^2, respectively). Both the L-axis and the ΔE-axis are scaled logarithmically ($\log_{10}$).

$l \leq 3$, it is not difficult to speculate as to the size of the energy-shifts of partial-waves beyond $l = 3$, and the associated difficulty in their extraction from LQCD calculations.

In order to estimate the amount of mixing of higher partial waves to a given phase-shift from the energy-eigenvalues, it is important to understand the expected contributions from (all of) the partial-waves. The energy-splitting of the T_1^- irrep in the $|\mathbf{n}|^2 = 1$-shell from

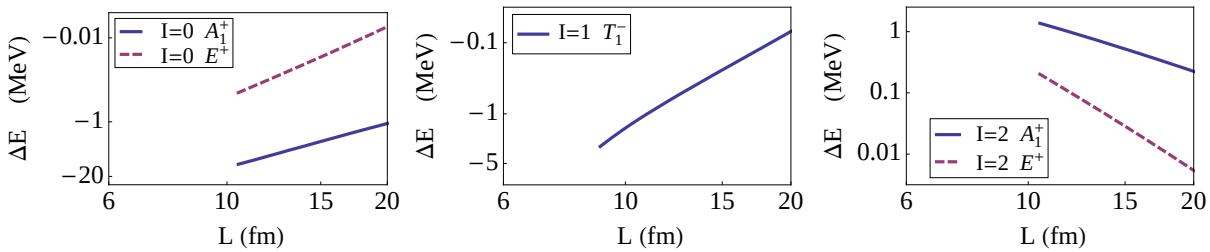

FIG. 34: The expected $\pi\pi$ energy-shifts in the $|\mathbf{n}|^2 = 4$ shell due to strong interactions. The left panel shows the shift in the $I = 0$ A_1^+, E^+ irreps (dominated by δ_0^0 and δ_2^0, respectively), the center panel shows the shift in the $I = 1$ T_1^- irrep (dominated by δ_1^1) and the right panel shows the shift in the $I = 2$ A_1^+, E^+ irreps (dominated by δ_0^2 and δ_2^2, respectively). Both the L-axis and the ΔE-axis are scaled logarithmically ($\log_{10}$).

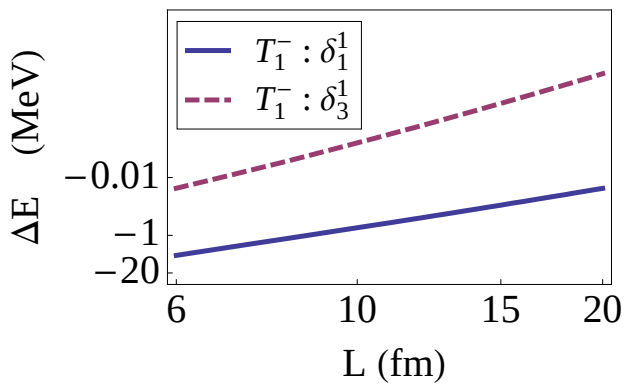

FIG. 35: The contributions to the energy-splitting of the T_1^- irrep in the $|\mathbf{n}|^2 = 1$-shell due to δ_1^1 and δ_3^1. Both the L-axis and the ΔE-axis are scaled logarithmically ($\log_{10}$).

the $l = 1$ phase-shift, δ_1^1, and the $l = 3$ phase-shift, δ_3^1, are shown in fig. 35. As expected, the contribution from δ_3^1 is approximately two-orders of magnitude smaller than that from δ_1^1 over the range of lattice volumes for which the analysis is applicable. Therefore, to high precision it is sufficient to use the perturbative expansion of the energy-splitting in terms of $\tan\delta_1^1$.

C. Signal-to-Noise Issues

There is also a signal-to-noise "problem" in the extraction of the δ_l for $l \geq 1$ as the signal-to-noise ratio degrades exponentially at large times. To demonstrate this behavior we return to the argument given by Lepage [58]. Consider the correlation function resulting from a source that creates a $\pi^+\pi^+$-state that transforms in the E^+ irrep of the cubic group,

$$\overline{x}(t) \;=\; \langle\hat{\theta}_{E^+}(t)\rangle \;=\; \langle 0|\; S_{E^+}(t) S^\dagger_{E^+}(0)\; |0\rangle \;\rightarrow\; Z_{E^+}\; e^{-E^{(\pi^+\pi^+)}_{0,E^+} t} \quad , \tag{42}$$

where $S_{E^+}(t)$ annihilates a $\pi^+\pi^+$ in the E^+ irrep at the time t. At large times this correlation function depends exponentially upon the ground-state energy which, in the absence of interactions, is $E^{(\pi^+\pi^+)}_{0,E^+} \;=\; 2\sqrt{\left(\frac{2\pi}{L}\right)^2 + m_\pi^2}$. The variance of this correlation function is

given by

$$\sigma^2(t) \;=\; \langle \Big(\hat{\theta}_{E^+}(t)\Big)^2 \rangle \;-\; \langle \hat{\theta}_{E^+}(t)\rangle^2 \;=\; \langle 0|\; S_{E^+}(t) S^\dagger_{E^+}(t) S^\dagger_{E^+}(0) S_{E^+}(0)\; |0\rangle \;-\; \langle \hat{\theta}_{E^+}(t)\rangle^2$$
$$= \sum_{\Gamma \in E^+ \otimes E^+} C_\Gamma \;\; \langle 0|\; \tilde{\mathcal{S}}_\Gamma(t) \tilde{\mathcal{S}}_\Gamma(0)\; |0\rangle \;-\; \langle \hat{\theta}_{E^+}(t)\rangle^2$$
$$\rightarrow \tilde{Z}_{A_1^+}\; e^{-2E^{(\pi^+\pi^+)}_{0,A_1^+} t} \;-\; Z^2_{E^+}\; e^{-2E^{(\pi^+\pi^+)}_{0,E^+} t} \;\; , \tag{43}$$

where C_Γ are the Clebsch-Gordan coefficients in the expansion $E^+ \otimes E^+ = A_1^+ \oplus A_2^+ \oplus E^+$ [53, 59, 60]. The energy, $\Delta_{\rm NS}$, that dictates the long-time behavior of the variance correlation function is that of the lowest-lying irrep composed of four pions, which is the lowest-lying A_1^+-irrep that has an energy of $2E^{(\pi^+\pi^+)}_{0,A_1^+} = 4m_\pi$ in the absence of interactions. Therefore, at large times, the noise-to-signal ratio behaves as

$$\frac{\sigma(t)}{\overline{x}(t)} \;\rightarrow\; \frac{\sqrt{\tilde{Z}_{A_1^+}}}{Z_{E^+}}\; e^{\Delta_{\rm NS} t} \;\;\; , \;\;\; \Delta_{\rm NS} \;=\; 2\; \left[\; \sqrt{\left(\frac{2\pi}{L}\right)^2 + m_\pi^2} - m_\pi \;\right] \;\;\; , \tag{44}$$

which grows exponentially at large times.

This argument generalizes to all of the cubic irreps, and the extraction of the δ_l for each $l \geq 1$ suffers from a signal-to-noise problem, with an energy-scale that is approximately

$$\Delta^{(|\mathbf{n}|^2)}_{\rm NS} \;=\; 2\; \left[\; \sqrt{\left(\frac{2\pi}{L}\right)^2 |\mathbf{n}|^2 + m_\pi^2} - m_\pi \;\right] \;\;\; . \tag{45}$$

Obviously, in large volumes, the degradation of the signal obtained for low-lying states will not dramatically impact the determination of the energy-eigenvalues as the energy-scale behaves as $\Delta^{(|\mathbf{n}|^2)}_{\rm NS} \rightarrow |\mathbf{n}|^2/(m_\pi L^2)$. However, for present-day calculations in modest lattice volumes, the degradation of the signal may impact the extraction of the phase-shifts in higher partial-waves, and numerical exploration is required to determine its impact.

V. CONCLUSION

We have explored the phenomenology of Lüscher's method in the extraction of the phase-shifts in higher partial-waves describing meson-meson scattering below inelastic thresholds using Lattice QCD, the formalism for which is contained in the works of Lüscher. The lowest-lying s-wave and p-wave interactions were explored in those works, and at the time, Lattice QCD calculations of scattering beyond the s-wave and p-wave were in the distant future. However, the rapidly increasing computational resources that are being directed towards Lattice QCD calculations will allow for the calculation of the phase-shifts in higher partial-waves in both mesonic and baryonic processes in the near future. We have considered the low-lying spectrum of two-meson states in a finite cubic lattice-volume, and determined contributions from the partial-waves with $l \leq 6$ and $l = 9$. There are a sufficient number of irreps of the cubic group that will allow for the calculation of the phase-shifts, δ_l for $l \leq 6$, and possibly $l = 9$. There are no irreps of the cubic group with ground-state energy-splittings that are dominated by interactions in the $l = 7$ and $l = 8$ partial-waves. As

such, there appears to be no clean way to calculate these phase-shifts from Lattice QCD calculations performed in cubic volumes. High precision calculations of the energy of states in other irreps may allow for their extraction by forming differences of energies, but this will require significantly more computational resources than the extraction of the phase-shifts in lower partial-waves. We have provided the structure of sources that will produce the irreps of the cubic group, in both momentum and position space, that will generate the relevant states in LQCD calculations. Further, we have given the explicit formula, and their perturbative solutions, that are required to analyze the results of such LQCD calculations. We recapitulate the leading contributions to the energy-eigenvalue equations and their solutions in the large-volume limit in table XXVI and table XXVII, respectively.

Experimental measurements of the $\pi\pi$ phase-shifts are difficult, with precision currently at the few-percent level in the s-wave and p-wave, but much larger uncertainties are associated with the phase-shifts in the higher partial-waves. It would appear that Lattice QCD calculations will be able to provide low-energy meson-meson phase-shifts in the low partial-waves with significantly more precision than the corresponding experimental measurements. While the contributions to energy-splittings rapidly become smaller with higher partial-waves, we conclude that it is presently possible to extract phase-shifts for partial-waves with $l \leq 3$. The implications of the recent preliminary calculations [20] of the $l = 2$ phase-shift, δ_2^2, at unphysical pion masses are very encouraging for future calculations.

APPENDIX A: BLOCK-DIAGONALIZATION OF $F^{(FV)}$

As the number of partial-waves with non-zero phase-shifts increases, so does the complexity of the calculation of the energy-eigenvalues in a finite cubic volume. To illustrate the method for determining the energy-eigenvalues, we provide the details of the calculation when $\delta_l \neq 0$ for $l \leq 4$. As is true in all cases involving parity-conserving interactions, the analysis in the even-parity sector ($l = 0, 2, 4$) decouples from that in the odd-parity sector ($l = 1, 3$). The calculations that are required for $\delta_l \neq 0$ for $l > 4$ become more complicated due to the dimensionality of the matrices involved, the contributions from the $\mathcal{Z}_{l,m}$ for higher values of l, and to multiple occurrences of the same cubic irreps. This last feature means that the diagonalization of the finite-volume functions, $F_{l;l}^{(FV)}$, are not dictated entirely by geometry due to mixing between the multiple occurrences of a given $\Gamma^{(i)}$. However, such calculations are a straightforward extension of what follows.

1. Odd-Parity Sector with $\delta_{1,3} \neq 0$

In the odd-parity sector with only $\delta_{1,3} \neq 0$, the finite-volume corrections are encapsulated in $F_-^{(FV)}$ which is a 10×10 matrix. It has block form

$$F_-^{(FV)} = \left(\begin{array}{c|c} F_{1;1}^{(FV)} & F_{1;3}^{(FV)} \\ \hline F_{3;1}^{(FV)} & F_{3;3}^{(FV)} \end{array} \right) , \tag{A1}$$

TABLE XXVI: A summary of the energy-eigenvalue equations for the lowest-lying state in each $\Gamma^{(i)}$ arising from the interaction in the dominant partial-wave.

l $[\Gamma^{(i)}]$	Leading Eigenvalue Equation	Section
0 $[A_1^+]$	$q\cot\delta_0 \;=\; \frac{2}{\sqrt{\pi}L}\,\mathcal{Z}_{0,0}\left(1;\tilde{q}^2\right)$	III A 1
1 $[T_1^-]$	$q^3\cot\delta_1 \;=\left(\frac{2\pi}{L}\right)^3 \frac{1}{\pi^{3/2}}\tilde{q}^2\,\mathcal{Z}_{0,0}\left(1;\tilde{q}^2\right)$	III B 3
2 $[E^+]$	$q^5\cot\delta_2 \;=\left(\frac{2\pi}{L}\right)^5 \frac{1}{\pi^{3/2}}\left(\tilde{q}^4\mathcal{Z}_{0,0}\left(1;\tilde{q}^2\right)+\frac{6}{7}\mathcal{Z}_{4,0}\left(1;\tilde{q}^2\right)\right)$	III A 3
2 $[T_2^+]$	$q^5\cot\delta_2 \;=\left(\frac{2\pi}{L}\right)^5 \frac{1}{\pi^{3/2}}\left(\tilde{q}^4\mathcal{Z}_{0,0}\left(1;\tilde{q}^2\right)-\frac{4}{7}\mathcal{Z}_{4,0}\left(1;\tilde{q}^2\right)\right)$	III A 5
3 $[T_2^-]$	$q^7\cot\delta_3 \;=\left(\frac{2\pi}{L}\right)^7 \frac{1}{\pi^{3/2}}\left(\tilde{q}^6\mathcal{Z}_{0,0}\left(1;\tilde{q}^2\right)-\frac{2\tilde{q}^2\mathcal{Z}_{4,0}\left(1;\tilde{q}^2\right)}{11}-\frac{60\mathcal{Z}_{6,0}\left(1;\tilde{q}^2\right)}{11\sqrt{13}}\right)$	III B 4
3 $[A_2^-]$	$q^7\cot\delta_3 \;=\left(\frac{2\pi}{L}\right)^7 \frac{1}{\pi^{3/2}}\left(\tilde{q}^6\mathcal{Z}_{0,0}\left(1;\tilde{q}^2\right)-\frac{12}{11}\tilde{q}^2\mathcal{Z}_{4,0}\left(1;\tilde{q}^2\right)+\frac{80}{11\sqrt{13}}\mathcal{Z}_{6,0}\left(1;\tilde{q}^2\right)\right)$	III B 1
4 $[T_1^+]$	$q^9\cot\delta_4 \;=\left(\frac{2\pi}{L}\right)^9 \frac{1}{\pi^{3/2}}\left(\tilde{q}^8\mathcal{Z}_{0,0}\left(1;\tilde{q}^2\right)-\frac{448\mathcal{Z}_{8,0}\left(1;\tilde{q}^2\right)}{143\sqrt{17}}-\frac{4\tilde{q}^2\mathcal{Z}_{6,0}\left(1;\tilde{q}^2\right)}{11\sqrt{13}}+\frac{54\tilde{q}^4\mathcal{Z}_{4,0}\left(1;\tilde{q}^2\right)}{143}\right)$	III A 4
5 $[E^-]$	$q^{11}\cot\delta_5 \;=\left(\frac{2\pi}{L}\right)^{11} \frac{1}{\pi^{3/2}}\times$ $\left(\tilde{q}^{10}\mathcal{Z}_{0,0}\left(1;\tilde{q}^2\right)-\frac{6\tilde{q}^6\mathcal{Z}_{4,0}\left(1;\tilde{q}^2\right)}{13}+\frac{32\tilde{q}^4\mathcal{Z}_{6,0}\left(1;\tilde{q}^2\right)}{17\sqrt{13}}-\frac{672\tilde{q}^2\mathcal{Z}_{8,0}\left(1;\tilde{q}^2\right)}{247\sqrt{17}}+\frac{1152\sqrt{21}\mathcal{Z}_{10,0}\left(1;\tilde{q}^2\right)}{4199}\right)$	III B 2
6 $[A_2^+]$	$q^{13}\cot\delta_6 \;=\left(\frac{2\pi}{L}\right)^{13} \frac{1}{\pi^{3/2}}\times$ $\left(\tilde{q}^{12}\mathcal{Z}_{0,0}\left(1;\tilde{q}^2\right)+\frac{6\tilde{q}^8\mathcal{Z}_{4,0}\left(1;\tilde{q}^2\right)}{17}-\frac{160\sqrt{13}\tilde{q}^6\mathcal{Z}_{6,0}\left(1;\tilde{q}^2\right)}{323}-\frac{40\tilde{q}^4\mathcal{Z}_{8,0}\left(1;\tilde{q}^2\right)}{19\sqrt{17}}\right.$ $\left.-\frac{2592\sqrt{21}\tilde{q}^2\mathcal{Z}_{10,0}\left(1;\tilde{q}^2\right)}{7429}+\frac{1980\mathcal{Z}_{12,0}\left(1;\tilde{q}^2\right)}{7429}+\frac{264\sqrt{1001}\mathcal{Z}_{12,4}\left(1;\tilde{q}^2\right)}{7429}\right)$	III A 2
9 $[A_1^-]$	$q^{19}\cot\delta_9 \;=\left(\frac{2\pi}{L}\right)^{19} \frac{1}{\pi^{3/2}}\times$ $\left(\tilde{q}^{18}\mathcal{Z}_{0,0}(1;\tilde{q}^2)-\frac{6\tilde{q}^{14}\mathcal{Z}_{4,0}(1;\tilde{q}^2)}{23}-\frac{32\sqrt{13}\tilde{q}^{12}\mathcal{Z}_{6,0}(1;\tilde{q}^2)}{115}-\frac{56\sqrt{17}\tilde{q}^{10}\mathcal{Z}_{8,0}(1;\tilde{q}^2)}{345}\right.$ $+\frac{1568\sqrt{7}\tilde{q}^8\mathcal{Z}_{10,0}(1;\tilde{q}^2)}{3335\sqrt{3}}+\frac{308\tilde{q}^6\mathcal{Z}_{12,0}(1;\tilde{q}^2)}{2139}+\frac{616\sqrt{1001}\tilde{q}^6\mathcal{Z}_{12,4}(1;\tilde{q}^2)}{20677}+\frac{53248\tilde{q}^4\mathcal{Z}_{14,0}(1;\tilde{q}^2)}{10695\sqrt{29}}$ $\left.-\frac{1664\sqrt{11}\tilde{q}^2\mathcal{Z}_{16,0}(1;\tilde{q}^2)}{3565\sqrt{3}}+\frac{832\sqrt{46189}\tilde{q}^2\mathcal{Z}_{16,4}(1;\tilde{q}^2)}{103385\sqrt{7}}+\frac{2206464\tilde{\mathcal{Z}}_{18,0}(1;\tilde{q}^2)}{103385\sqrt{37}}+\frac{28288\sqrt{3553}\mathcal{Z}_{18,4}(1;\tilde{q}^2)}{20677\sqrt{259}}\right)$	III B 5

TABLE XXVII: The perturbative expansions of the energy-eigenvalues of the lowest-lying state in each $\Gamma^{(i)}$.

$\lvert\mathbf{n}\rvert^2$ $[\Gamma^{(i)}]$	$\lvert q\rvert^2$
$0\ [A_1^+]$	$-\frac{4\pi a_0}{L^3}\left[\ 1\ -2.8373\left(\frac{a_0}{L}\right)+6.3752\left(\frac{a_0}{L}\right)^2\ \right]\ +\ ...$
$1\ [T_1^-]$ $1\ [E^+]$	$\frac{4\pi^2}{L^2}\left[\ 1-\frac{3}{\pi^2}\tan\delta_1\left(1-0.3653\tan\delta_1\right)\ +\ ...\right]$ $\frac{4\pi^2}{L^2}\left[\ 1-\frac{15}{2\pi^2}\tan\delta_2\left(1-1.5672\tan\delta_2\right)\ +\ ...\right]$
$2\ [T_2^+]$ $2\ [T_2^-]$	$\frac{4\pi^2}{L^2}\left[\ 2-\frac{15}{2\sqrt{2}\pi^2}\tan\delta_2\left(1-0.4830\tan\delta_2\right)\ +\ ...\right]$ $\frac{4\pi^2}{L^2}\left[\ 2-\frac{105}{8\sqrt{2}\pi^2}\tan\delta_3\ +\ ...\right]$
$3\ [A_2^-]$	$\frac{4\pi^2}{L^2}\left[\ 3-\frac{140}{9\sqrt{3}\pi^2}\tan\delta_3\ +\ ...\right]$
$5\ [T_1^+]$ $5\ [A_2^+]$	$\frac{4\pi^2}{L^2}\left[\ 5-\frac{2268}{125\sqrt{5}\pi^2}\tan\delta_4\ +\ ...\right]$ $\frac{4\pi^2}{L^2}\left[\ 5-\frac{162162}{3125\sqrt{5}\pi^2}\tan\delta_6\ +\ ...\right]$
$6\ [E^-]$	$\frac{4\pi^2}{L^2}\left[\ 6-\frac{385}{12\sqrt{6}\pi^2}\tan\delta_5\ +\ ...\right]$
$14\ [A_1^-]$	$\frac{4\pi^2}{L^2}\left[\ 14-\frac{4208972625}{46118408\sqrt{14}\pi^2}\tan\delta_9\ +\ ...\right]$

where the component matrices in the $|l,m\rangle$-basis are [8]

$$
\begin{aligned}
F^{(FV)}_{1;1} &= \frac{1}{\pi^{3/2}}\,\frac{1}{\tilde{q}}\,\mathcal{Z}_{0,0}(1;\tilde{q}^2)\;\;\mathrm{diag}\,(1,1,1) \\
F^{(FV)}_{1;3} &= \left(F^{(FV)}_{3;1}\right)^T = \frac{1}{\pi^{3/2}}\,\frac{1}{\tilde{q}^5}\,\mathcal{Z}_{4,0}(1;\tilde{q}^2)\;\;\frac{2}{\sqrt{21}}\begin{pmatrix} 0 & 0 & -\sqrt{\frac{3}{2}} & 0 & 0 & 0 & -\sqrt{\frac{5}{2}} \\ 0 & 0 & 0 & 2 & 0 & 0 & 0 \\ -\sqrt{\frac{5}{2}} & 0 & 0 & 0 & -\sqrt{\frac{3}{2}} & 0 & 0 \end{pmatrix} \\
\overline{F}^{(FV)}_{3;3} &= \frac{1}{\pi^{3/2}}\,\frac{1}{\tilde{q}}\,\mathcal{Z}_{0,0}(1;\tilde{q}^2)\;\;\mathrm{diag}\,(1,1,1,1,1,1,1) \\
&\quad + \frac{1}{\pi^{3/2}}\,\frac{1}{\tilde{q}^5}\,\mathcal{Z}_{4,0}(1;\tilde{q}^2)\;\;\frac{1}{11}\begin{pmatrix} 3 & 0 & 0 & 0 & \sqrt{15} & 0 & 0 \\ 0 & -7 & 0 & 0 & 0 & 5 & 0 \\ 0 & 0 & 1 & 0 & 0 & 0 & \sqrt{15} \\ 0 & 0 & 0 & 6 & 0 & 0 & 0 \\ \sqrt{15} & 0 & 0 & 0 & 1 & 0 & 0 \\ 0 & 5 & 0 & 0 & 0 & -7 & 0 \\ 0 & 0 & \sqrt{15} & 0 & 0 & 0 & 3 \end{pmatrix} \\
&\quad + \frac{1}{\pi^{3/2}}\,\frac{1}{\tilde{q}^7}\,\mathcal{Z}_{6,0}(1;\tilde{q}^2)\;\;\frac{5}{33\sqrt{13}}\begin{pmatrix} -1 & 0 & 0 & 0 & 7\sqrt{15} & 0 & 0 \\ 0 & 6 & 0 & 0 & 0 & -42 & 0 \\ 0 & 0 & -15 & 0 & 0 & 0 & 7\sqrt{15} \\ 0 & 0 & 0 & 20 & 0 & 0 & 0 \\ 7\sqrt{15} & 0 & 0 & 0 & -15 & 0 & 0 \\ 0 & -42 & 0 & 0 & 0 & 6 & 0 \\ 0 & 0 & 7\sqrt{15} & 0 & 0 & 0 & -1 \end{pmatrix} \quad ,
\end{aligned}
\tag{A2}
$$

where the relevant relations between the $\mathcal{Z}_{l,m}$, that can be found in eq. (B7), have been used, and where $\mathrm{diag}(a,b,...)$ denotes a diagonal matrix. It is convenient to first diagonalize the $F^{(FV)}_{l;l}$ blocks ($F^{(FV)}_{1;1}$ is already diagonal in this basis). The block-diagonal matrix, S_-, is defined to have the form

$$
S_- \;=\; \left(\begin{array}{c|c} S_{11} & 0 \\ \hline 0 & S_{33} \end{array}\right) \quad , \tag{A3}
$$

and when acting on $F^{(FV)}_-$ produces a matrix, $\overline{F}^{(FV)}_- \;=\; S_-.F^{(FV)}_-.S^\dagger_-$, which can be rearranged into block-diagonal form where each block is associated with a $\Gamma^{(i)}$. The matrices $\cos\delta$ and $\sin\delta$ in eq. (3) are invariant under this transformation,

$$
\overline{\cos}\delta \;=\; \mathrm{diag}\,(c_1,c_1,c_1,c_3,c_3,c_3,c_3,c_3,c_3,c_3) \quad , \tag{A4}
$$

[8] Explicitly, the basis is $\{|1,1\rangle, |1,0\rangle, |1,-1\rangle, |3,3\rangle, |3,2\rangle, |3,1\rangle, |3,0\rangle, |3,-1\rangle, |3,-2\rangle, |3,-3\rangle\}$.

where c_1 and c_3 denote $\cos\delta_1$ and $\cos\delta_3$, respectively, and similarly for $\overline{\sin}\delta$. The components of S_- in eq. (A3) are

$$S_{11} = \begin{pmatrix} 1 & 0 & 0 \\ 0 & 1 & 0 \\ 0 & 0 & 1 \end{pmatrix} \quad , \quad S_{33} = \begin{pmatrix} 0 & 0 & -\sqrt{\frac{5}{8}} & 0 & 0 & 0 & \sqrt{\frac{3}{8}} \\ 0 & \frac{1}{\sqrt{2}} & 0 & 0 & 0 & \frac{1}{\sqrt{2}} & 0 \\ -\sqrt{\frac{3}{8}} & 0 & 0 & 0 & \sqrt{\frac{5}{8}} & 0 & 0 \\ 0 & -\frac{1}{\sqrt{2}} & 0 & 0 & 0 & \frac{1}{\sqrt{2}} & 0 \\ 0 & 0 & \sqrt{\frac{3}{8}} & 0 & 0 & 0 & \sqrt{\frac{5}{8}} \\ \sqrt{\frac{5}{8}} & 0 & 0 & 0 & \sqrt{\frac{3}{8}} & 0 & 0 \\ 0 & 0 & 0 & 1 & 0 & 0 & 0 \end{pmatrix} \quad , \tag{A5}$$

and the matrix $\overline{F}_-^{(FV)}$ is of the form

$$\overline{F}_-^{(FV)} = \left(\begin{array}{c|c} \overline{F}_{1;1}^{(FV)} & \overline{F}_{1;3}^{(FV)} \\ \hline \overline{F}_{3;1}^{(FV)} & \overline{F}_{3;3}^{(FV)} \end{array}\right) \quad , \tag{A6}$$

where

$$\begin{aligned}
\overline{F}_{1;1}^{(FV)} &= \frac{1}{\pi^{3/2}} \frac{1}{\tilde{q}} \mathcal{Z}_{0,0}(1;\tilde{q}^2) \ \ \mathrm{diag}\,(1,1,1) \\
\overline{F}_{1;3}^{(FV)} &= \left(\overline{F}_{3;1}^{(FV)}\right)^T = \frac{1}{\pi^{3/2}} \frac{1}{\tilde{q}^5} \mathcal{Z}_{4,0}(1;\tilde{q}^2) \ \frac{4}{\sqrt{21}} \begin{pmatrix} 0 & 0 & 0 & 0 & -1 & 0 & 0 \\ 0 & 0 & 0 & 0 & 0 & 0 & 1 \\ 0 & 0 & 0 & 0 & 0 & -1 & 0 \end{pmatrix} \\
\overline{F}_{3;3}^{(FV)} &= \frac{1}{\pi^{3/2}} \frac{1}{\tilde{q}} \mathcal{Z}_{0,0}(1;\tilde{q}^2) \ \ \mathrm{diag}\,(1,1,1,1,1,1,1) \\
&\quad + \frac{1}{\pi^{3/2}} \frac{1}{\tilde{q}^5} \mathcal{Z}_{4,0}(1;\tilde{q}^2) \ \frac{2}{11} \ \ \mathrm{diag}\,(-1,-1,-1,-6,3,3,3) \\
&\quad + \frac{1}{\pi^{3/2}} \frac{1}{\tilde{q}^7} \mathcal{Z}_{6,0}(1;\tilde{q}^2) \ \frac{20}{33\sqrt{13}} \ \ \mathrm{diag}\,(-9,-9,-9,12,5,5,5) \quad .
\end{aligned} \tag{A7}$$

From the structure of $\overline{F}_-^{(FV)}$ it is clear that the ordering of the $\Gamma^{(i)}$ along the diagonal of $\overline{F}_{3;3}^{(FV)}$ is T_2^-, A_2^- and T_1^-, respectively, and the equations that dictate the energy-eigenvalues of each of the $\Gamma^{(i)}$, given in eqs. (31), (35), and (39), follow directly from eq. (A7). The matrix S_- that diagonalizes $F_-^{(FV)}$ is independent of the $\mathcal{Z}_{l,m}$ functions because, with each relevant $\Gamma^{(i)}$ occurring only once, the decomposition depends upon geometry only.

2. Even-Parity Sector with $\delta_{0,2,4} \neq 0$

In the even-parity sector with only $\delta_{0,2,4} \neq 0$, the finite-volume corrections are encapsulated in $F_+^{(FV)}$ which is a 15×15 matrix. It has block form

$$F_+^{(FV)} = \left(\begin{array}{c|c|c} F_{0;0}^{(FV)} & F_{0;2}^{(FV)} & F_{0;4}^{(FV)} \\ \hline F_{2;0}^{(FV)} & F_{2;2}^{(FV)} & F_{2;4}^{(FV)} \\ \hline F_{4;0}^{(FV)} & F_{4;2}^{(FV)} & F_{4;4}^{(FV)} \end{array} \right) , \tag{A8}$$

where

$$\begin{aligned}
F_{0;0}^{(FV)} &= \frac{1}{\pi^{3/2}} \frac{1}{\tilde{q}} \mathcal{Z}_{0,0}(1;\tilde{q}^2) \ , \quad F_{0;2}^{(FV)} = \begin{pmatrix} 0 & 0 & 0 & 0 & 0 \end{pmatrix} \\
F_{0;4}^{(FV)} &= \frac{1}{\pi^{3/2}} \frac{1}{\tilde{q}^5} \mathcal{Z}_{4,0}(1;\tilde{q}^2) \begin{pmatrix} \sqrt{\frac{5}{14}} & 0 & 0 & 0 & 1 & 0 & 0 & 0 & \sqrt{\frac{5}{14}} \end{pmatrix} \\
F_{2;2}^{(FV)} &= \frac{1}{\pi^{3/2}} \frac{1}{\tilde{q}} \mathcal{Z}_{0,0}(1;\tilde{q}^2) \ \mathrm{diag}\,(1,1,1,1,1) \\
&\quad + \frac{1}{\pi^{3/2}} \frac{1}{\tilde{q}^5} \mathcal{Z}_{4,0}(1;\tilde{q}^2) \frac{1}{7} \begin{pmatrix} 1 & 0 & 0 & 0 & 5 \\ 0 & -4 & 0 & 0 & 0 \\ 0 & 0 & 6 & 0 & 0 \\ 0 & 0 & 0 & -4 & 0 \\ 5 & 0 & 0 & 0 & 1 \end{pmatrix}
\end{aligned}$$

$$\begin{aligned}
F_{2;4}^{(FV)} &= \frac{1}{\pi^{3/2}} \frac{1}{\tilde{q}^5} \mathcal{Z}_{4,0}(1;\tilde{q}^2) \frac{10\sqrt{3}}{77\sqrt{2}} \begin{pmatrix} 0 & 0 & -3\sqrt{2} & 0 & 0 & 0 & -\sqrt{2} & 0 & 0 \\ 0 & 0 & 0 & 1 & 0 & 0 & 0 & -\sqrt{7} & 0 \\ -2\sqrt{\frac{7}{3}} & 0 & 0 & 0 & 2\sqrt{\frac{10}{3}} & 0 & 0 & 0 & -2\sqrt{\frac{7}{3}} \\ 0 & -\sqrt{7} & 0 & 0 & 0 & 1 & 0 & 0 & 0 \\ 0 & 0 & -\sqrt{2} & 0 & 0 & 0 & -3\sqrt{2} & 0 & 0 \end{pmatrix} \\
&+ \frac{1}{\pi^{3/2}} \frac{1}{\tilde{q}^7} \mathcal{Z}_{6,0}(1;\tilde{q}^2) \frac{5\sqrt{3}}{11\sqrt{13}} \begin{pmatrix} 0 & 0 & 1 & 0 & 0 & 0 & -7 & 0 & 0 \\ 0 & 0 & 0 & -2\sqrt{2} & 0 & 0 & 0 & 2\sqrt{14} & 0 \\ -\sqrt{\frac{21}{2}} & 0 & 0 & 0 & \sqrt{15} & 0 & 0 & 0 & -\sqrt{\frac{21}{2}} \\ 0 & 2\sqrt{14} & 0 & 0 & 0 & -2\sqrt{2} & 0 & 0 & 0 \\ 0 & 0 & -7 & 0 & 0 & 0 & 1 & 0 & 0 \end{pmatrix}
\end{aligned}$$

$$
\begin{aligned}
F_{4;4}^{(FV)} \;=\; & \frac{1}{\pi^{3/2}}\,\frac{1}{\tilde{q}}\,\mathcal{Z}_{0,0}(1;\tilde{q}^2)\;\;\mathrm{diag}\,(1,1,1,1,1,1,1,1,1) \\
& + \frac{1}{\pi^{3/2}}\,\frac{1}{\tilde{q}^5}\,\mathcal{Z}_{4,0}(1;\tilde{q}^2)\,\frac{27}{1001}\begin{pmatrix}
14 & 0 & 0 & 0 & \sqrt{70} & 0 & 0 & 0 & 0 \\
0 & -21 & 0 & 0 & 0 & 5\sqrt{7} & 0 & 0 & 0 \\
0 & 0 & -11 & 0 & 0 & 0 & 15 & 0 & 0 \\
0 & 0 & 0 & 9 & 0 & 0 & 0 & 5\sqrt{7} & 0 \\
\sqrt{70} & 0 & 0 & 0 & 18 & 0 & 0 & 0 & \sqrt{70} \\
0 & 5\sqrt{7} & 0 & 0 & 0 & 9 & 0 & 0 & 0 \\
0 & 0 & 15 & 0 & 0 & 0 & -11 & 0 & 0 \\
0 & 0 & 0 & 5\sqrt{7} & 0 & 0 & 0 & -21 & 0 \\
0 & 0 & 0 & 0 & \sqrt{70} & 0 & 0 & 0 & 14
\end{pmatrix} \\
& + \frac{1}{\pi^{3/2}}\,\frac{1}{\tilde{q}^7}\,\mathcal{Z}_{6,0}(1;\tilde{q}^2)\,\frac{1}{11\sqrt{13}}\begin{pmatrix}
-4 & 0 & 0 & 0 & 6\sqrt{70} & 0 & 0 & 0 & 0 \\
0 & 17 & 0 & 0 & 0 & -3\sqrt{7} & 0 & 0 & 0 \\
0 & 0 & -22 & 0 & 0 & 0 & -42 & 0 & 0 \\
0 & 0 & 0 & -1 & 0 & 0 & 0 & -3\sqrt{7} & 0 \\
6\sqrt{70} & 0 & 0 & 0 & 20 & 0 & 0 & 0 & 6\sqrt{70} \\
0 & -3\sqrt{7} & 0 & 0 & 0 & -1 & 0 & 0 & 0 \\
0 & 0 & -42 & 0 & 0 & 0 & -22 & 0 & 0 \\
0 & 0 & 0 & -3\sqrt{7} & 0 & 0 & 0 & 17 & 0 \\
0 & 0 & 0 & 0 & 6\sqrt{70} & 0 & 0 & 0 & -4
\end{pmatrix} \\
& + \frac{1}{\pi^{3/2}}\,\frac{1}{\tilde{q}^9}\,\mathcal{Z}_{8,0}(1;\tilde{q}^2)\,\frac{7}{143\sqrt{17}}\begin{pmatrix}
1 & 0 & 0 & 0 & \sqrt{70} & 0 & 0 & 0 & 65 \\
0 & -8 & 0 & 0 & 0 & -8\sqrt{7} & 0 & 0 & 0 \\
0 & 0 & 28 & 0 & 0 & 0 & 28 & 0 & 0 \\
0 & 0 & 0 & -56 & 0 & 0 & 0 & -8\sqrt{7} & 0 \\
\sqrt{70} & 0 & 0 & 0 & 70 & 0 & 0 & 0 & \sqrt{70} \\
0 & -8\sqrt{7} & 0 & 0 & 0 & -56 & 0 & 0 & 0 \\
0 & 0 & 28 & 0 & 0 & 0 & 28 & 0 & 0 \\
0 & 0 & 0 & -8\sqrt{7} & 0 & 0 & 0 & -8 & 0 \\
65 & 0 & 0 & 0 & \sqrt{70} & 0 & 0 & 0 & 1
\end{pmatrix}
\end{aligned}
\tag{A9}
$$

which can be made partially block-diagonalized by

$$
S_+ \;=\; \left(\begin{array}{c|c|c}
S_{0,0} & 0 & 0 \\ \hline
0 & S_{22} & 0 \\ \hline
0 & 0 & S_{44}
\end{array}\right) \quad , \tag{A10}
$$

with

$$S_{0,0} \;=\; 1 \;\;,\;\; S_{22} \;=\; \begin{pmatrix} -\frac{1}{\sqrt{2}} & 0 & 0 & 0 & \frac{1}{\sqrt{2}} \\ 0 & 0 & 0 & 1 & 0 \\ 0 & 1 & 0 & 0 & 0 \\ \frac{1}{\sqrt{2}} & 0 & 0 & 0 & \frac{1}{\sqrt{2}} \\ 0 & 0 & 1 & 0 & 0 \end{pmatrix}$$

$$S_{44} \;=\; \begin{pmatrix} \frac{\sqrt{7}}{2\sqrt{6}} & 0 & 0 & 0 & -\frac{\sqrt{5}}{2\sqrt{3}} & 0 & 0 & 0 & \frac{\sqrt{7}}{2\sqrt{6}} \\ 0 & 0 & \frac{1}{\sqrt{2}} & 0 & 0 & 0 & \frac{1}{\sqrt{2}} & 0 & 0 \\ -\frac{1}{\sqrt{2}} & 0 & 0 & 0 & 0 & 0 & 0 & 0 & \frac{1}{\sqrt{2}} \\ 0 & 0 & 0 & \frac{\sqrt{7}}{2\sqrt{2}} & 0 & 0 & 0 & \frac{1}{2\sqrt{2}} & 0 \\ 0 & \frac{1}{2\sqrt{2}} & 0 & 0 & 0 & \frac{\sqrt{7}}{2\sqrt{2}} & 0 & 0 & 0 \\ \frac{\sqrt{5}}{2\sqrt{6}} & 0 & 0 & 0 & \frac{\sqrt{7}}{2\sqrt{3}} & 0 & 0 & 0 & \frac{\sqrt{5}}{2\sqrt{6}} \\ 0 & 0 & 0 & -\frac{1}{2\sqrt{2}} & 0 & 0 & 0 & \frac{\sqrt{7}}{2\sqrt{2}} & 0 \\ 0 & 0 & -\frac{1}{\sqrt{2}} & 0 & 0 & 0 & \frac{1}{\sqrt{2}} & 0 & 0 \\ 0 & -\frac{\sqrt{7}}{2\sqrt{2}} & 0 & 0 & 0 & \frac{1}{2\sqrt{2}} & 0 & 0 & 0 \end{pmatrix} \quad . \tag{A11}$$

After this partial-diagonalization, finite-volume function becomes $\overline{F}_{+}^{(FV)} \;=\; S_{+}.F_{+}^{(FV)}.S_{+}^{\dagger}$ where

$$\begin{aligned}
\overline{F}_{0,0}^{(FV)} \;&=\; \frac{1}{\pi^{3/2}}\,\frac{1}{\tilde{q}}\;\mathcal{Z}_{0,0}(1;\tilde{q}^2) \;\;,\;\; \overline{F}_{0;2}^{(FV)} \;=\; \begin{pmatrix} 0 & 0 & 0 & 0 & 0 \end{pmatrix} \\
\overline{F}_{0;4}^{(FV)} \;&=\; \frac{1}{\pi^{3/2}}\,\frac{1}{\tilde{q}^5}\;\mathcal{Z}_{4,0}(1;\tilde{q}^2)\;\frac{2\sqrt{3}}{\sqrt{7}}\begin{pmatrix} 0 & 0 & 0 & 0 & 0 & 1 & 0 & 0 & 0 \end{pmatrix} \\
\overline{F}_{2;2}^{(FV)} \;&=\; \frac{1}{\pi^{3/2}}\,\frac{1}{\tilde{q}}\;\mathcal{Z}_{0,0}(1;\tilde{q}^2)\;\;\mathrm{diag}\,(1,1,1,1,1) \\
&\quad+\; \frac{1}{\pi^{3/2}}\,\frac{1}{\tilde{q}^5}\;\mathcal{Z}_{4,0}(1;\tilde{q}^2)\;\frac{2}{7}\;\mathrm{diag}\,(-2,-2,-2,3,3)
\end{aligned}$$

$$\begin{aligned}
\overline{F}_{2;4}^{(FV)} \;&=\; \frac{1}{\pi^{3/2}}\,\frac{1}{\tilde{q}^5}\;\mathcal{Z}_{4,0}(1;\tilde{q}^2)\;\frac{20\sqrt{3}}{77}\begin{pmatrix} 0 & 0 & 0 & 0 & 0 & 0 & 0 & -1 & 0 \\ 0 & 0 & 0 & 0 & 0 & 0 & 0 & 0 & 1 \\ 0 & 0 & 0 & 0 & 0 & 0 & -1 & 0 & 0 \\ 0 & -2 & 0 & 0 & 0 & 0 & 0 & 0 & 0 \\ -2 & 0 & 0 & 0 & 0 & 0 & 0 & 0 & 0 \end{pmatrix} \\
&\quad+\; \frac{1}{\pi^{3/2}}\,\frac{1}{\tilde{q}^7}\;\mathcal{Z}_{6,0}(1;\tilde{q}^2)\;\frac{40\sqrt{3}}{11\sqrt{13}}\begin{pmatrix} 0 & 0 & 0 & 0 & 0 & 0 & 0 & 1 & 0 \\ 0 & 0 & 0 & 0 & 0 & 0 & 0 & 0 & -1 \\ 0 & 0 & 0 & 0 & 0 & 0 & 1 & 0 & 0 \\ 0 & -\frac{3}{4} & 0 & 0 & 0 & 0 & 0 & 0 & 0 \\ -\frac{3}{4} & 0 & 0 & 0 & 0 & 0 & 0 & 0 & 0 \end{pmatrix} \quad .
\end{aligned} \tag{A12}$$

$$
\begin{aligned}
\overline{F}^{(FV)}_{4;4} &= \frac{1}{\pi^{3/2}}\,\frac{1}{\tilde{q}}\;\mathcal{Z}_{0,0}(1;\tilde{q}^2)\;\;\mathrm{diag}\,(1,1,1,1,1,1,1,1,1) \\
&+ \frac{1}{\pi^{3/2}}\,\frac{1}{\tilde{q}^5}\;\mathcal{Z}_{4,0}(1;\tilde{q}^2)\;\frac{54}{1001}\;\mathrm{diag}\,(2,2,7,7,7,14,-13,-13,-13) \\
&+ \frac{1}{\pi^{3/2}}\,\frac{1}{\tilde{q}^7}\;\mathcal{Z}_{6,0}(1;\tilde{q}^2)\;\frac{4}{11\sqrt{13}}\;\mathrm{diag}\,(-16,-16,-1,-1,-1,20,5,5,5) \\
&+ \frac{1}{\pi^{3/2}}\,\frac{1}{\tilde{q}^9}\;\mathcal{Z}_{8,0}(1;\tilde{q}^2)\;\frac{392}{1001\sqrt{17}}\;\mathrm{diag}\,(7,7,-8,-8,-8,10,0,0,0) \quad . \qquad \text{(A13)}
\end{aligned}
$$

It is clear from the form of the matrix $\overline{F}^{(FV)}_{+}$ that the ordering of the $\Gamma^{(i)}$ in the $\overline{F}^{(FV)}_{4;4}$-block is E^+, T_1^+, A_1^+ and T_2^+, respectively, and the equations that dictate the energy-eigenvalues of each of the $\Gamma^{(i)}$, given in eqs. (9), (20), (25), and (29), follow directly from these expressions.

APPENDIX B: $\mathcal{Z}_{l,m}(1;\tilde{q}^2)$ FUNCTIONS

The two-hadron Green functions in the finite lattice volume depend upon summations over plane-wave states subject to periodic boundary conditions and with amplitudes that depend upon the strength of the interactions in each of the partial-waves that generate the two-hadron T-matrix. The summations that define the energy-eigenvalues in the volume are [1, 2]

$$
\mathcal{Z}_{l,m}(1;\tilde{q}^2) \;=\; \sum_{\mathbf{n}} \frac{|\mathbf{n}|^l\; Y_{lm}(\Omega_{\mathbf{n}})}{[\;|\mathbf{n}|^2-\tilde{q}^2\;]} \quad , \qquad \text{(B1)}
$$

a special case of the sums defined in eq. (5). The $l=0$ summation is special as it requires UV regulation in order to be defined, while sums with $l \geq 1$ are finite due to contribution from the solitary Y_{lm}. However, brute-force evaluation of the sums is quite inefficient and Lüscher presented a method to evaluate the sums that exponentially accelerates their evaluation [1, 2], making use of the Poisson resummation formula. In this appendix, we reproduce Lüscher's results, and then present each of the $\mathcal{Z}_{l,m}(1;\tilde{q}^2)$ that contribute to the energy-eigenvalues considered in the body of this paper.

Numerical evaluation of the $\mathcal{Z}_{0,0}(1;\tilde{q}^2)$ can be evaluated by brute force through the definition

$$
\mathcal{Z}_{0,0}(1;\tilde{q}^2) \;=\; \frac{1}{\sqrt{4\pi}}\;\lim_{\Lambda_{\mathbf{n}}\to\infty}\left[\;\sum_{\mathbf{n}}^{\Lambda_{\mathbf{n}}}\frac{1}{|\mathbf{n}|^2-\tilde{q}^2}\;-\;4\pi\Lambda_{\mathbf{n}}\;\right] \quad , \qquad \text{(B2)}
$$

or through the exponentially-accelerated relation [1, 2, 61] [9]

$$\mathcal{Z}_{0,0}(1;\tilde{q}^2) \;=\; \pi e^{\tilde{q}^2}(2\tilde{q}^2-1) \;+\; \frac{e^{\tilde{q}^2}}{2\sqrt{\pi}} \sum_{\mathbf{n}} \frac{e^{-|\mathbf{n}|^2}}{|\mathbf{n}|^2-\tilde{q}^2} - \frac{\pi}{2}\int_0^1 dt\; \frac{e^{t\tilde{q}^2}}{t^{3/2}} \left(4t^2\tilde{q}^4 \;-\; \sum_{\mathbf{m}\neq\mathbf{0}} e^{\frac{-\pi^2|\overline{\mathbf{m}}|^2}{t}} \right) \quad . \tag{B4}$$

For $l \neq 0$, the exponentially accelerated evaluation can be accomplished with [10]

$$\mathcal{Z}_{l,m}(1;\tilde{q}^2) \;=\; \sum_{\mathbf{n}} \frac{|\mathbf{n}|^l\; Y_{lm}(\Omega_{\mathbf{n}})\; e^{-\Lambda(|\mathbf{n}|^2-\tilde{q}^2)}}{[\;|\mathbf{n}|^2-\tilde{q}^2\;]} + \sum_{\mathbf{p}} \int_0^{\Lambda} d\lambda\; \left(\frac{\pi}{\lambda}\right)^{l+3/2}\; e^{\lambda\tilde{q}^2}\; |\mathbf{p}|^l\; Y_{lm}(\Omega_{\mathbf{p}})\; e^{-\frac{\pi^2|\mathbf{p}|^2}{\lambda}} \quad . \tag{B6}$$

There are exact relations that exist between the $\mathcal{Z}_{l,m}(1;\tilde{q}^2)$ for fixed l:

$$\begin{aligned}
\mathcal{Z}_{4,\pm4}(1;\tilde{q}^2) \;&=\; \sqrt{\frac{5}{14}}\mathcal{Z}_{4,0}(1;\tilde{q}^2) \\
\mathcal{Z}_{6,\pm4}(1;\tilde{q}^2) \;&=\; -\sqrt{\frac{7}{2}}\;\mathcal{Z}_{6,0}(1;\tilde{q}^2) \\
\mathcal{Z}_{8,\pm4}(1;\tilde{q}^2) \;&=\; \frac{\sqrt{154}}{33}\;\mathcal{Z}_{8,0}(1;\tilde{q}^2) \quad , \quad \mathcal{Z}_{8,\pm8}(1;\tilde{q}^2) \;=\; \frac{\sqrt{1430}}{66}\;\mathcal{Z}_{8,0}(1;\tilde{q}^2) \\
\mathcal{Z}_{10,\pm4}(1;\tilde{q}^2) \;&=\; -\sqrt{\frac{66}{65}}\;\mathcal{Z}_{10,0}(1;\tilde{q}^2) \quad , \quad \mathcal{Z}_{10,\pm8}(1;\tilde{q}^2) \;=\; -\sqrt{\frac{187}{130}}\;\mathcal{Z}_{10,0}(1;\tilde{q}^2) \\
\mathcal{Z}_{12,\pm8}(1;\tilde{q}^2) \;&=\; \sqrt{\frac{429}{646}}\;\mathcal{Z}_{12,0}(1;\tilde{q}^2) \;-\; 4\sqrt{\frac{42}{323}}\;\mathcal{Z}_{12,\pm4}(1;\tilde{q}^2) \\
\mathcal{Z}_{12,\pm12}(1;\tilde{q}^2) \;&=\; 4\sqrt{\frac{91}{7429}}\;\mathcal{Z}_{12,0}(1;\tilde{q}^2) \;+\; 9\sqrt{\frac{11}{7429}}\;\mathcal{Z}_{12,\pm4}(1;\tilde{q}^2)
\end{aligned}$$

---

[9] The Poisson resummation formula

$$\sum_{\mathbf{n}} \delta^3(\mathbf{y}-\mathbf{n}) \;=\; \sum_{\mathbf{m}} e^{i2\pi\mathbf{m}\cdot\mathbf{y}} \quad , \tag{B3}$$

has been used in obtaining eq. (B4).

[10] We have used a relation that is similar to that used by Lüscher [2],

$$\int d^3\mathbf{x}\; g(\mathbf{x})\; e^{-\lambda|\mathbf{x}|^2}\; e^{i2\pi\mathbf{p}\cdot\mathbf{x}} \;=\; g(\frac{-i}{2\pi}\nabla_{\mathbf{p}}) \int d^3\mathbf{x}\; e^{-\lambda|\mathbf{x}|^2}\; e^{i2\pi\mathbf{p}\cdot\mathbf{x}} \;=\; \left(\frac{\pi}{\lambda}\right)^{3/2}\; g(\frac{i\pi}{\lambda}\mathbf{p})\; e^{-\frac{\pi^2|\mathbf{p}|^2}{\lambda}} \quad . \tag{B5}$$

$$
\begin{aligned}
\mathcal{Z}_{14,\pm4}(1;\tilde{q}^2) &= -\frac{3}{2}\sqrt{\frac{143}{595}}\,\mathcal{Z}_{14,0}(1;\tilde{q}^2) \quad , \quad \mathcal{Z}_{14,\pm8}(1;\tilde{q}^2) \;=\; -\sqrt{\frac{741}{1190}}\,\mathcal{Z}_{14,0}(1;\tilde{q}^2) \\
\mathcal{Z}_{14,\pm12}(1;\tilde{q}^2) &= -\frac{1}{2}\sqrt{\frac{437}{119}}\,\mathcal{Z}_{14,0}(1;\tilde{q}^2) \\
\mathcal{Z}_{16,\pm8}(1;\tilde{q}^2) &= -6\sqrt{\frac{6}{805}}\mathcal{Z}_{16,4}(1;\tilde{q}^2) \;+\; \sqrt{\frac{442}{2185}}\mathcal{Z}_{16,0}(1;\tilde{q}^2) \\
\mathcal{Z}_{16,\pm12}(1;\tilde{q}^2) &= -\frac{31}{5}\sqrt{\frac{13}{483}}\mathcal{Z}_{16,4}(1;\tilde{q}^2) \;+\; \frac{16}{5}\sqrt{\frac{17}{437}}\mathcal{Z}_{16,0}(1;\tilde{q}^2) \\
\mathcal{Z}_{16,\pm16}(1;\tilde{q}^2) &= 4\sqrt{\frac{754}{74865}}\mathcal{Z}_{16,4}(1;\tilde{q}^2) \;+\; 7\sqrt{\frac{493}{135470}}\mathcal{Z}_{16,0}(1;\tilde{q}^2) \\
\mathcal{Z}_{18,\pm8}(1;\tilde{q}^2) &= -\frac{58}{5}\sqrt{\frac{22}{161}}\mathcal{Z}_{18,4}(1;\tilde{q}^2) \;-\; \frac{3}{5}\sqrt{\frac{646}{23}}\mathcal{Z}_{18,0}(1;\tilde{q}^2) \\
\mathcal{Z}_{18,\pm12}(1;\tilde{q}^2) &= \frac{501}{5}\sqrt{\frac{11}{4669}}\mathcal{Z}_{18,4}(1;\tilde{q}^2) \;+\; \frac{16}{5}\sqrt{\frac{323}{667}}\mathcal{Z}_{18,0}(1;\tilde{q}^2) \\
\mathcal{Z}_{18,\pm16}(1;\tilde{q}^2) &= -4\sqrt{\frac{3162}{23345}}\mathcal{Z}_{18,4}(1;\tilde{q}^2) \;-\; \sqrt{\frac{19437}{6670}}\mathcal{Z}_{18,0}(1;\tilde{q}^2) \quad . \qquad \text{(B7)}
\end{aligned}
$$

Unlike the cases of $l = 0, 4, 6, 8, 10, 14$ which have only one occurrence of the A_1^+ irrep in their decomposition, $l = 12, 16, 18$ have two, and as such the $\mathcal{Z}_{12,\pm4k}$ (k is an integer) are not simply proportional to $\mathcal{Z}_{12,0}$, as demonstrated in eq. (B7), and a similar statement can be made about $\mathcal{Z}_{16,\pm4k}$ and $\mathcal{Z}_{18,\pm4k}$.

In an effort to better understand the origins of the structure of the functions determining the energy-eigenvalues of each of the $\Gamma^{(i)}$, it is useful to explicitly display the functions $\mathcal{Z}_{l,m}(1;\tilde{q}^2)$. The function $\mathcal{Z}_{0,0}(1;\tilde{q}^2)$ is shown in the body of this paper in fig. 1. As discussed by Lüscher, the functions $\mathcal{Z}_{l,m}(1;\tilde{q}^2)$ vanish for all odd-l, and also vanishes for $l = 2$. The function $\mathcal{Z}_{4,0}(1;\tilde{q}^2)$ is shown in fig. 36, and exhibits some structure that is not present in $\mathcal{Z}_{0,0}(1;\tilde{q}^2)$. There are branches of $\mathcal{Z}_{4,0}(1;\tilde{q}^2)$ that are non-monotonic, for instance, between $\tilde{q}^2 = 1$ and $\tilde{q}^2 = 2$. This behavior is found in all of the $\mathcal{Z}_{l,m}$'s with $l > 0$. The functions $\mathcal{Z}_{8,0}(1;\tilde{q}^2)$ and $\mathcal{Z}_{10,0}(1;\tilde{q}^2)$ are shown in fig. 37, $\mathcal{Z}_{12,0}(1;\tilde{q}^2)$ and $\mathcal{Z}_{12,4}(1;\tilde{q}^2)$ in fig. 38, $\mathcal{Z}_{14,0}(1;\tilde{q}^2)$ in fig. 39, $\mathcal{Z}_{16,0}(1;\tilde{q}^2)$ and $\mathcal{Z}_{16,4}(1;\tilde{q}^2)$ in fig. 40, and finally $\mathcal{Z}_{18,0}(1;\tilde{q}^2)$ and $\mathcal{Z}_{18,4}(1;\tilde{q}^2)$ in fig. 41.

In constructing the perturbative expressions for the energy-eigenvalues in terms of the δ_l, the leading contributions result from the residue of the pole of the leading function. We present a few of these residues of the $\mathcal{Z}_{l,m}(1;\tilde{q}^2)$ functions in table XXVIII and table XXIX.

APPENDIX C: PERTURBATIVE EXPRESSIONS

In many instances the energy-shifts due to the interactions are small because the phase-shift is small and/or the lattice volume is large. In such instances, a perturbative expression can be used to extract the phase-shift from an energy-eigenvalue instead of solving the full expression, as discussed by Lüscher [1, 2]. The energy-eigenvalues for a given $\Gamma^{(i)}$ in a given $|\mathbf{n}|^2$-shell, and more specifically $\tilde{q}^2$, can be expanded in terms of the dimensionless quantity

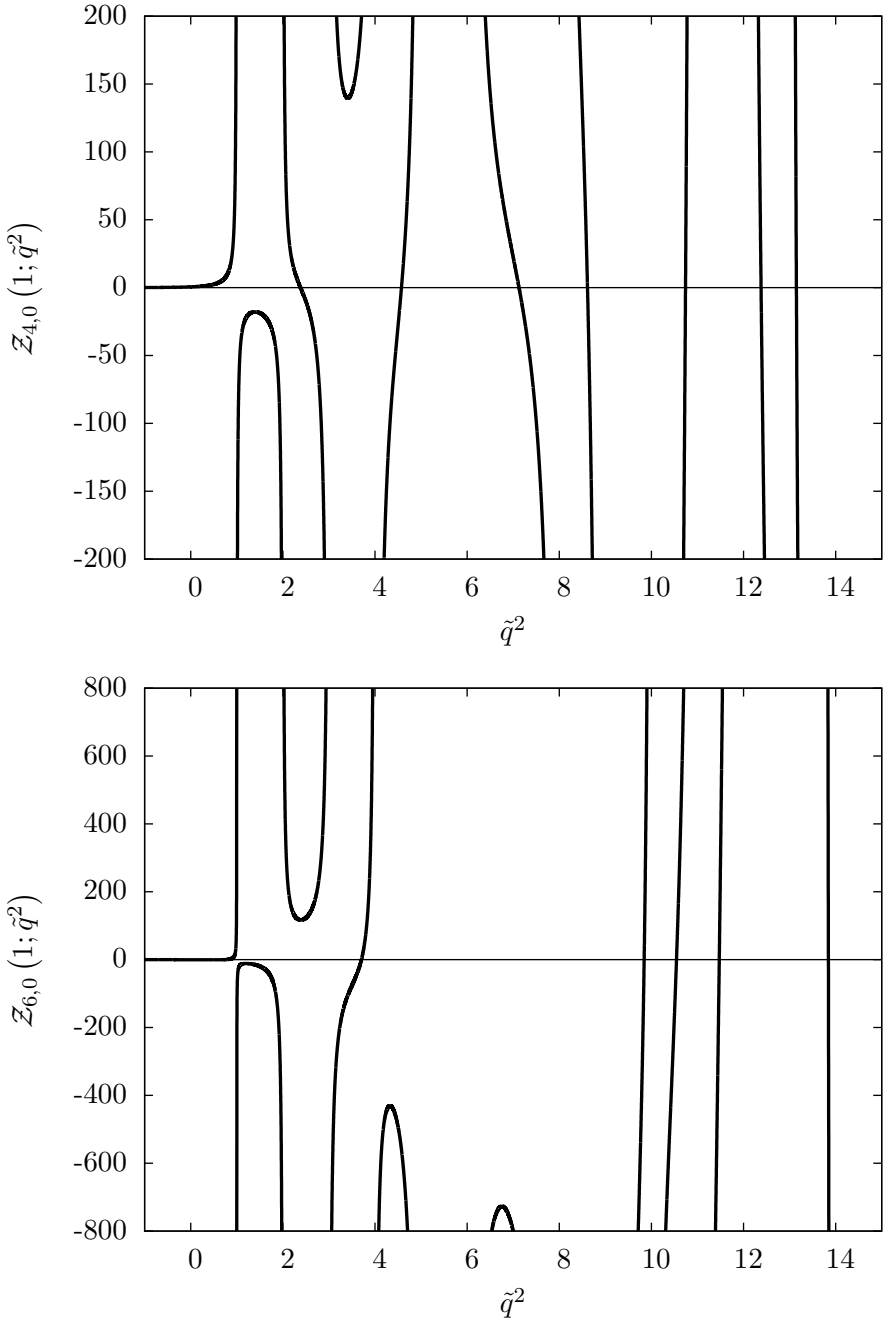

FIG. 36: The function $\mathcal{Z}_{4,0}(1;\tilde{q}^2)$ (top-panel) and $\mathcal{Z}_{6,0}(1;\tilde{q}^2)$ (bottom-panel).

$\left(L^{(2l+1}q^{2l+1}\cot\delta_l^I\right)^{-1}$ [11]. In the case of a single partial-wave, the general form for the energy

[11] The corresponding expansion that is appropriate for systems near unitarity, an expansion in terms of $(Lq\cot\delta)$ for s-wave interactions that is small for large scattering lengths, can be found in Ref. [56].

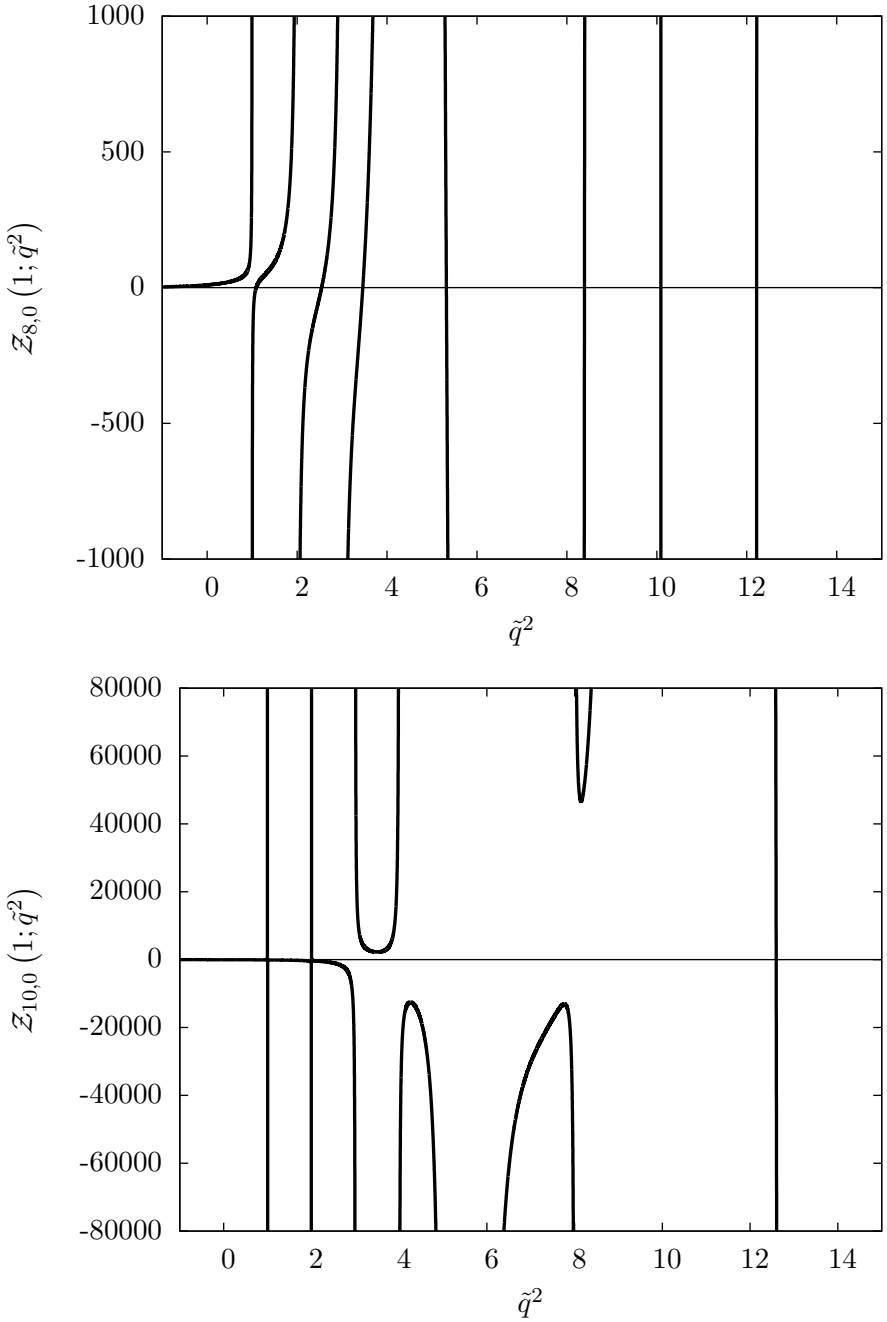

FIG. 37: The function $\mathcal{Z}_{8,0}(1;\tilde{q}^2)$ (top-panel) and $\mathcal{Z}_{10,0}(1;\tilde{q}^2)$ (bottom-panel).

of an irrep, $\Gamma^{(i)}$, in the $|\mathbf{n}|^2$-shell is

$$q^{2l+1}\cot\delta_l^I \;=\; \frac{1}{\pi L}\,\left(\frac{2\pi}{L}\right)^{2l}\left[\frac{\alpha_{-1}^{(|\mathbf{n}|^2,\Gamma^{(i)})}}{\delta\tilde{q}^2} \;+\; \alpha_0^{(|\mathbf{n}|^2,\Gamma^{(i)})} \;+\; \alpha_1^{(|\mathbf{n}|^2,\Gamma^{(i)})}\delta\tilde{q}^2 \;+\; ...\right] \quad , \text{(C1)}$$

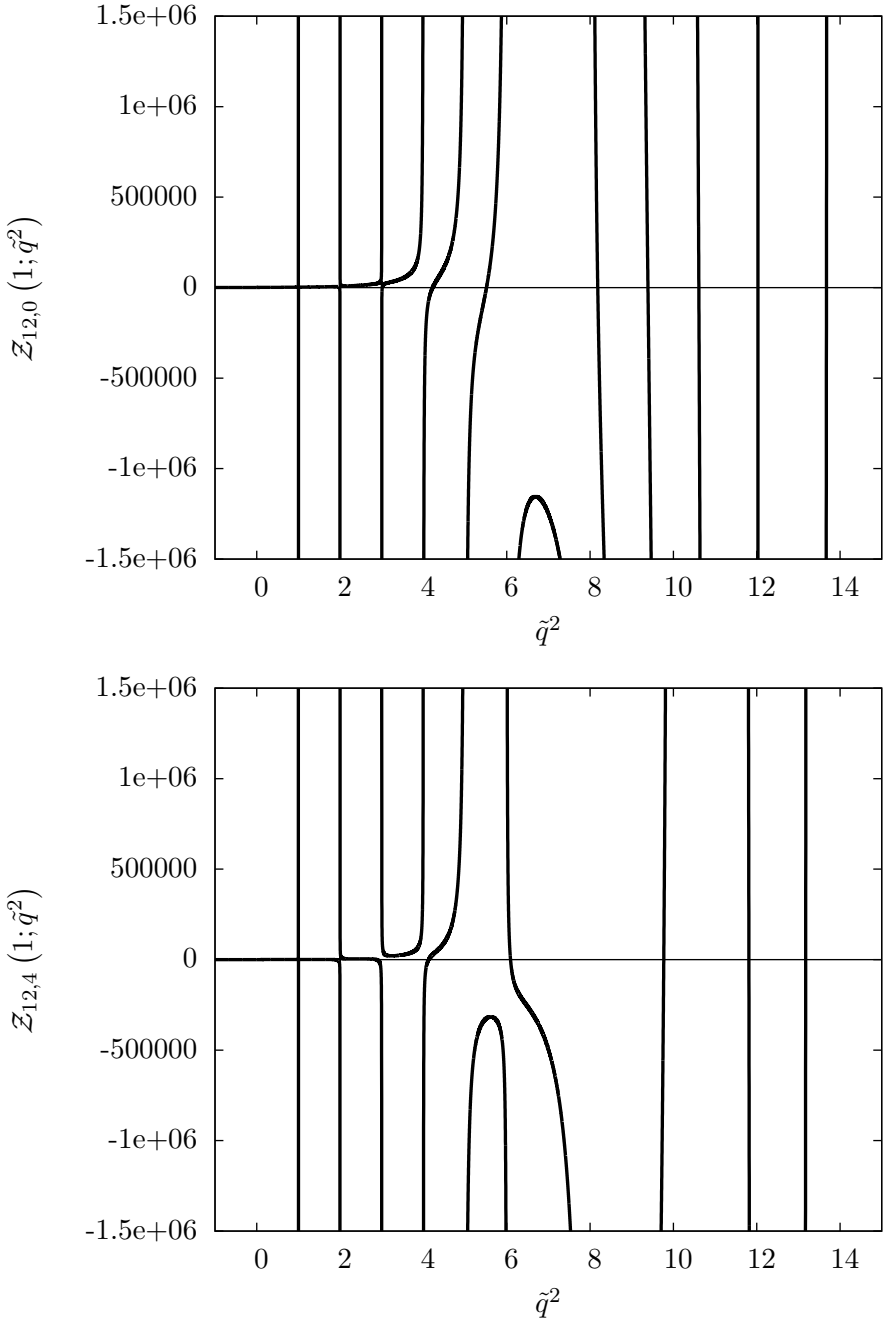

FIG. 38: The function $\mathcal{Z}_{12,0}(1;\tilde{q}^2)$ (top-panel) and $\mathcal{Z}_{12,4}(1;\tilde{q}^2)$ (bottom-panel).

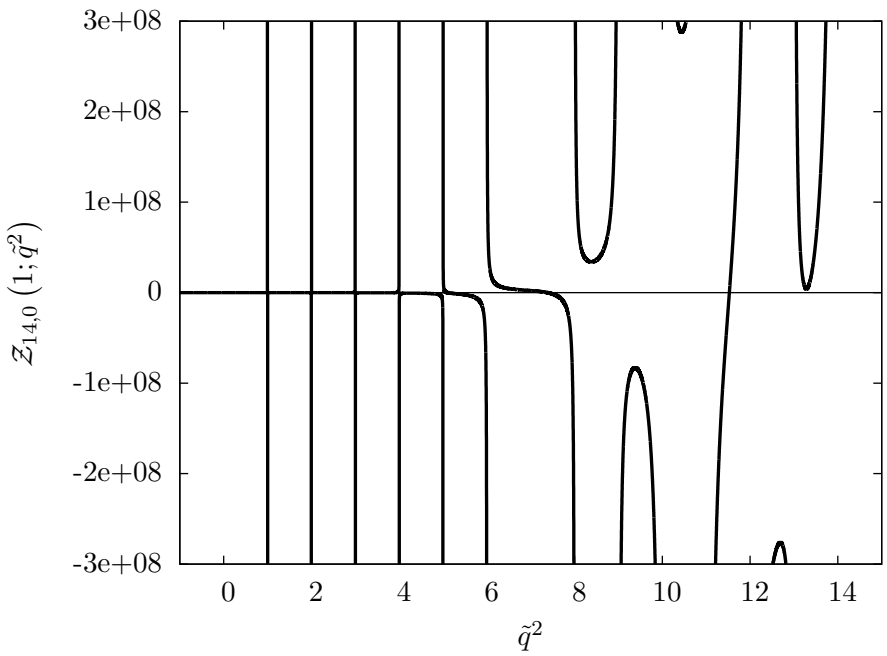

FIG. 39: The function $\mathcal{Z}_{14,0}(1;\tilde{q}^2)$.

TABLE XXVIII: Residues of the functions $\sqrt{4\pi}\ \mathcal{Z}_{l,m}(1;\tilde{q}^2)$ for $l \leq 12$, i.e. the coefficient of $-\frac{1}{\tilde{Q}^2}$ where $\tilde{q}^2 = |\mathbf{n}|^2 + \tilde{Q}^2$.

$\lvert\mathbf{n}\rvert^2$	$R\left[\sqrt{4\pi}\mathcal{Z}_{0,0}\right]$	$R\left[\sqrt{4\pi}\mathcal{Z}_{4,0}\right]$	$R\left[\sqrt{4\pi}\mathcal{Z}_{6,0}\right]$	$R\left[\sqrt{4\pi}\mathcal{Z}_{8,0}\right]$	$R\left[\sqrt{4\pi}\mathcal{Z}_{10,0}\right]$	$R\left[\sqrt{4\pi}\mathcal{Z}_{12,0}\right]$	$R\left[\sqrt{4\pi}\mathcal{Z}_{12,4}\right]$
0	1	0	0	0	0	0	0
1	6	$\frac{21}{2}$	$\frac{3\sqrt{13}}{4}$	$\frac{99\sqrt{17}}{32}$	$\frac{65\sqrt{21}}{64}$	$\frac{3715}{256}$	$\frac{75\sqrt{1001}}{512}$
2	12	-21	$-\frac{39\sqrt{13}}{2}$	$\frac{891\sqrt{17}}{16}$	$-\frac{65\sqrt{21}}{32}$	-$\frac{43885}{128}$	$-\frac{8085\sqrt{1001}}{256}$
3	8	-84	$48\sqrt{13}$	$99\sqrt{17}$	$-520\sqrt{21}$	$\frac{2225}{2}$	$-\frac{555\sqrt{1001}}{4}$
4	6	168	$48\sqrt{13}$	$792\sqrt{17}$	$1040\sqrt{21}$	59440	$600\sqrt{1001}$
5	24	210	$-255\sqrt{13}$	$-\frac{13365\sqrt{17}}{8}$	$-\frac{204425\sqrt{21}}{16}$	$\frac{21172895}{64}$	$\frac{1262535\sqrt{1001}}{128}$
6	24	-378	$333\sqrt{13}$	$-\frac{51381\sqrt{17}}{8}$	$\frac{408915\sqrt{21}}{16}$	$\frac{58441035}{64}$	$-\frac{324765\sqrt{1001}}{128}$
14	48	-4116	$-1806\sqrt{13}$	$-\frac{455301\sqrt{17}}{4}$	$\frac{19718335\sqrt{21}}{8}$	$\frac{2472346835}{32}$	$\frac{309589035\sqrt{1001}}{64}$

where the solutions to eq. (C1) can be written as

$$\begin{aligned}
\tilde{q}^2_{|\mathbf{n}|^2,\Gamma} &= |\mathbf{n}|^2 + \delta\tilde{q}^2 = \left(\frac{qL}{2\pi}\right)^2 \\
&= |\mathbf{n}|^2 \ + \ g_0^{(|\mathbf{n}|^2,\Gamma^{(i)})}\ \tan\delta_l^I \ \left(\ 1 \ + \ g_1^{(|\mathbf{n}|^2,\Gamma^{(i)})}\tan\delta_l^I \ + \ g_2^{(|\mathbf{n}|^2,\Gamma^{(i)})}\tan^2\delta_l^I \ + \ ...\right) \\
&+ \ h_0^{(|\mathbf{n}|^2,\Gamma^{(i)})}\ \frac{\frac{d}{d(Lq)^2}\left((Lq)^{2l+1}\cot\delta_l^I\right)}{\left[(Lq)^{2l+1}\cot\delta_l^I\right]^3} \ + \ ... \quad , \qquad \text{(C2)}
\end{aligned}$$

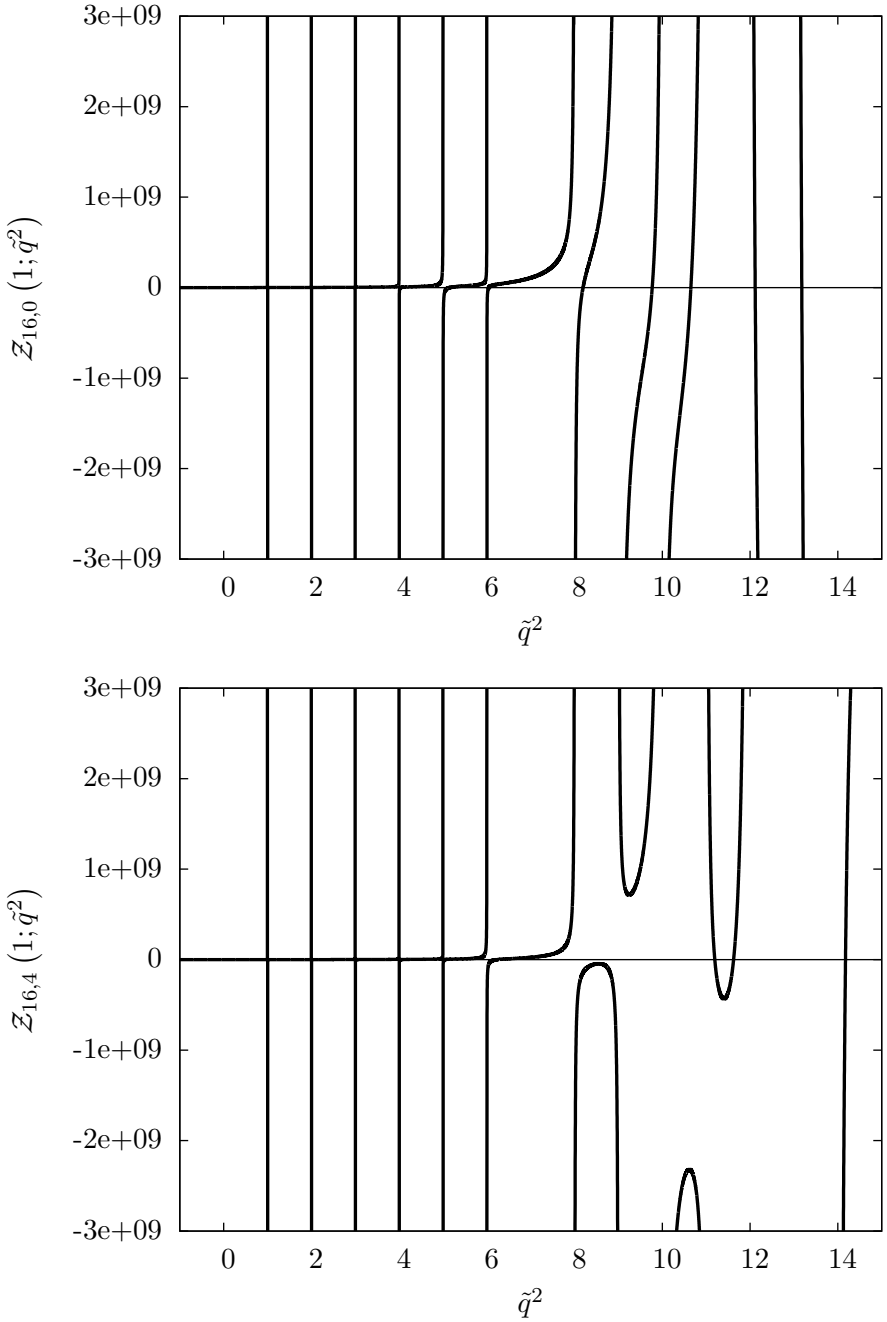

FIG. 40: The functions $\mathcal{Z}_{16,0}(1;\tilde{q}^2)$ (top-panel) and $\mathcal{Z}_{16,4}(1;\tilde{q}^2)$ (bottom-panel).

where the phase-shift is evaluated at the unperturbed energy of the state, and the coefficients are

$$g_0^{(|\mathbf{n}|^2,\Gamma^{(i)})} = \frac{\alpha_{-1}^{(|\mathbf{n}|^2,\Gamma^{(i)})}}{2\pi^2|\mathbf{n}|^{2l+1}} \quad , \quad g_1^{(|\mathbf{n}|^2,\Gamma^{(i)})} = \frac{\alpha_0^{(|\mathbf{n}|^2,\Gamma^{(i)})}}{2\pi^2|\mathbf{n}|^{2l+1}}$$
$$g_2^{(|\mathbf{n}|^2,\Gamma^{(i)})} = \frac{(\alpha_0^{(|\mathbf{n}|^2,\Gamma^{(i)})})^2 + \alpha_{-1}^{(|\mathbf{n}|^2,\Gamma^{(i)})}\alpha_1^{(|\mathbf{n}|^2,\Gamma^{(i)})}}{2\pi^2|\mathbf{n}|^{2l+1}} \quad . \tag{C3}$$

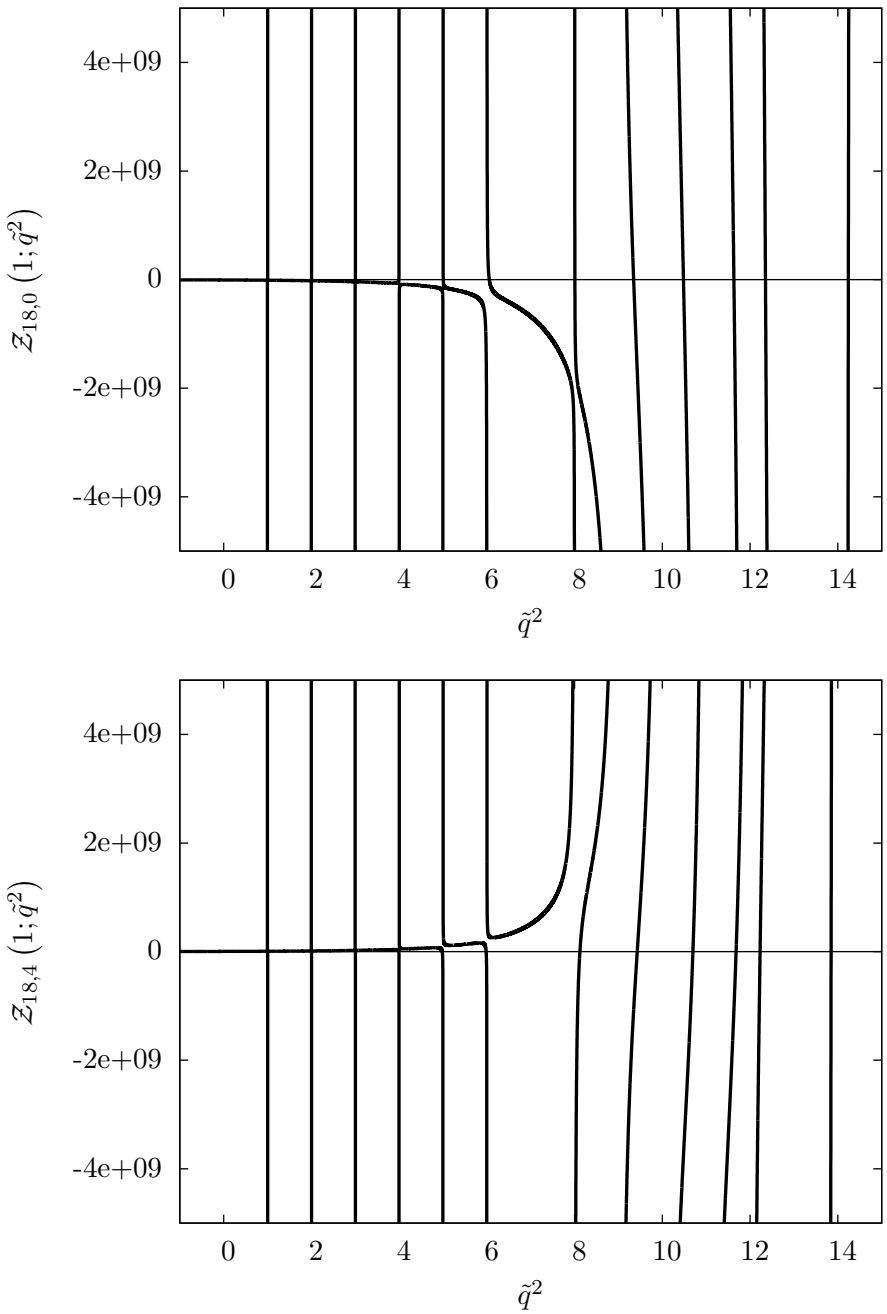

FIG. 41: The functions $\mathcal{Z}_{18,0}(1;\tilde{q}^2)$ (top-panel) and $\mathcal{Z}_{18,4}(1;\tilde{q}^2)$ (bottom-panel).

For the terms in eq. (C2), the contributions scale as

$$\tilde{q}^2_{|\mathbf{n}|^2,\Gamma} \sim \mathcal{O}\left(1\right) + \mathcal{O}\left(\frac{1}{L^{2l+1}}\right) + \mathcal{O}\left(\frac{1}{L^{4l+2}}\right) + \mathcal{O}\left(\frac{1}{L^{6l+3}}\right) + \mathcal{O}\left(\frac{1}{L^{4l+4}}\right) + \ldots\,, \quad \text{(C4)}$$

from which it can be determined when the contributions from higher partial-waves become important. For instance, the energy-shifts in the T_1^- irrep are dominated by δ_1, and the

TABLE XXIX: Residues of the functions $\sqrt{4\pi}\ \mathcal{Z}_{l,m}(1;\tilde{q}^2)$ for $14 \leq l \leq 18$, i.e. the coefficient of $-\frac{1}{\tilde{Q}^2}$ where $\tilde{q}^2 = |\mathbf{n}|^2 + \tilde{Q}^2$.

$\lvert\mathbf{n}\rvert^2$	$R\left[\sqrt{4\pi}\mathcal{Z}_{14,0}\right]$	$R\left[\sqrt{4\pi}\mathcal{Z}_{16,0}\right]$	$R\left[\sqrt{4\pi}\mathcal{Z}_{16,4}\right]$	$R\left[\sqrt{4\pi}\mathcal{Z}_{18,0}\right]$	$R\left[\sqrt{4\pi}\mathcal{Z}_{18,4}\right]$
1	$\frac{595\sqrt{29}}{512}$	$\frac{22819\sqrt{33}}{8192}$	$\frac{33\sqrt{323323}}{4096}$	$\frac{20613\sqrt{37}}{16384}$	$-\frac{39\sqrt{920227}}{8192}$
2	$-\frac{52955\sqrt{29}}{256}$	$\frac{2627491\sqrt{33}}{4096}$	$\frac{5937\sqrt{323323}}{2048}$	$-\frac{234021\sqrt{37}}{8192}$	$\frac{9063\sqrt{920227}}{4096}$
3	$3570\sqrt{29}$	$-\frac{135261\sqrt{33}}{16}$	$\frac{873\sqrt{323323}}{8}$	$-12453\sqrt{37}$	$18\sqrt{920227}$
4	$19040\sqrt{29}$	$182552\sqrt{33}$	$528\sqrt{323323}$	$329808\sqrt{37}$	$-1248\sqrt{920227}$
5	$-\frac{9356375\sqrt{29}}{128}$	$\frac{3105175795\sqrt{33}}{2048}$	$\frac{1267665\sqrt{323323}}{1024}$	$-\frac{2195267925\sqrt{37}}{4096}$	$-\frac{12933225\sqrt{920227}}{2048}$
6	$-\frac{144911655\sqrt{29}}{128}$	$\frac{1849263939\sqrt{33}}{2048}$	$\frac{15619473\sqrt{323323}}{1024}$	$-\frac{40787860977\sqrt{37}}{4096}$	$-\frac{26504469\sqrt{920227}}{2048}$
14	$\frac{6869655205\sqrt{29}}{64}$	$-\frac{12080581399901\sqrt{33}}{1024}$	$\frac{4554268593\sqrt{323323}}{512}$	$\frac{44894607368667\sqrt{37}}{2048}$	$\frac{51258039399\sqrt{920227}}{1024}$

TABLE XXX: The coefficients, $g_i^{(|\mathbf{n}|^2,A_1^+)}$ that contribute to the perturbative expansion of the energy-eigenvalues of states in the A_1^+ irrep of the cubic group, as given in eq. (C2), in terms of s-wave phase-shift δ_0.

$\lvert\mathbf{n}\rvert^2$	$g_0^{(\lvert\mathbf{n}\rvert^2,A_1^+)}$	$g_1^{(\lvert\mathbf{n}\rvert^2,A_1^+)}$	$g_2^{(\lvert\mathbf{n}\rvert^2,A_1^+)}$
1	$-\frac{3}{\pi^2}$	-0.06137	-0.3542
2	$-\frac{3\sqrt{2}}{\pi^2}$	-0.1826	-0.3618
3	$-\frac{4}{\sqrt{3}\pi^2}$	-0.1981	-0.1996
4	$-\frac{3}{2\pi^2}$	0.2415	-0.1328
5	$-\frac{12}{\sqrt{5}\pi^2}$	0.1590	-0.5155
6	$-\frac{2\sqrt{6}}{\pi^2}$	-0.4798	-0.2025

expansion is of the form

$$\tilde{q}^2_{|\mathbf{n}|^2,T_1^-} \sim \mathcal{O}(1) + \mathcal{O}\left(\frac{1}{L^3}\right) + \mathcal{O}\left(\frac{1}{L^6}\right) + \mathcal{O}\left(\frac{1}{L^9}\right) + \mathcal{O}\left(\frac{1}{L^8}\right) + \ldots \quad , \tag{C5}$$

respectively, and the $l = 3$ partial-wave first contributes at $\mathcal{O}\left(\frac{1}{L^7}\right)$. In the case of the T_1^+ irrep, which is dominated by δ_4, the expansion is of the form

$$\tilde{q}^2_{|\mathbf{n}|^2,T_1^+} \sim \mathcal{O}(1) + \mathcal{O}\left(\frac{1}{L^9}\right) + \mathcal{O}\left(\frac{1}{L^{18}}\right) + \mathcal{O}\left(\frac{1}{L^{27}}\right) + \mathcal{O}\left(\frac{1}{L^{20}}\right) + \ldots \quad , \tag{C6}$$

and δ_6 contributions are of the form $\mathcal{O}(L^{-13})$. Therefore, the order at which the higher partial-waves contribute in the large-volume limit depends upon the $\Gamma^{(i)}$.

The perturbative expansions of the lowest few A_1^+ energy-eigenvalues in terms of the $l = 0$ phase-shift δ_0 were given by Lüscher [1], and here we simply extend those results to levels with $|\mathbf{n}|^2 \leq 6$ with the coefficients given in table XXX. The energy of the A_1^+ state in the $|\mathbf{n}|^2 = 0$ level can be expressed in terms of the s-wave scattering parameters defining the

TABLE XXXI: The coefficients, $g_i^{(|\mathbf{n}|^2,T_1^{-(1)})}$ that contribute to the perturbative expansion of the energy-eigenvalues of states in the (first occurrence of the) T_1^- irrep of the cubic group, as given in eq. (C2), in terms of $l=1$ phase-shift δ_1.

$\|\mathbf{n}\|^2$	$g_0^{(\|\mathbf{n}\|^2,T_1^{-(1)})}$	$g_1^{(\|\mathbf{n}\|^2,T_1^{-(1)})}$	$g_2^{(\|\mathbf{n}\|^2,T_1^{-(1)})}$
1	$-\frac{3}{\pi^2}$	-0.3653	-0.2058
2	$-\frac{3\sqrt{2}}{\pi^2}$	-0.3975	-0.1979
3	$-\frac{4}{\sqrt{3}\pi^2}$	-0.2761	-0.1471
4	$-\frac{3}{2\pi^2}$	0.2035	-0.1589
5	$-\frac{12}{\sqrt{5}\pi^2}$	0.05024	-0.5555
6	$-\frac{2\sqrt{6}}{\pi^2}$	-0.5625	-0.07659

TABLE XXXII: The coefficients, $g_i^{(|\mathbf{n}|^2,E^{+(1)})}$ that contribute to the perturbative expansion of the energy-eigenvalues of states in the (first occurrence of the) E^+ irrep of the cubic group, as given in eq. (C2), in terms of $l=2$ phase-shift δ_2.

$\|\mathbf{n}\|^2$	$g_0^{(\|\mathbf{n}\|^2,E^{+(1)})}$	$g_1^{(\|\mathbf{n}\|^2,E^{+(1)})}$	$g_2^{(\|\mathbf{n}\|^2,E^{+(1)})}$
1	$-\frac{15}{2\pi^2}$	-1.5672	2.5842
2	$-\frac{15}{4\sqrt{2}\pi^2}$	-0.8065	0.54
4	$-\frac{15}{4\pi^2}$	0.3272	-0.421
5	$-\frac{78}{5\sqrt{5}\pi^2}$	-0.447	-0.4331
6	$-\frac{5}{2\pi^2}\sqrt{\frac{3}{2}}$	-0.7884	0.3746

low-energy behavior of the phase-shift, and it is well-known that

$$\tilde{q}^2_{|\mathbf{0}|^2,A_1^+} = -\frac{a_0}{\pi L}\left(1 + c_1\left(\frac{a_0}{L}\right) + c_2\left(\frac{a_0}{L}\right)^2 + ...\right) + ... \quad . \tag{C7}$$

where the particle-physics convention for defining the scattering length has been used, and the coefficients are $c_1 = -2.8373$ and $c_2 = 6.3752$.

An important point to note is that the perturbative energy-shifts that are presented in table XXX-table XXXIII are for one of the occurrences of the $\Gamma^{(i)}$ that form a given $|\mathbf{n}|^2$-shell. Other occurrences are unperturbed at leading order. When multiple occurrences of a given irrep appear in a given $|\mathbf{n}|^2$-shell, the leading interactions will perturb the energy of one combination, while leaving the other states unperturbed, but the interactions in higher partial-waves will perturb these remaining states. The expansion coefficients for the lowest-lying T_1^- (dominated by δ_1^1), the E^+ and T_2^+ (both dominated by δ_2^I) are shown in table XXXI, table XXXII, and table XXXIII, respectively. We note that the coefficients in the perturbative expansion of the energy-eigenstates in the T_1^- irrep given in table XXXI differ from those given by Lüscher [2]. This can be attributed to the fact that $q^{(2l+1)}\cot\delta_l$

TABLE XXXIII: The coefficients, $g_i^{(|\mathbf{n}|^2,T_2^{+(1)})}$ that contribute to the perturbative expansion of the energy-eigenvalues of states in the (first occurrence of the) T_2^+ irrep of the cubic group, as given in eq. (C2), in terms of $l=2$ phase-shift δ_2.

$\|\mathbf{n}\|^2$	$g_0^{(\|\mathbf{n}\|^2,T_2^{+(1)})}$	$g_1^{(\|\mathbf{n}\|^2,T_2^{+(1)})}$	$g_2^{(\|\mathbf{n}\|^2,T_2^{+(1)})}$
2	$-\frac{15}{2\sqrt{2}\pi^2}$	-0.4830	-0.1828
3	$-\frac{20}{3\sqrt{3}\pi^2}$	-0.6737	0.2128
5	$-\frac{48}{5\sqrt{5}\pi^2}$	0.2004	-0.4515
6	$-\frac{5\sqrt{\frac{3}{2}}}{\pi^2}$	-0.5497	-0.0902

TABLE XXXIV: The coefficients, $g_0^{(|\mathbf{n}|^2,\Gamma)}$ that contribute to the perturbative expansion of the energy-eigenvalues of states in the A_2^-, T_2^-, T_1^+, E^- and A_2^+, as given in eq. (C2), in terms of dominant phase-shifts δ_3, δ_3, δ_4, δ_5, and δ_6, respectively. Also given are the coefficients in the perturbative expansion of the second occurrence of E^+, T_2^+, T_1^- and T_2^-, in terms of dominant phase-shifts δ_4, δ_4, δ_3, and δ_5, respectively.

$\|\mathbf{n}\|^2$	$g_0^{(\|\mathbf{n}\|^2,A_2^-)}$	$g_0^{(\|\mathbf{n}\|^2,T_2^-)}$	$g_0^{(\|\mathbf{n}\|^2,T_1^+)}$	$g_0^{(\|\mathbf{n}\|^2,E^-)}$	$g_0^{(\|\mathbf{n}\|^2,A_2^+)}$	$g_0^{(\|\mathbf{n}\|^2,E^{+(2)})}$	$g_0^{(\|\mathbf{n}\|^2,T_2^{+(2)})}$	$g_0^{(\|\mathbf{n}\|^2,T_1^{-(2)})}$	$g_0^{(\|\mathbf{n}\|^2,T_2^{-(2)})}$
2	0	$-\frac{105}{8\sqrt{2}\pi^2}$	0	0	0	0	0	0	0
3	$-\frac{140}{9\sqrt{3}\pi^2}$	0	0	0	0	0	0	0	0
5	0	$-\frac{84}{5\sqrt{5}\pi^2}$	$-\frac{2268}{125\sqrt{5}\pi^2}$	0	$-\frac{162162}{3125\sqrt{5}\pi^2}$	$-\frac{23814}{1625\sqrt{5}\pi^2}$	0	$-\frac{252}{25\sqrt{5}\pi^2}$	$-\frac{74844}{3125\sqrt{5}\pi^2}$
6	$-\frac{35\sqrt{\frac{2}{3}}}{3\pi^2}$	$-\frac{35}{4\sqrt{6}\pi^2}$	$-\frac{35\sqrt{2}}{4\sqrt{3}\pi^2}$	$-\frac{385}{12\sqrt{6}\pi^2}$	0	0	$-\frac{245\sqrt{2}}{36\sqrt{3}\pi^2}$	$-\frac{175\sqrt{2}}{36\sqrt{3}\pi^2}$	0

can be expanded in a power-series in energy about threshold [12], as performed in this work, while $q\cot\delta_l$ does not have such an expansion for $l>0$. For the remaining irreps, the T_2^-, A_2^-, T_1^+, A_2^+ and E^-, the expansion converges rapidly with just one non-trivial term, $\mathcal{O}\left(\tan\delta_l^I\right)$. The leading coefficients for these expansion of the energy-eigenvalues for each of these irreps are given in table XXXIV, along with the coefficients in the expansions for the second occurrences of the E^+, T_2^+, T_1^- and T_2^-. The perturbative expansion of the lowest-lying A_1^- state is given in table XXVII.

ACKNOWLEDGMENTS

We would like to thank David Kaplan for inspiring discussions. The work of TL was performed under the auspices of the U.S. Department of Energy by Lawrence Livermore National Laboratory under Contract DE-AC52-07NA27344 and the UNEDF SciDAC grant

[12] This is the effective range expansion which is valid below the threshold of the t-channel cut, $|\mathbf{q}|=m_\pi$ for $\pi\pi\to\pi\pi$.

DE-FC02-07ER41457. The work of MJS was supported in part by the U.S. Dept. of Energy under Grant No. DE-FG02-97ER41014.

[1] M. Luscher, Commun. Math. Phys. **105**, 153 (1986).
[2] M. Luscher, Nucl. Phys. B **354**, 531 (1991).
[3] T. Luu, M. J. Savage, A. Schwenk and J. P. Vary, Phys. Rev. C **82**, 034003 (2010) [arXiv:1006.0427 [nucl-th]].
[4] I. Stetcu, B. R. Barrett, U. van Kolck and J. P. Vary, Phys. Rev. A **76**, 063613 (2007) [arXiv:0705.4335 [cond-mat.other]].
[5] E. Epelbaum, H. Krebs, D. Lee and U. G. Meissner, Eur. Phys. J. A **45**, 335 (2010) [arXiv:1003.5697 [nucl-th]].
[6] J. E. Mandula, G. Zweig and J. Govaerts, Nucl. Phys. B **228**, 91 (1983).
[7] K. Rummukainen and S. A. Gottlieb, Nucl. Phys. B **450**, 397 (1995) [arXiv:hep-lat/9503028].
[8] C. h. Kim, C. T. Sachrajda and S. R. Sharpe, Nucl. Phys. B **727**, 218 (2005) [arXiv:hep-lat/0507006].
[9] T. Luu, PoS **LATTICE2008**, 246 (2008) [arXiv:0810.2331 [hep-lat]].
[10] S. Kreuzer and H. W. Hammer, Phys. Lett. B **694**, 424 (2011) [arXiv:1008.4499 [hep-lat]].
[11] S. Kreuzer and H. W. Hammer, Phys. Lett. B **673**, 260 (2009) [arXiv:0811.0159 [nucl-th]].
[12] S. R. Beane, P. F. Bedaque, K. Orginos and M. J. Savage [NPLQCD Collaboration], Phys. Rev. D **73**, 054503 (2006) [arXiv:hep-lat/0506013].
[13] S. R. Beane, T. C. Luu, K. Orginos, A. Parreno, M. J. Savage, A. Torok and A. Walker-Loud, Phys. Rev. D **77**, 014505 (2008) [arXiv:0706.3026 [hep-lat]].
[14] X. Feng, K. Jansen and D. B. Renner, Phys. Lett. B **684**, 268 (2010) [arXiv:0909.3255 [hep-lat]].
[15] S. R. Beane, P. F. Bedaque, T. C. Luu, K. Orginos, E. Pallante, A. Parreno and M. J. Savage, Phys. Rev. D **74**, 114503 (2006) [arXiv:hep-lat/0607036].
[16] J. Nagata, S. Muroya and A. Nakamura, Phys. Rev. C **80**, 045203 (2009) [arXiv:0812.1753 [hep-lat]].
[17] S. R. Beane, T. C. Luu, K. Orginos, A. Parreno, M. J. Savage, A. Torok and A. Walker-Loud [NPLQCD Collaboration], Phys. Rev. D **77**, 094507 (2008) [arXiv:0709.1169 [hep-lat]].
[18] S. R. Beane, W. Detmold, K. Orginos and M. J. Savage, arXiv:1004.2935 [hep-lat].
[19] R. Briceno, *private communication*
[20] J. J. Dudek, R. G. Edwards, M. J. Peardon, D. G. Richards and C. E. Thomas, arXiv:1011.6352 [hep-ph].
[21] Q. Liu [RBC Collaboration and UKQCD Collaboration], PoS **LAT2009**, 101 (2009) [arXiv:0910.2658 [hep-lat]].
[22] S. R. Sharpe, R. Gupta and G. W. Kilcup, Nucl. Phys. B **383**, 309 (1992).
[23] R. Gupta, A. Patel and S. R. Sharpe, Phys. Rev. D **48**, 388 (1993) [arXiv:hep-lat/9301016].
[24] Y. Kuramashi, M. Fukugita, H. Mino, M. Okawa and A. Ukawa, Phys. Rev. Lett. **71**, 2387 (1993).
[25] Y. Kuramashi, M. Fukugita, H. Mino, M. Okawa and A. Ukawa, [arXiv:hep-lat/9312016].
[26] M. Fukugita, Y. Kuramashi, H. Mino, M. Okawa and A. Ukawa, Phys. Rev. Lett. **73**, 2176 (1994) [arXiv:hep-lat/9407012].
[27] C. Gattringer, D. Hierl and R. Pullirsch [Bern-Graz-Regensburg Collaboration], Nucl. Phys. Proc. Suppl. **140**, 308 (2005) [arXiv:hep-lat/0409064].
[28] M. Fukugita, Y. Kuramashi, M. Okawa, H. Mino and A. Ukawa, Phys. Rev. D **52**, 3003 (1995)

[arXiv:hep-lat/9501024].
[29] H. R. Fiebig, K. Rabitsch, H. Markum and A. Mihaly, Few Body Syst. **29**, 95 (2000) [arXiv:hep-lat/9906002].
[30] S. Aoki *et al.* [JLQCD Collaboration], Nucl. Phys. Proc. Suppl. **83**, 241 (2000) [arXiv:hep-lat/9911025].
[31] C. Liu, J. h. Zhang, Y. Chen and J. P. Ma, [arXiv:hep-lat/0109010].
[32] C. Liu, J. h. Zhang, Y. Chen and J. P. Ma, Nucl. Phys. B **624**, 360 (2002) [arXiv:hep-lat/0109020].
[33] S. Aoki *et al.* [CP-PACS Collaboration], Nucl. Phys. Proc. Suppl. **106**, 230 (2002) [arXiv:hep-lat/0110151].
[34] S. Aoki *et al.* [JLQCD Collaboration], Phys. Rev. D **66**, 077501 (2002) [arXiv:hep-lat/0206011].
[35] S. Aoki *et al.* [CP-PACS Collaboration], Nucl. Phys. Proc. Suppl. **119**, 311 (2003) [arXiv:hep-lat/0209056].
[36] S. Aoki *et al.* [CP-PACS Collaboration], Phys. Rev. D **67**, 014502 (2003) [arXiv:hep-lat/0209124].
[37] K. J. Juge [BGR Collaboration], Nucl. Phys. Proc. Suppl. **129**, 194 (2004) [arXiv:hep-lat/0309075].
[38] N. Ishizuka and T. Yamazaki, Nucl. Phys. Proc. Suppl. **129**, 233 (2004) [arXiv:hep-lat/0309168].
[39] S. Aoki *et al.* [CP-PACS Collaboration], [arXiv:hep-lat/0503025].
[40] S. Aoki *et al.* [CP-PACS Collaboration], Nucl. Phys. Proc. Suppl. **140**, 305 (2005) [arXiv:hep-lat/0409063].
[41] T. Yamazaki *et al.* [CP-PACS Collaboration], Phys. Rev. D **70**, 074513 (2004) [arXiv:hep-lat/0402025].
[42] A. Torok *et al.*, Phys. Rev. D **81**, 074506 (2010) [arXiv:0907.1913 [hep-lat]].
[43] S. R. Beane, P. F. Bedaque, K. Orginos and M. J. Savage, Phys. Rev. Lett. **97**, 012001 (2006) [arXiv:hep-lat/0602010].
[44] S. R. Beane, P. F. Bedaque, T. C. Luu, K. Orginos, E. Pallante, A. Parreno and M. J. Savage [NPLQCD Collaboration], Nucl. Phys. A **794**, 62 (2007) [arXiv:hep-lat/0612026].
[45] S. Aoki, T. Hatsuda and N. Ishii, Comput. Sci. Dis. **1**, 015009 (2008) [arXiv:0805.2462 [hep-ph]].
[46] S. R. Beane *et al.* [NPLQCD Collaboration], Phys. Rev. D **81**, 054505 (2010) [arXiv:0912.4243 [hep-lat]].
[47] S. R. Beane *et al.* [NPLQCD Collaboration], arXiv:1012.3812 [hep-lat].
[48] M. Gockeler, R. Horsley, Y. Nakamura, D. Pleiter, P. E. L. Rakow, G. Schierholz and J. Zanotti [QCDSF Collaboration], PoS **LATTICE2008**, 136 (2008) [arXiv:0810.5337 [hep-lat]].
[49] J. Frison *et al* [BMW Collaboration], [arXiv:1011.3413 [hep-lat]].
[50] C. Liu, X. Feng and S. He, Int. J. Mod. Phys. A **21**, 847 (2006) [arXiv:hep-lat/0508022].
[51] S. Aoki, T. Hatsuda and N. Ishii, Prog. Theor. Phys. **123**, 89 (2010) [arXiv:0909.5585 [hep-lat]].
[52] Z. Y. Niu, D. C. Du, B. Z. Guo, N. Li, C. Liu and H. Liu, Phys. Rev. D **82**, 054501 (2010) [arXiv:1005.5571 [hep-lat]].
[53] **Group Theory: Application to the Physics of Condensed Matter**, M.S. Dresselhaus, G. Dresselhaus, A. Jorio, Springer-Verlag, 2008. ISBN 978-3-540-32897-1.
[54] **Group Theory and Quantum Mechanics** M. Tinkham, Dover Publications, 2003 ISBN-

13:978-0-486-43247-2.

[55] P. F. Bedaque, I. Sato and A. Walker-Loud, Phys. Rev. D **73**, 074501 (2006) [arXiv:hep-lat/0601033].

[56] S. R. Beane, P. F. Bedaque, A. Parreno and M. J. Savage, Phys. Lett. B **585**, 106 (2004) [arXiv:hep-lat/0312004].

[57] R. Kaminski, J. R. Pelaez and F. J. Yndurain, Phys. Rev. D **77**, 054015 (2008) [arXiv:0710.1150 [hep-ph]].

[58] G. P. Lepage, 'The Analysis Of Algorithms For Lattice Field Theory," Invited lectures given at TASI'89 Summer School, Boulder, CO, Jun 4-30, 1989. Published in Boulder ASI 1989:97-120 (QCD161:T45:1989).

[59] D. C. Moore and G. T. Fleming, Phys. Rev. D **74**, 054504 (2006) [arXiv:hep-lat/0607004].

[60] S. Basak *et al.* [Lattice Hadron Physics Collaboration (LHPC)], Phys. Rev. D **72**, 074501 (2005) [arXiv:hep-lat/0508018].

[61] W. Detmold and M. J. Savage, Nucl. Phys. A **743**, 170 (2004) [arXiv:hep-lat/0403005].